

**EFFECT OF THERMOMECHANICAL PROCESSING ON MICROSTRUCTURAL  
REFINEMENT AND SUPERPLASTIC BEHAVIOUR OF  
Ti-6.8Al-3.2Mo-1.8Zr-0.3Si ALLOY**

*A Thesis Submitted  
in Partial Fulfilment of the Requirements  
for the Degree of*  
**MASTER OF TECHNOLOGY**

*by*  
**KARADGE MALLIKARJUN BABURAO**

*to the*  
**DEPARTMENT OF MATERIALS AND METALLURGICAL ENGINEERING  
INDIAN INSTITUTE OF TECHNOLOGY KANPUR  
JANUARY, 1998**

***DEDICATED***

***TO***

***AVI & APPAJI***

- 4 MAY 1998 MME  
CENTRAL LIBRARY  
11.1 KANPLIB  

---

No. A 125414

MME-1998-M- BAB-EFF

Entered in System

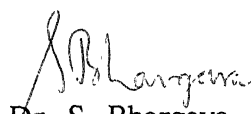
Nimisha  
4.6.98



CERTIFICATE

Kanpur.  
Submitted on 12.01.98

It is certified that the work contained in the thesis entitled, "Effect of Thermo-mechanical Processing on Microstructural Refinement and Superplastic Behaviour of Ti-6.8Al-3.2Mo-1.8Zr-0.3Si Alloy" by Karadge Mallikarjun Baburao has been carried out under my supervision and that this work has not been submitted elsewhere for a degree.

  
Dr. S. Bhargava

Professor

Department of Materials and Metallurgical Engineering

Indian Institute of technology, Kanpur-208016 (INDIA)



## ACKNOWLEDGEMENTS

I would like to express my deep sense of gratitude and indebtedness to Prof. S. Bhargava for his valuable guidance, encouragement and inspirational discussions through out the course of this investigation. It has truly been a learning experience to associate with him and work towards the completion of this work.

I am extremely thankful to Mr.S.Suwas for whole-heartedly extending his valuable time as well as encouraging moral support during the course of this project work.

I am grateful to Mr.K.P.Mukherjee, Mr.Kumar, Mr.Jain, Mr Umashankar,Mr.Laxmi, Mr.Pal and the workshop staff for their assistance in the experimental work.

The association, cooperation and support given by my friends Shailesh and Patro gratefully acknowledged.

Thanks are also due to my friends, Pravin, Bupesh, Santosh, Babu, Anirban, Giri, Bikash etc for extending their cooperation whenever needed.

January 1998

I.I.T.,Kanpur.

(Karadge Mallikarjun. Baburao)

## CONTENTS

ACKNOWLEDGEMENT	(iii)
LIST OF TABLES	(viii)
LIST OF FIGURES	( ix )
ABSTRACT	(xvi)
Chapter 1    Introduction	1
 Chapter 2    Literature Review	 5
2.1    Specific properties and applications of titanium and its alloys	5
2.2    Classification of titanium alloys	8
2.2.1 $\alpha$ alloys	9
2.2.2    Near $\alpha$ alloys	11
2.2.3    ( $\alpha+\beta$ ) alloys	11
2.2.4    Near $\beta$ alloys	11
2.2.5 $\beta$ alloys	14
2.3    Importance of ( $\alpha+\beta$ ) alloys	14
2.4    Microstructural control in ( $\alpha+\beta$ ) alloys	15
2.4.1    Microstructural features	15
2.4.2    Effect of heat treatment on microstructure	16
2.4.3    Effect of hot working on microstructure	18
2.4.4    Thermomechanical Processing	22

2.5	Texture in ( $\alpha+\beta$ ) alloys	22
2.6	Forming of titanium alloys	23
2.7	Superplastic forming of titanium alloys	27
2.7.1	Superplasticity	27
2.7.2	Metallurgical variables affecting superplasticity	29
2.7.3	Applications of superplastic forming	37
<b>Chapter 3</b>	<b>Experimental Procedure</b>	<b>39</b>
3.1	Starting Material	39
3.2	Thermomechanical processing	39
3.2.1	Equipments for thermomechanical processing	41
3.2.2	Thermomechanical processing schedule	42
3.3	Characterization techniques	44
3.3.1	Microstructural characterization	44
3.3.2	Structural Characterization	45
3.3.3	Mechanical Testing	45
<b>Chapter 4</b>	<b>Results and Discussion</b>	<b>47</b>
4.1	Structure of Ti-632Si alloy prior to its thermomechanical processing in the $\beta$ phase field	48
4.2	Effect of thermomechanical processing variables on conditioning of grains of Ti-632 alloy	51

4.2.1	Effect of recrystallization temperature on $\beta$ grain size	51
4.2.2	Effect of temperature and thickness reduction on the characteristics of $\beta$ grains	51
4.2.3	Effect of $\beta$ rolling temperature and thickness reduction on the characteristic features of the as-quenched structure	59
4.2.4	Effect of $\beta$ -annealing on the structure of hot rolled alloy	61
4.2.5	Comparison between conditions of water quenched $\beta$ grains as oriented by varying the thermomechanical processing of Ti-632Si alloy in the $\beta$ phase field	65
4.3	Effect of thermomechanical processing variables in the $(\alpha+\beta)$ phase field on phase field on the microstructural refinement in Ti-632Si alloy	65
4.3.1	Effect of the hot rolling temperature on the morphology of primary $\alpha$	67
4.3.2	Effect of conditioning of $\beta$ grains on microstructural refinements in Ti-632Si alloy after rolling in $(\alpha+\beta)$ phase field	76
4.4	Effect of recrystallization annealing in $(\alpha+\beta)$ phase field on the $(\alpha+\beta)$ hot rolled Ti-632Si alloy	79
4.4.1	Effect of recrystallization temperature and time on the annealing behaviour	82
4.4.2	Effect of $\alpha$ platelet thickness on the post	88

4.5	Superplastic behaviour of thermomechanically processed Ti-632Si alloy	93
4.5.1	Effect of temperature and strain rate on strain rate sensitivity of thermomechanically processed Ti-632Si alloy	94
4.5.2	Effect of temperature on elongation till failure	99
4.5.3	Microstructural changes in Ti-632Si alloy during superplastic deformation	104
4.5.4	Activation energy for superplastic deformation	106
4.5.5	Effect of recrystallization on the superplastic behaviour	106
4.5.6	Effect of thermomechanical processing on elongation till failure	115
<b>CONCLUSIONS</b>		121
<b>SUGGESTIONS FOR FURTHER WORK</b>		123
<b>REFERENCES</b>		124

## LIST OF TABLES

Table 2.1	Physical Properties Of Elemental Titanium.	6
Table 2.2	Mechanical properties Of Some Structural Titanium Alloys.	7
Table 2.3	Classification Of U.S.Technical Multicomponent Alloys.	12
Table 2.4	Aluminium And Molybdenum Equivalences Of A Series Of U.S. Titanium Alloys.	13
Table 2.5	Properties Of A Textured Titanium Alloy Plate.	25
Table 2.6	Summary Of Superplastic Characteristics Of Titanium Alloys.	27A
Table 2.7	Activation Energies For Superplastic Deformation And Self-Diffusion In Titanium Alloys.	35
Table 3.1	Chemical Composition Of The As Recieved Alloy.	39

## LIST OF FIGURES

Fig.2.1	Schematic Phase Diagram Of Binary Titanium Alloy Systems. (a) Alpha Stabilized.    (b) Beta Stabilized.	10
Fig.2.2	Schematic CCT Diagram Showing The Effect Of Cooling Rate On The Constitution Of An ( $\alpha+\beta$ ) Ti Alloy.	17
Fig.2.3	Schematic Illustration Of Formation Of Widmanstatten Structure In Ti-6Al-4V Alloy.	17
Fig.2.4	Light Micrographs Illustrating Effect Of Beta Stabilizing Alloying Elements On Size And Distribution Of Alpha Phase Packets In Beta Processed Materials: (a) Packets, Which Contain Single Alpha-Phase Variant, Are Large In Ti-6-4. (b) Single Variant Packets Are Smaller In Ti-6-6-2. (c) Packets Are Smallest In Ti-6-2-4-6.	19
Fig.2.5	Light Micrographsa Illustrating Effect Of Processing On Microstructure: (a) Forged In Beta Phase Field And Air Cooled. (b) Quenched From Beta Phase Field.	20
Fig.2.6	Light Micrographs Demonstrating Dependence Of Primary Alpha Morphology On Forging Treatment: (a) Equiaxed Primary Alpha Resulting From Extensive Hot Working. (b) Elongated Primary Alpha Resulting From Light Hot Working.	20
Fig.2.7	Textures In ( $\alpha+\beta$ ) Titanium Alloys.	24

Fig.2.8	Graphs Illustrating Effects Of Average Grain Size On Flow Stress And Strain rate Sensitivity ('m') Value For Ti-6Al-4V At 1200 °K.	30
Fig.2.9	Graph Illustrating Effect Of Texture On Total Elongation For Ti-6Al-5V.	32
Fig.2.10	Variation Of $\alpha$ Volume Fraction With Temperature For Three Ti Alloys.	32
Fig.2.11	Graphs Illustrating Effects Of Temperature And Alpha Volume Fraction On The Flow Stress And Strain Rate Sensitivity ('m') Values For Ti-6Al-4V.	33
Fig.2.12	Effect Of Temperature On Maximum Elongations In Ti-6Al-4V.	36
Fig.2.13	Superplastically Formed Nacelle Frame Showing Savings Potential.	38
Fig.2.14	Potential Superplastic Forming Applications In The Avionics Compartment.	38
Fig.3.1	Micrograph Of The As Recieved Material (Ti-6.8Al-3.2Mo-1.8Zr-0.3Si).	40
Fig.3.2	Schematic Illustration Of The Thermomechanical Processing Routes Followed In The Present Study. (a) Route 1. (b) Route 2. (c) Route	43A
Fig.3.3	Flowsheet Of Three Different Thermomechanical Processing Routes Followed In The Present Study.	43
Fig.4.1	Micrographs Showing The Martensitic Structure With Prior $\beta$ Grain Boundaries After Solutionizing And Quenching From Different Temperatures. (a) 1050°C (b) 1150°C.	49
Fig.4.2	Micrograph Showing Martensitic Structure Consisting Of Partially Disordered Array Of Individual Platelets Of Acicular $\alpha$ Martensite After Quenching From 1050°C.	49
Fig.4.3	X-Ray Diffraction Pattern For As Solutionised Sample	50



Quenched From 1050°C.

Fig.4.4	Schematic Representation Of The $\beta$ -Processes Studied.	52
Fig.4.5	Flowsheet Of The $\beta$ -Processes Used.	52A
Fig.4.6	Microstructures Of Ti-632Si Rolled At 1050°C, W/Q. (a) 20 %      (b) 40 %      (c) 60 %.	54
Fig.4.7	Microstructures Of Ti-632Si Rolled At 1150°C, W/Q. (a) 20 %      (b) 40 %      (c) 60 %.	55
Fig.4.8	Graph Illustrating The Effect Of Rolling Thickness Reductions (%) And Temperatures On Beta Grain Aspect Ratio.	56
Fig.4.9	Micrographs Showing Formation Of Shear Bands (Hairline Structures) After 60% Thickness Reduction At 1050°C, W/Q.	57
Fig.4.10	Presence Of Fine Equiaxed Grains In The As Rolled Samples(1050°C, 60 % Thickness Reduction, W/Q).	58
Fig.4.11	Graph Illustrating The Effect Of Rolling Thickness Reductions And Temperatures On Martensite Aspect Ratio.	60
Fig.4.12	Micrographs Illustrating Recrystallization Structures After Annealing Of The Beta Rolled Specimens In The Beta Phase Field (1020°C) At Different Time Intervals. (a) 10s, (b) 15s, (c) 20s, (d) 30s.	62
Fig.4.13	Graph Showing Variation Of Volume Fraction Of Recrystallized Beta Grains Annealed At 1020°C With $\ln(\text{Annealing Time, s})$ .	63
Fig.4.14	Graph Showing Reduction In Vicker's Microhardness (VHN) With $\ln(\text{Annealing Time, s})$ After Annealing At 1020 °C.	64
Fig.4.15	Variation Of Martensite Aspect Ratios With Different $\beta$ Processing Routes.	66
Fig.4.16	Micrographs Of Specimens ( $\alpha+\beta$ ) Rolled At Three Different Temperatures With 60 % Thickness Reduction Following Route 3 Of The Thermomechanical Processing	69

Routes.

(a) 850 °C (b) 900 °C (c) 950 °C.

Fig.4.17	Length Distribution Of The $\alpha$ Plates In The Specimens Rolled In ( $\alpha+\beta$ ) Field At Different Temperatures.	70
Fig.4.18	Thickness Distribution Of The $\alpha$ Plates In The Specimens Rolled In ( $\alpha+\beta$ ) Field At Different Temperatures.	71
Fig.4.19	Aspect Ratio Distribution Of The $\alpha$ Plates In The Specimens Rolled In ( $\alpha+\beta$ ) Field At Different Temperatures.	72
Fig.4.20	Graph Showing Variation In $\alpha$ Aspect Ratio With Respect To ( $\alpha+\beta$ ) Rolling Temperature.	73
Fig.4.21	Graph Showing Variation In $\alpha$ Grain Size With Respect To ( $\alpha+\beta$ ) Rolling Temperature.	74
Fig.4.22	Scheme Of Division Of $\alpha$ -Phase Plate During Deformation In The ( $\alpha+\beta$ ) Field.	75
Fig.4.23	Microstructures Of Typical Breakups Of $\alpha$ Lamellae By The $\beta$ Penetration As Occurring In The Specimen Rolled At 950°C.	77
Fig.4.24	Micrographs Of Specimens Rolled At 1050 °C Following Different Thermomechanical Processing Routes. (a) Route 1 (b) Route 2 (c) Route 3.	78
Fig.4.25	Bar Graph Showing Variation In $\alpha$ Aspect Ratios In The As Rolled Specimens Obtained By Three Thermomechanical Processing Routes.	80
Fig.4.26	Bar Graph Showing Variation In $\alpha$ Grain Size In The As Rolled Specimens Obtained By Three Thermomechanical Processing Routes.	81
Fig.4.27	Micrographs Of The Specimens Annealed At 800°C At Different Times After Rolling In The ( $\alpha+\beta$ ) Phase Field At 850 °C Following Route 3. (a) 0.5 h (b) 2 h (c) 4h.	83

Fig.4.28	Micrographs Of The Specimens Annealed At 850 °C At Different Times After ( $\alpha+\beta$ ) Rolling At 850 °C Following Route 3. (a) 0.5 h (b) 2 h (c) 4h.	84
Fig.4.29	Graph Illustrating Variation In $\alpha$ Aspect Ratio After Annealing At 800°C and 850°C At Different Times In As ( $\alpha+\beta$ ) Rolled (850°C) Specimens Following Route 3.	85
Fig.4.30	Graph Illustrating Variation In $\alpha$ Grain Size After Annealing At 800°C and 850°C At Different Times In As ( $\alpha+\beta$ ) Rolled (850°C) Specimens Following Route 3.	86
Fig.4.31	Schematic Representation Of The Conversion Of $\alpha$ Platelike Structure To Equiaxed Structure During Post Deformation Annealing.	87
Fig.4.32	Micrographs Of The Specimens Annealed At 800°C For 1 Hour Following 60 % Thickness Reductions In ( $\alpha+\beta$ ) Rolling At Different Temperatures (Route 3). (a) 850°C (b) 900°C (c) 950°C.	89
Fig.4.33	Micrographs Of The Specimens Annealed At 850 °C For 1 Hour Following 60 % Thickness Reductions In ( $\alpha+\beta$ ) Rolling At Different Temperatures (Route 3). (a) 850°C (b) 900°C (c) 950°C.	90
Fig.4.34	Bar Graph Illustrating Variation In $\alpha$ Grain Aspect Ratios After Annealing At 800°C and 850°C For 1 Hour Of The Samples Rolled At Three Different ( $\alpha+\beta$ ) Temperatures.	91
Fig.4.35	Bar Graph Illustrating Variation In $\alpha$ Grain Sizes After Annealing At 800°C and 850°C For 1 Hour Of The Samples Rolled At Three Different ( $\alpha+\beta$ ) Temperatures.	92
Fig.4.36	Load vs Elongation Curves For Route 3 As Rolled Specimens Tested ( Strain Rate Jump Tests )	95

	At Three Different Temperatures. (a) 850°C (b) 900°C (c) 950°C.	
Fig.4.37	Graph Illustrating $\ln(\text{Flow Stress})$ As A Function Of $\ln(\text{Strain Rate})$ For As Rolled Specimens Of Route 3 Tested ( Strain Rate Jump Tests ) At Three Different Temperatures.	98
Fig.4.38	Effect Of Temperature On Strain Rate Sensitivity ( 'm' ) As A Function Of Strain Rate For As Rolled Specimens processed By Route 3.	100
Fig.4.39	Load vs Elongation Curve For Route 3 Sample Tested At Two Different Temperatures and Strain rate : $5.5 \times 10^{-3}$ (a) 900°C (b) 925°C.	101
Fig.4.40	X-Ray Diffraction Pattern For As Rolled Route 3 Specimen Water Quenched From 850°C Directly After Rolling.	105
Fig.4.41	Micrographs Of The Elongated As Rolled Route 3 Specimen Tested ( Elongation To Failure Test ) At 900°C And Strain Rate $5.5 \times 10^{-3}$ /s At Different Locations.	105A
Fig.4.42	Microstructure Of The Specimen Adjacent To The Fracture Tip Showing The Propagation Of Cracks (Testing Conditions : Temperature 900 °C, Strain Rate = $5.5 \times 10^{-3}$ )	107
Fig.4.43	Graph Of $\ln(\text{Strain Rate})$ vs $\ln[1/(RT)]$ For Three Different Flow Stresses Obtained From Fig 4.37.	108
Fig.4.44	Load vs Elongation Curves For Route 3 Annealed Specimens Tested ( Strain Rate Jump Tests ) At 900°C. (Annealed At 850°C For 1 Hour)	110
Fig.4.45	Load vs Elongation Curves For Route 3 Annealed Specimens Tested ( Strain Rate Jump Tests ) At	111

900°C. (Annealed At 850°C For 4 Hours)

Fig.4.46	Graph Illustrating $\ln(\text{Flow Stress})$ As A Function Of $\ln(\text{Strain Rate})$ For Route 3 Annealed Specimens Tested ( Strain rate Jump Tests ) At 900°C.	112
Fig.4.46(A)	Effect Of Recrystallization On Strain Rate Sensitivity ('m') As A Function Of Strain Rate For Route 3 Annealed Specimens Tested ( Strain Rate Jump Tests ) At 900°C.	113
Fig.4.47	Microstructure Of The As Rolled ( $\alpha+\beta$ ) Alloy Reheated At 900 °C, Soaked For 15 Min and Subsequently Water Quenched.	114
Fig.4.48	Load vs Elongation Curves For As Rolled Specimens Tested (Elongation To Failure) At 900 °C (a) Route 1    (b) Route 2    (c) Route 3.	116
Fig.4.49	Bar Graph Showing Comparison Of Flow Stresses For Superplastic Deformation For As Rolled Specimens Processed By Three Different Routes. (Testing Conditions : Temperature 900°C, Strain Rate = $5.5 \times 10^{-3}$ ).	118
Fig.4.50	Bar Graph Showing Comparison Of Maximum Elongations Obtained For As Rolled Specimens Produced By Three Different Thermomechanical Processing Routes.(Testing Conditions : Temperature 900°C, Strain Rate = $5.5 \times 10^{-3}$ ).	119
Fig.4.51	Photograph Showing Elongated samples After Superplastic Tensile Testing.	119A

## Chapter 1

### INTRODUCTION

In the decade of 1950's, a wonder metal called titanium burst upon the industrial world through its use as an alloy in the gas turbine engines [1]. The light weight and excellent corrosion resistance of titanium alloys led to expansion of its use into air frames and petrochemical and marine environments. The story of titanium alloys is an intriguing one, replete with the boom-and-bust cyclic fluctuations associated with a material largely tied to aerospace/military applications.

Titanium alloys are usually divided into three major classes [2]. These basic alloy groups are defined by the phases predominant in their microstructure near room temperature and are referred to as alpha ( $\alpha$ ) alloys, alpha + beta ( $\alpha+\beta$ ) alloys and beta ( $\beta$ ) alloys. The group : ( $\alpha+\beta$ ) alloys, consist of largest number of superplastic alloys. These alloys are formulated so that both the hexagonal alpha ( $\alpha$ ) phase and the bcc beta ( $\beta$ ) phase coexist at room temperature. A large variety of properties can be obtained in the  $\alpha+\beta$  alloys as a result of deformation and heat treatment that alters both the phase compositions and amounts of  $\alpha$  and  $\beta$  phase.

Morphology of the primary  $\alpha$  phase in the ( $\alpha+\beta$ ) titanium alloys is of considerable importance from the point of view of controlling their static and dynamic mechanical properties. The presence of equiaxed (low aspect ratio)  $\alpha$  phase in the microstructures promotes ductility at low temperatures, fatigue crack initiation resistance and elevated temperature flow characteristics [3]. Similarly improved fracture toughness, fatigue crack propagation resistance, creep and stress rupture strengths are obtained in microstructures possessing lamellar ( high aspect ratio ) primary  $\alpha$  phase [3]. Further, dimensional characteristics in both these morphologies play an important role in influencing mechanical properties of these type of titanium alloys.

Though ( $\alpha+\beta$ ) type of titanium posses a good combination of mechanical properties and are vieved as excellent candidate materials for many advanced aerospace and other engineering

applications, they suffer from the drawback of poor workability [4]. The buy-to-fly ratio for manufacturing components from titanium alloys is therefore very low. Superplastic forming of components of titanium alloys has therefore emerged as one of the commercially viable production route [5]. Fortunately most of the  $(\alpha+\beta)$  titanium alloys display superplastic properties over a given temperature-strain rate regime [6]. However, microstructural state of the alloy has important bearing on such properties and one of the essential requirements for undergoing the superplastic flow in appropriate temperature-strain rate regime is that these alloys consist of the  $(\alpha+\beta)$  structure in which the primary  $\alpha$  exists in a very fine equiaxed morphology [6]. Obtaining fine equiaxed structure in the starting preform material of two phase titanium alloys, so that they can be further shaped by superplastic forming, has therefore become one of the major goals in processing  $(\alpha+\beta)$  titanium alloys [7]. Thermomechanical processing, both in the single phase  $\beta$  as well as two phase  $(\alpha+\beta)$  fields, is the most effective method of modifying and controlling the morphology of the primary  $\alpha$  phase. While the lamellar  $\alpha$  morphology arises during slow cooling of the alloy through the  $(\alpha+\beta)$  two phase field, equiaxed morphology generally results from the recrystallization / mill annealing of the structure which is obtained by imparting sufficiently large deformation in the alloy below its  $\beta$ -transus temperature [6].

The deformation behaviour of the  $(\alpha+\beta)$  alloys in the two phase field is strongly influenced by the deformation characteristics of the difficult-to-form HCP  $\alpha$  phase. It occurs both by slip and as well as twinning, though the contribution of the latter at higher temperatures is low [8]. Further as observed by the nature of the stress-strain curves, and also supported by the TEM analysis of the structure,  $(\alpha+\beta)$  titanium alloys soften by dynamic recovery and/or by dynamic recrystallization during their hot deformation [9]. Metallographic investigations indicate that  $\alpha$  lamellae elongate and work harden during deformation. Therefore, sub-boundaries and shear bands develop within deformed  $\alpha$  lamellae, the misorientation between which increases with the degree of deformation. Hot deformation degree, if exceeding a critical value, may also lead to the fracturing of deforming  $\alpha$  lamellae and give rise to primary  $\alpha$  lamellae of smaller aspect ratio [10]. Subsequent breakup of  $\alpha$  lamellae to equiaxed morphology occurs during subsequent recrystallization annealing when the  $\beta$  phase penetrates across the lamellar width along the sub boundaries or shear bands. Nature of the starting microstructure characterised by lamellae width, therefore, affects the evolution of equiaxed microstructures in  $(\alpha+\beta)$  titanium

alloys. Other variables namely strain, strain rate, temperature and number of passes determine the amount of stored energy for static recovery and recrystallization processes. These factors, in turn, play an important role in microstructural evolution during annealing of the hot deformed alloy. Thus, the transformation of primary lamellar  $\alpha$  morphology to the equiaxed  $\alpha$  morphology by thermomechanical processing is strongly influenced by (i) the degree of prior deformation in the  $\beta$  phase field, (ii) working temperature and (iii) the mode of deformation applied. While the first two parameters, i.e. the degree of prior deformation and the working temperature, influence the morphology of primary  $\alpha$  as well as the texture, the mode of deformation ( as governed by the stress and strain fields set up in the workpiece ) primarily influences the texture, in turn, affects the  $\alpha$  phase morphology during recrystallization annealing. However, no homogeneous distribution of  $\alpha$  and  $\beta$  phases is generally obtained after a thermomechanical processing as reported in the existing literatures.

To reduce structural weight and fabrication costs of titanium alloys, increasing attention is being given to near-net shape processing techniques. Superplastic forming (SPF) has emerged as a practical fabrication method and attention has begun to be focussed on improving SPF by optimizing the material and process parameters. Recently widespread results have shown that SPF with or without concurrent Diffusion Bonding (DB) can result in substantial cost savings (> 50% of conventionally fabricated components), creating greatest interest in SPF method [11].

To date most SPF work was concentrated on Ti-6Al-4V in the temperature range 900 - 925°C [12]. While the behaviour of this alloy has been more than adequate to meet the current design concepts, imaginable innovations possible with SPF have led to the desire for improved performance. Consideration of microstructural requirements for SPF behaviour [12] indicate that it can be achieved by using a fine equiaxed microstructural with approximately equal properties of the two phases at the forming temperature. This type of microstructure can be effectively achieved by thermomechanical processing [13]. It is seen that changes in the  $\alpha$  morphology from lamellar to equiaxed are a direct result of prior deformation, deformation temperature and mode of deformation applied.

The ( $\alpha+\beta$ ) alloy of titanium with a composition Ti-6.8Al-3.2Mo-1.8Zr-0.3Si, finds



application as aeroengine turbine components. Presence of about 0.3% of Si in this alloy improves the creep resistance [14] and also affects the microstructure and static strength [15]. However, precipitation of silicates in these alloys causes embrittlement. While silicon in the form of silicates reduces room temperature fatigue life [16], in solution, it enhances the high temperature fatigue life [17]. Results and understanding of the stability of microstructures development of suitable microstructures for further processing should give directives in making decisions for prolonged application of this alloy in jet engines.

### 1.3 AIMS OF PRESENT STUDY

The present study was undertaken to study

- (1) the process of microstructural refinement in Ti-632Si alloy by involving the conditioning of
  - (a)  $\beta$  grains and
  - (b) acicular  $\alpha$  prior to hot rolling in the  $(\alpha+\beta)$  phase field ;
- (2) the effect of recrystallization annealing in the  $(\alpha+\beta)$  phase field on formation of equiaxed primary  $\alpha$  in thermomechanically treated Ti-632Si alloy ;
- (3) the superplastic behaviour of thermomechanically treated Ti-632Si alloy.

## Chapter 2

### LITERATURE REVIEW

#### 2.1 SPECIFIC PROPERTIES AND APPLICATIONS OF TITANIUM AND ITS ALLOYS:

Titanium possesses an outstanding combination of physical, chemical and mechanical properties. It is a low density element and can be greatly strengthened by alloying and mechanical working. It is non-magnetic in nature and shows a relatively lower thermal expansion coefficient. Some of the important physical properties of titanium have been shown in Table No. 2.1.

Ability of titanium and its alloys to passivate provide them a higher degree of immunity against a wide range of acidic, alkaline and saline media and thus makes them useful corrosion resistant materials. Similarly these alloys can be used upto  $\sim 750^{\circ}\text{K}$  without any problem of oxidation.

With strength capability most equal to that of low carbon steels and density nearly half (56%) of them, titanium alloys can be strengthened to achieve a specific strength (strength per unit weight) equal to that of ultra-high strength steels. The specific fracture toughness (fracture toughness ( $K_{Ic}$ ) per unit weight) of titanium alloys is superior to most of the structural materials. Most of the titanium alloys developed to date also show an excellent combination of creep and fatigue strength making them well suited for dynamically loaded structural components. Further, most of the dual phase titanium alloys of the family represented by Ti-6Al-4V can exist a high value of strain rate sensitivity approaching to unity which puts them among the most desirable candidate materials for superplastic forming/isothermal forging. Selected mechanical properties of some titanium structural alloys are shown in Table No. 2.2.

## Physical properties of Elemental Titanium

Atomic Number	22
Atomic weight	47.90
Atomic Volume	10.6 W/D
Covalent Radius	1.32 Å
First Ionisation Energy	158 k-cal/g-mole
Thermal Neutron Absorption Cross Section	5.6 barns/atom
Crystal Structure	Alpha : HCP, $\leq 1155.5$ K Beta : BCC, $\geq 1155.5$ K
Color	Dark Grey
Density	4.51 g/cm <sup>3</sup>
Melting Point	1941 $\pm$ 10 K
Solidus/Liquidus	1998 $\pm$ 10 K
Boiling Point	3533 K
Specific Heat (At 25 °C)	0.518 J/kg K
Thermal Conductivity	9.0 BTU/hr ft <sup>2</sup> °F
Heat Of Fusion	440 kJ/kg
Heat Of Vaporization	9.83 MJ/kg
Specific Gravity	4.5
Modulus Of Elasticity	1.027 * 10 <sup>11</sup> N/m <sup>2</sup>
Young's Modulus Of Elasticity	102.7 GPa
Poisson's Ratio	0.41
Coefficient Of Friction	0.8 at 40 m/min
Specific Resistance	554 $\mu$ ohm <sup>-mm</sup>
Coefficient Of Thermal Expansion	8.64 * 10 <sup>-6</sup> /°C
Electrical Conductivity	3% IACS (Copper 100%)
Electrical Resistivity	47.8 $\mu$ ohm-cm
Temperature Coefficient Of Electrical Resistance	0.0026 /°C
Magnetic Susceptibility	3.17 emu/g

Table 1.1                      Physical Properties Of Elemental Titanium

Alloy	Tensile strength (min) (MPa/kg )	Yield strength(min) (MPa/kg)	Elong- ation (%)	Reduction in area (%)	Charpy impact stren- gth (J)	Fatigue streng- th(MPa)	Fracture tough- ness MPa $\sqrt{m}$
Ti-5Al- 2.5 Sn (ELI)	807	745	16	--	26	485-495	
Ti-6Al- 4V	993 -1172	924 -1103	15	35	19	489-620	32-123
Ti-6Al- 2Sn-4Zr- 6Mo	1269	1172	10	23	--	620-751	26-34
Ti-13V- 11Cr-3 Al	1220	1172	8	--	--	--	--
4340 (Ultra high strength steel)	1965	1482	--	--	--	--	71
Al alloy (20240)	185.495	75-395	13-20	--	--	--	90-140
Mg alloy (A2318)	255-290	150-220	15-21	--	4	--	

Note: Range is provided in certain cases since property values depend on microstructural state. Minimum values are given where range is not specified.

Table 2.2 Mechanical Properties Of Some Structural Titanium Alloys.

Due to the excellent corrosion resistance displayed by titanium and its alloys, they find extensive applications in heat exchangers, reactor vessels desalination plants, steam turbine blades, condenser tubings and several other components in chemical, marine, petrochemical, offshore and power generation industries. Its non-toxicity and biocompatibility in addition to excellent corrosion resistance, is made use of in prosthetic devices such as heart-valve parts and leg bone replacements or splints. Applications related to corrosion resistance and biocompatible properties account for about 30% titanium.

Majority of the demand for titanium alloys, however, is from aerospace industries where high specific strengths make them an attractive choice for air frames, blades and other parts of both low as well as high pressure compressors of turbine engine. Though strength efficiency is the prime consideration for such applications other requirements like fatigue life, fracture toughness, creep, microstructural stability at high temperatures may also have to be met depending on nature of application. To meet these multifarious requirements different alloys have been developed.

## 2.2 CLASSIFICATION OF TITANIUM ALLOYS [2]

Pure titanium has two allotropic forms, the low temperature hcp  $\alpha$  phase and the elevated temperature ( $\alpha \rightarrow \beta$ ) bcc  $\beta$  phase. the allotropic transformation temperature being 882.5°C (1155.5K) [19,20]. Alloying elements added tends to preferentially stabilize one or other of the three phases.

Elements like Al, C, O, N, Sn, etc., when added to titanium raise the transformation temperature (commonly referred to as  $\beta$ -transus) of the alloy and thus stabilize the  $\alpha$  phases to a temperature higher than 882.5 °C. These elements are referred to as  $\alpha$  stabilizers. Rosenberg has suggested the following expression [21] for aluminum equivalent Al\* of the alloy:

$$Al^* = [Al] + [Zr]/6 + [Sn]/5 + 10 [O+C+2N] \text{ wt\%}$$

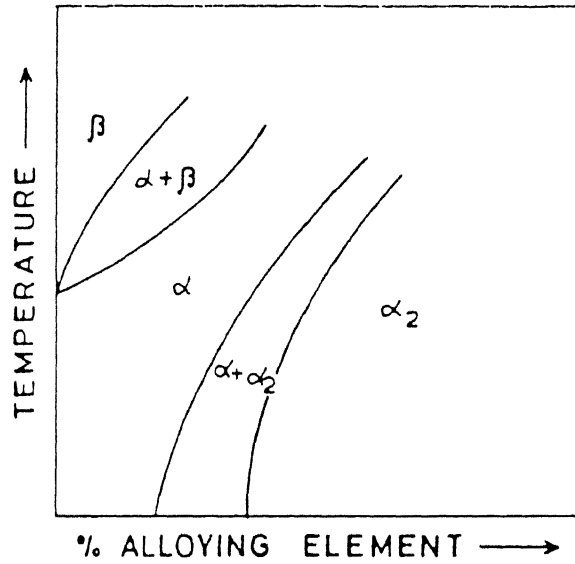
Elements like Mo, V, Ni, Mn, Cu, Cr, Fe, H, Si wt when added to titanium, lower the  $\beta$  transus temperature and hence are known as  $\beta$  stabilizers. Molchanova [19] has suggested the following expression for Mo equivalent  $Mo^*$  of the alloy:

$$Mo^* = [Mo] + [Ta]/5 + [Nb]/3.6 + [W]/2.5 + [V]/1.5 + 1.25 [CR] + 1.25 [Ni] + 1.7 [Mn] + 1.7 [Co] + 2.5 [Fe]$$

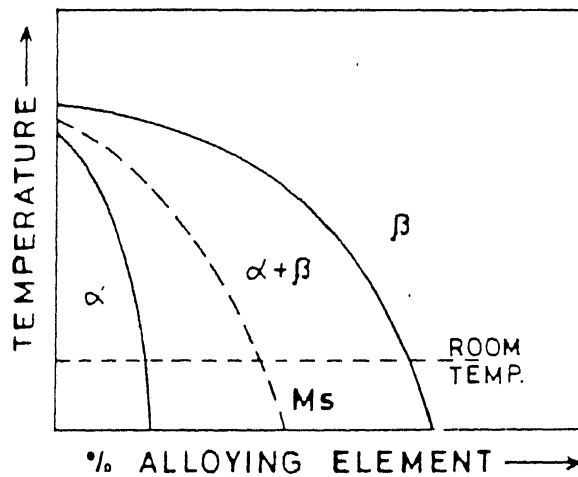
Variation of  $\beta$  transus temperature with the percentage of alloying additives can be obtained from the phase diagrams. Schematic phase diagrams [22] for Ti- $\alpha$  stabilizers and Ti- $\beta$  stabilizers (isomorphous) have been shown in figure 2.1. The Figure 2.1 (a) is a representative of  $\alpha$ -stabilizing addition, indicating increasing alloying addition result in an increase in the  $\beta$  transus temperature, to eventually the formation of a hexagonal ordered compound  $\alpha_2$ . The Figure 2.1(b) is the representative of the equilibrium diagram for the  $\beta$  isomorphous stabilizers, indicating increasing alloying additions result in both a decrease of  $\beta$  transus temperature and the volume fraction of the low temperature  $\alpha$ -phase present at a particular temperature. Thus the type and concentration of alloying elements determine the equilibrium concentration which forms the basis for classification of titanium alloys. Depending on the type of alloying addition made, titanium alloys can be  $\alpha$ , near  $\alpha$ ,  $\alpha+\beta$ , near  $\beta$  or  $\beta$  alloys.

### 2.2.1 $\alpha$ Alloys

These alloys contain only  $\alpha$  stabilizers as alloying elements and hence the room temperature microstructure consists of hcp  $\alpha$ -phase only. Due to the single phase nature of these alloys no microstructural strengthening can be achieved in them. Solid solution strengthening [21] of them is also limited because an aluminium equivalent (Al) of more than 9.0 promotes the formation of the brittle phase  $\alpha_2$ . These alloys, according to Wood [23], are characterized by satisfactory strength, toughness, creep resistance, and weldability. Furthermore the absence of a ductile-brittle transformation, a property of the bcc structure, renders  $\alpha$  alloys suitable for cryogenic applications [24]. However, these alloys have poor workability. Examples of these alloys are CP Ti and Ti-5Al-2.5 Sn, both of which find significant commercial applications. Some of the important  $\alpha$  alloys with their Aluminium and Molybdenum equivalences are shown in Table No. 2.3 and 2.4 [23,25].



(a)  $\alpha$  - STABILIZED



(b)  $\beta$  - STABILIZED

Fig. 2.1 Schematic Phase Diagrams Of Binary Ti Alloy Systems.

### 2.2.2 Near $\alpha$ -alloys

Small additions 1.2 wt% of  $\beta$  stabilizers to alpha ( $\alpha$ ) alloys give rise to near  $\alpha$  alloys. By such additions problems related to low strength and poor hot workability of high aluminium compositions are eliminated and a compromise is effected between the higher strength which is available with alpha-beta ( $\alpha+\beta$ ) alloys and better high temperature stability and weldability which are characteristics of  $\alpha$  alloys. Examples of these alloys are Ti-11Sn-2.25 Al-5Zr-1Mo-0.25Si, Ti-6Al-2Sn-4Zr-2Mo-0.1Si, Ti-6Al-5Zr-0.5Mo-0.3Si all of which find applications as turbine engine components. Some of the important near  $\alpha$  alloys with their aluminium and molybdenum equivalences are given in Table 2.3 and 2.4 [23,25].

### 2.2.3 ( $\alpha + \beta$ ) Alloys

The  $\alpha+\beta$  alloys are such that at equilibrium, usually at room temperature, they support a mixture of  $\alpha$  and  $\beta$  phases. Somewhat higher additions of  $\beta$  stabilizers (4.6%) in Ti alloys stabilize small vol. fraction of  $\beta$  phase in the microstructure. In practice the  $\alpha+\beta$  alloys usually contain mixtures of both  $\alpha$  and  $\beta$  stabilizers [2]. Morphology of both the phases ( $\alpha$  and  $\beta$ ) can be considerably varied by controlling various heat treatment and mechanical working parameters. A wide range of different property levels can therefore be achieved in these alloys. The simplest of such alloys, and one upon which most attention has been undoubtedly lavished, is Ti-6Al-4V. Although this particular alloy is difficult to form even in the annealed condition [24],  $\alpha+\beta$  alloys generally exhibit good fabricability as well as high room temperature strength and moderate elevated temperature strength. They may contain between 10 to 50%  $\beta$  phase at room temperature; if they contain more than 20% they are not weldable. Other important alloys are shown in Tables 2.3 and 2.4 [23,25]. All these alloys find extensive use in the aerospace industry.

### 2.2.4 Near $\beta$ -Alloys

Still larger additions of  $\beta$  stabilizers can cause retention of  $\beta$  phase at room temperature. Therefore, near beta alloys [2]. These alloys show excellent cold formability in which high strengths can also be achieved through proper heat treatment. Examples of these alloys are shown in Tables 2.3 and 2.4 [23,25]. This family of alloys has emerged for commercial applications only in the recent past.



**Table 2.3**  
**Classification of U.S. Technical Multicomponent Alloys**

Composition, wt%	Classification
Ti-5Al-2.5Sn	$\alpha$
Ti-8Al-1Mo-1V Ti-6Al-2Sn-4Zr-2Mo	Near $\alpha$
Ti-6Al-4V Ti-6Al-6V-2Sn Ti-3Al-2.5V	$\alpha + \beta$
Ti-6Al-2Sn-4Zr-6Mo Ti-5Al-2Sn-2Zr-4Cr-4Mo Ti-10V-2Fe-3Al	Near $\beta$
Ti-13V-11Cr-3Al Ti-15V-3Cr-3Al-3Sn Ti-3Al-8V-6Cr-4Mo-4Zr Ti-8Mo-8V-2Fe-3Al Ti-11.5Mo-6Zr-4.5Sn	$\beta$

Alloy classification and composition, wt. %	Aluminum equivalency, wt. %				Molybdenum equivalency, wt. %								
	[Al]	$\frac{[Zr]}{6}$	$\frac{[Sn]}{3}$	[Al] <sub>eq</sub>	[Mo]	$\frac{[Ta]}{5}$	$\frac{[Nb]}{3.6}$	$\frac{[V]}{1.5}$	1.25[Cr]	1.25[Ni]	1.7[Mn]	1.7[Co]	2.5[Fe] [Mo] <sub>eq</sub>
<b>Alpha and near-alpha alloys</b>													
Ti-0.8Ni-0.3Mo					0.3		..			1.0			1.3
Ti-5Al-2.5Sn	5.0		0.8	5.8	...				...	..			..
Ti-3Al-1Mo-1V	8.0			8.0	1.0			0.7					1.7
Ti-6Al-2Sn-4Zr-2Mo-0.1Si	6.0	0.7	0.7	7.4	2.0		..						2.0
Ti-6Al-2Nb-1Ta-0.8Mo	6.0			6.0	0.8	0.2	0.6						1.6
Ti-2.23Al-1.1Sn-5Zr-1Mo	2.3	0.8	3.7	6.8	1.0								1.0
Ti-5Al-5Sn-2Zr-2Mo	5.0	0.3	1.7	7.0	2.0			..					2.0
<b>Alpha-beta alloys</b>													
Ti-6Al-4V	6.0			6.0				2.7					2.7
Ti-6Al-6V-2Sn	6.0		0.7	6.7	..			4.0					4.0
Ti-7Al-4Mo	7.0			7.0	4.0								4.0
Ti-4.5Al-5Mo-1.5Cr	4.5			4.5	5.0				1.9				6.9
Ti-6Al-2Sn-4Zr-6Mo	6.0	0.7	0.7	7.4	6.0								6.0
Ti-5Al-2Sn-2Zr-4Mo-4Cr	5.0	0.3	0.7	6.0	4.0		..		5.0				9.0
Ti-6Al-2Sn-2Zr-2Mo-2Cr	6.0	0.3	0.7	7.0	2.0		...	..	2.5				4.5
Ti-3Al-2.5V	3.0			3.0				1.7					1.7
Ti-10V-2Fe-3Al	3.0			3.0	...			6.7				5.0	11.7
<b>Beta alloys (metastable)</b>													
Ti-8Mn				..				..			13.6		13.6
Ti-11.5Mo-6Zr-4.5Sn		1.0	0.4	1.4	11.5								11.5
Ti-10V-2Fe-3Al	3.0			3.0	...			6.7		..			5.0
Ti-15V-3Cr-3Al-3Sn	3.0		1.0	4.0	..		..	10.0	3.8				13.8
Ti-13V-11Cr-3Al	3.0			3.0	..		...	8.7	13.8				22.5
Ti-8Mo-8V-2Fe-3Al	3.0		..	3.0	8.0		..	5.3				5.0	18.3
Ti-3Al-5V-6Cr-4Mo-4Zr	3.0	0.7	..	3.7	4.0		..	5.3	7.5				16.8

Table 2.4 Aluminium and Molybdenum Equivalences of a Series of U.S. Titanium Alloys

### 2.2.5 Beta Alloys

These alloys contain very large amount of  $\beta$  stabilizers which gives them high densities, poor ductilities, poor oxidation resistance and of less commercial importance. Beta alloys, according to Wood [23], are extremely formable. They are however, prone to ductile brittle transition [26] and along with other bcc phase alloys, are unsuitable for low temperature applications [24]. Some of the beta alloys are shown in Tables 2.3 and 2.4 [15,17]. Ti-Nb alloys can be used as low temperature superconductors but their commercial importance is not very high.

Since the present investigation is concerned with the Titanium alloy : Ti-6.8Al-3.2Mo-1.8Zr-0.3Si, an ( $\alpha+\beta$ ) alloy, the discussion henceforth will only be confined to the family of  $\alpha+\beta$  alloys.

## 2.3 IMPORTANCE OF ( $\alpha+\beta$ ) ALLOYS

As a class, ( $\alpha+\beta$ ) alloys account for more than 75 % of all Titanium used [27]. Alpha-Beta alloys have been designed to combine the better part of properties of both alpha and near-beta alloys. Because of the dual phase structure consisting of  $\alpha$  and  $\beta$  phases, a wide range of microstructural features, varying in size and morphology of both the constituent phases can be obtained in them. Since the rule of mixture is not followed by them [28], a considerable amount of microstructural strengthening can be imparted to them. Thus for the same alloy it is possible to have a wide range of property levels by altering the morphology and size of its microstructural constituents. Yield strength (0.2 %), tensile strength and ductility do not get influenced by a large degree by alteration of the microstructure, but, properties involving dynamic loading such as fracture toughness, fatigue strength, fatigue crack propagation rate (FCP) get influenced by the microstructural changes to a very large degree. Similarly creep resistance and creep rupture strength and superplastic behaviour are known to vary drastically with the microstructural state of the material.

## 2.4 MICROSTRUCTURAL CONTROL IN ( $\alpha$ + $\beta$ ) ALLOYS

Microstructures are characterized by nature of phases present, their shape, size morphology which in turn are functions of heat treatment and working schedule before we go into the details. let us look at some of the prominent microstructural features in titanium alloys.

### 2.4.1 Microstructural Features [29]

- (a) **Primary Alpha ( $\alpha_p$ )** - It refers to the alpha phase in a crystallographic structure that is retained from the last high temperature ( $\alpha$ + $\beta$ ) working or heat treatment. Morphology of primary  $\alpha$  is influenced by prior thermomechanical history and may vary from lamellar to equiaxed grains.
- (b) **Alpha Prime ( $\alpha'$ )** - A supersaturated non-equilibrium hexagonal alpha phase formed by a diffusionless transformation of the beta phase. It occurs as fine, randomly oriented needles.
- (c) **Secondary Alpha** - Alpha phase generated from alpha prime on reheating in two phase field is designated as secondary alpha. It shows lamellar structure whose dimensions are function of temperature and time of heating.
- (d) **Grain Boundary Alpha** - Primary alpha outlining prior beta grain boundaries are referred to as grain boundary alpha. It evolves by heterogeneous transformation when cooled slowly from the beta to the alpha-beta phase field. Thickness and continuity of the layer depends on cooling rate and alloy composition.
- (e) **Alpha Double Prime ( $\alpha''$ )** - It refers to a supersaturated, non-equilibrium orthorhombic phase formed by diffusionless transformation of the beta phase in certain alloys like Ti-Mo, Ti-Nb etc. which have high concentration of beta stabilizers.
- (f) **Metastable Beta** - Refers to the beta phase which is retained at room temperature instead of undergoing martensitic transformation. Prior beta grain boundaries are visible whose sizes are function of temperature and time of solutionizing in the beta phase field.
- (g) **Alpha ( $\alpha_2$ )** - Refers to the ordered alpha phase  $Ti_3Al$  produced by segregation of alloying elements and existing as small precipitates.
- (h) **Silicides** - In high silicon bearing alloys silicon combines with titanium and other

alloying elements to form complex compounds known as silicides e.g.,  $\text{Ti}_3\text{Si}_3$ , Ti-Mo-Si etc. which exist as precipitates in the matrix.

#### 2.4.2 Effect of Heat Treatment on Microstructure

Heat treatment of titanium alloys are done for a variety of reasons - to reduce residual stresses known as stress relieving, generate acceptable combination of ductibility, machinability and dimensional and structural stability known as annealing. to increase strength and optimize special properties as fracture toughness fatigue strength, creep strength etc. The latter requirements are made by proper choice of thermal cycling to generate microstructures yielding requisite properties. The basis for microstructural manipulation during heat treatment of titanium alloys centres around the beta-alpha phase transformation which takes place in these alloys during cooling transformation can occur either by nucleation and growth mechanism yielding Widmanstatten structure or martensitic depending on the alloy composition and the cooling rate [10]. Figure 2.2 gives a schematic representation of the continuous cooling transformation diagram of an  $\alpha+\beta$  titanium alloy.

When the alloy is slowly cooled below the  $\beta$  transus alpha begins to nucleate at  $\beta$  grain boundaries with a crystallographic Burgers orientation relationship :

$$\begin{aligned} (0001)_\alpha // \{011\}_\beta \\ <1120>_\alpha // <111>_\beta \end{aligned}$$

Because of the close atomic matching along this common nucleation plane, the alpha phase thickens relatively slowly perpendicular to it but grows faster along it leading to plate like structure. A schematic illustration of the formation of Widmanstatten structure is shown in Fig. 2.3. Even when cooling at rates when nucleation and growth mechanism is operative morphology of the alpha phase is influenced by alloy content and cooling rates for e.g., during slow cooling (or in alloys leaner in  $\beta$  stabilizers) the Widmanstatten alpha plates form in colonies or packets of plates all of which belong to the same variant of the orientation relationship between the alpha and beta phases. With increase in cooling rates or increase in beta stabilizers

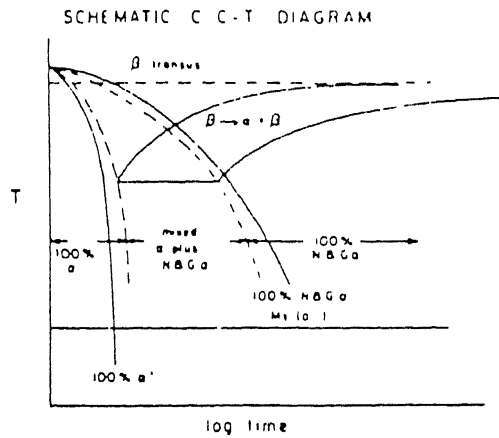


Fig. 2.2 Schematic CCT Diagram Showing The Effect Of Cooling Rate On The Constitution Of An  $(\alpha+\beta)$  Ti Alloy.

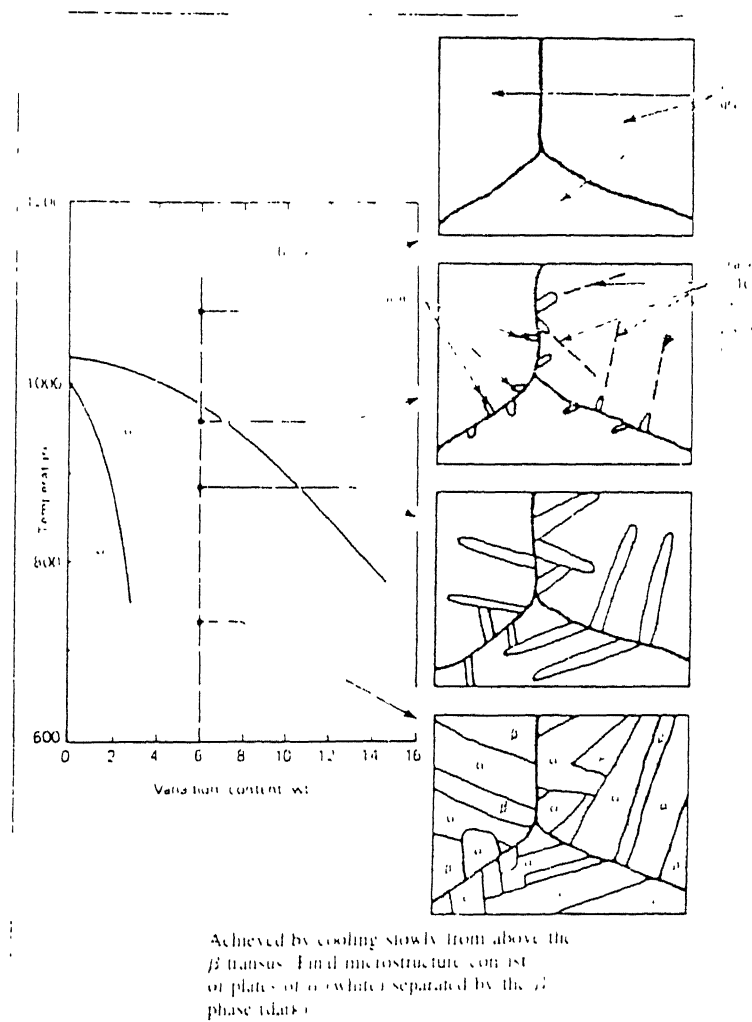


Fig. 2.3 Schematic Illustration Of Formation of Widmanstätten Structure In Ti-6Al-4V Alloy.

content nucleation of additional variants become more prevalent and the number of plates in the Widmanstätten alpha decreases until a point is reached when the transformed region consists of a random mixture of  $\alpha$ -plates belonging to different variants of the orientation relationship (Figure 2.4).

Rapid quenching from the beta phase field leads to formation of randomly oriented needle shaped martensite ( $\alpha''$ ) (Figure 2.5) which is supersaturated with beta stabilizing elements like Mo and V. Increasing beta stabilizer content not only shifts the cooling curve for nucleation and growth transformation to the right leading to evolution of  $\alpha''$  at lower cooling rates but also depresses the  $M_f$  (Martensite finish temperature) the latter causing incomplete transformation resulting in some metastable beta being found at room temperature. Subsequent aging of martensite leads to nucleation of beta phase at plate boundaries and internal substructures (such as twins) [30] followed by growth. Diffusion of excess beta-stabilizing elements from supersaturated  $\alpha''$  is utilized during growth with the latter gradually transforming to equilibrium  $\alpha$  [31]. Resulting fine lamellar or acicular alpha shows superior creep properties and higher fracture toughness values [32]

A wider range of microstructures can be produced by a combination of heat treatment and mechanical working than is possible through heat treatment alone [33]. Development of equiaxed alpha as one of the constituent phases form the basis of most of them as it shows clear advantages over lamellar structures in certain properties such as higher strengths, ductility and formability [34,35], better hydrogen tolerance and low cycle fatigue properties [36]. Thus both fabrication as well as microstructural evolution can be effected by proper control of deformation parameters during high temperature working - a process known as thermomechanical treatment [37].

### 2.4.3 Effect of Hot Working on Microstructure

Deformation of alpha-beta alloys is governed by the deformation characteristics of the difficult to deform hcp alpha phase. Deformation takes place by both slip and twinning though contribution of the latter is low [38,39]. Lamellar alpha phase elongate and strain harden on

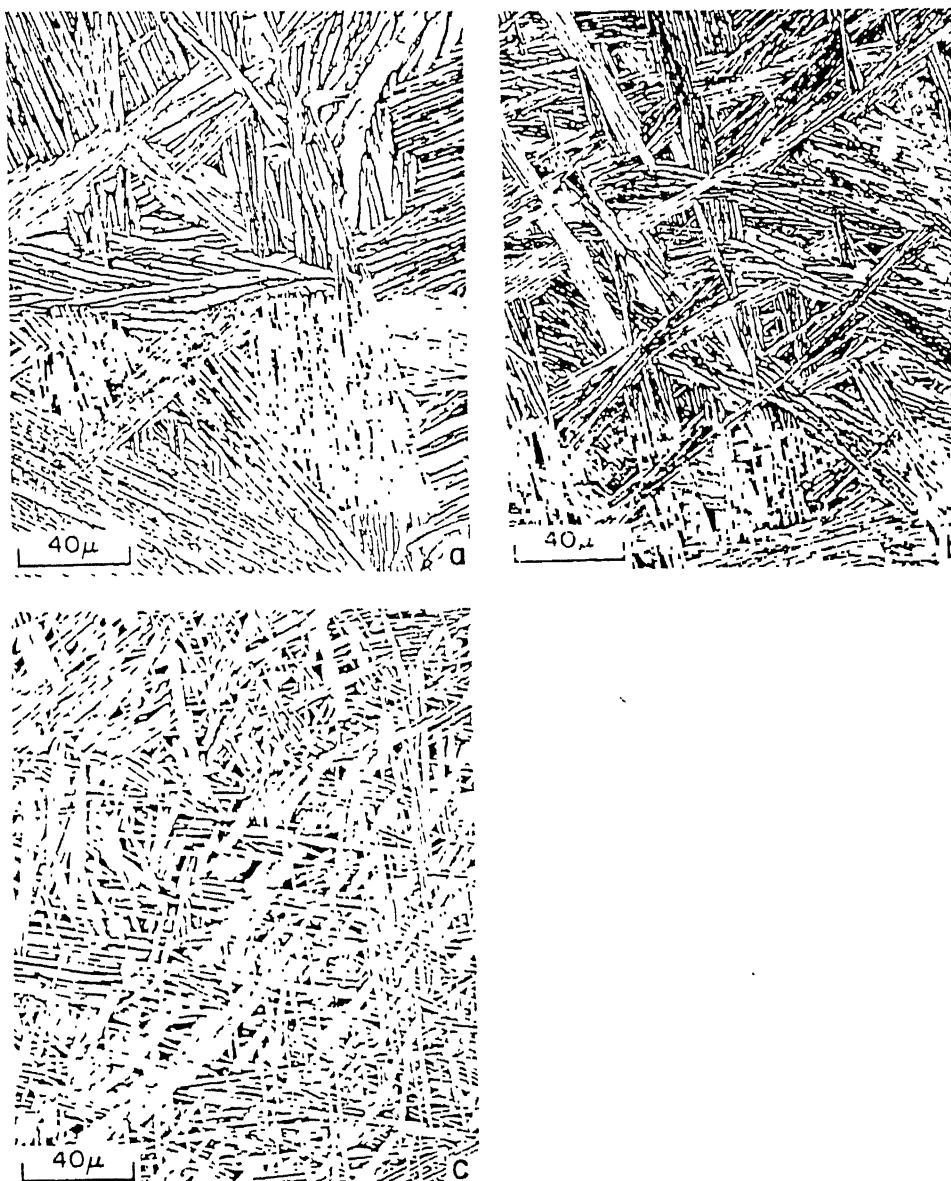


Fig. 2.4 Light Micrographs Illustrating Effect Of  $\beta$ -Stabilizing Alloying Elements On Size And Distribution Of  $\alpha$ -Phase Packets In  $\beta$ -Processed Materials:

- (a) Packets Which Contain Single  $\alpha$ -Phase Variant , Are Large In Ti-6-4.
- (b) Single Variant Packets Are Smaller In Ti-6-6-2.
- (c) Packets Are Smallest In Ti-6-4-2-6.



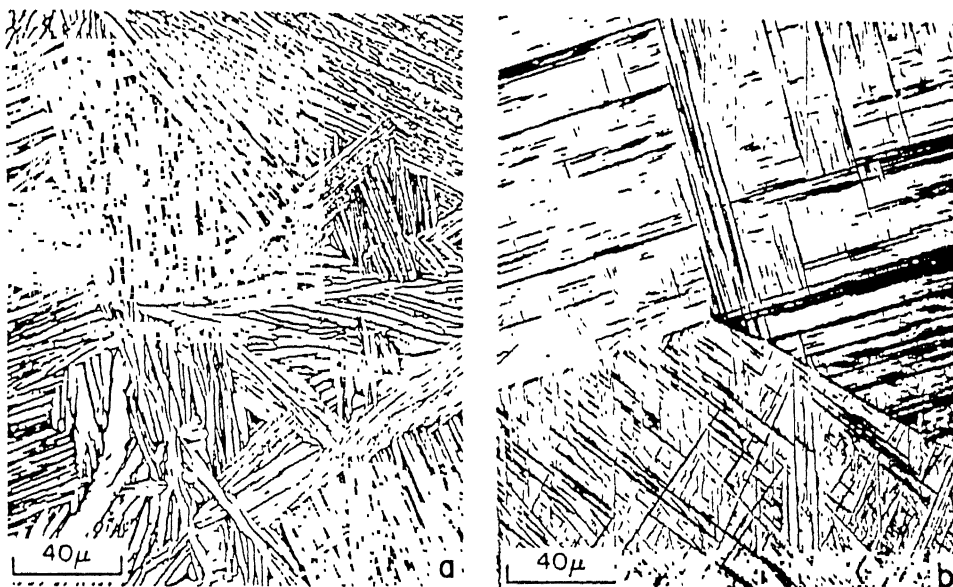


Fig. 2.5 Light Micrographs Illustrating Effect Of Processing On Microstructure:  
 (a) Forged In  $\beta$ -Phase Field And Air cooled.  
 (b) Quenched From  $\beta$ -Phase Field.

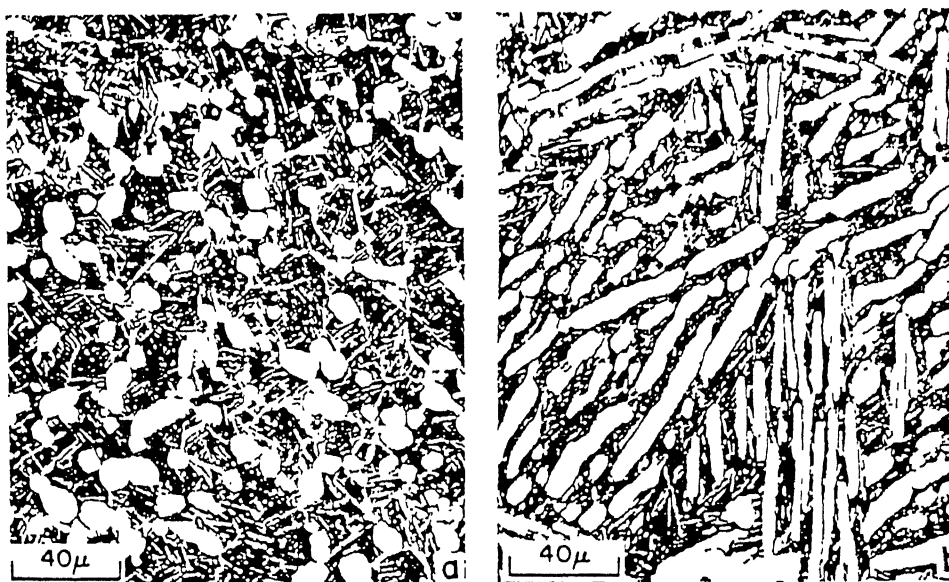


Fig. 2.6 Light Micrographs Demonstrating Dependence Of Primary  $\alpha$  Morphology On Forging Treatment:  
 (a) Equiaxed Primary  $\alpha$  Resulting From Extensive Hot Working.  
 (b) Elongated Primary  $\alpha$  Resulting From Light Hot Working.

working along with formation of sub-boundaries and shear bands, the misorientation of which increases with increasing degree of working [13]. Higher degree of working leads to fracturing of lamellae into small aspect ratio alpha grains [40] (Figure 2.6). Subsequent break-up to equiaxed morphology occurs during annealing when the beta phase penetrates across the lamellar width along the sub-boundaries or shear bands [41]. Nature of the starting microstructure characterized by lamellae width therefore affects the evolution of microstructures [40]. Other variables like strain [40], strain rate [38], temperature [41], number of passes [42] determine amount of stored energy for static recovery and recrystallization processes which also play an important role in evolution of microstructure during annealing. Kinetics of the dynamic softening mechanisms operative which determine the amount of stored energy is governed by these variables. Alpha-beta alloys soften by dynamic recovery and recrystallization as seen by the nature of the stress strain curve and electron microscopy observations [42].

Hot working can be done by either forging or rolling but the latter is preferred since it leads to alignment of grains along preferred orientations which can be made use of to get better tensile properties along certain directions.

Deformation in the  $\beta$ -phase field offers well known technological advantages. In addition, microstructural requirements can be met by properly controlling variables related to deformation and recrystallization. It is well known that dynamic recovery is the dominant softening mechanism in the deformation of  $\beta$ -phase [42] which manifests itself with the development of a highly recovered substructure from the initial  $\beta$  grains. An advantage  $\beta$  processing is that at the higher temperature at which it takes place, the silicon [in Silicon bearing alloys] can be retained in solid solution during the operation, thereby leading to a product with improved creep strength [43]. On the other hand high temperatures associated may result in (i) a large  $\beta$  grain size, (ii) coarse Widmanstatten structure on cooling to room temperature.

#### 2.4.4 Thermomechanical Processing

The properties of  $\alpha+\beta$  alloys are strongly dependent on microstructure. Thermomechanical processing is the most effective method to modify the  $\alpha+\beta$  morphology [13]. Changes in  $\alpha$  morphology from lamellar to equiaxed one are direct result of amount of prior deformation, working temperature and mode of deformation applied followed by annealing temperature and time. Chen and colleagues, for examples, have devoted considerable attention to the relationship between the microstructure and mechanical properties of Ti-6Al-2Sn-4Zr-2Mo-0.1Si forgings. Previous section have briefly indicated the characteristics of  $\alpha+\beta$  and  $\beta$  deformation factors that might be taken into consideration in the design of processing operations in general are -

- (1) The starting microstructure
- (2) The start and finish temperatures
- (3) The extent of deformation and,
- (4) The rate of which the deformation takes place. In achieving the desired final microstructure, hence mechanical properties, two more thermal variables are available for control and adjustment.
  - (i) the cooling rate from the final working operation, and
  - (ii) the final heat treatment.

This entire sequence of operations is known as thermomechanical processing [44]

#### 2.5 TEXTURES IN $\alpha+\beta$ ALLOYS

Ti alloys show strong textures which produce pronounced anisotropies in mechanical properties primarily due to lower crystallographic symmetry of hcp  $\alpha$ Ti. By proper control of deformation variables texture as a means of strengthening can be utilized to fabricate components having higher strengths along particular directions.

Intense textures are found in the Ti6Al4V alloy especially if the material was heavily deformed in the  $(\alpha+\beta)$  phase field. Quite different textures are observed depending on

deformation mode and on deformation temperature [44,45]. The most prominent textures are the Basal Texture (Figure 2.7(a)), where the basal planes are parallel to the rolling plane and which is achieved by cross-rolling at low temperature [46]. When sheets of Ti and its alloys have basal texture or texture close to it, then the material has isotropic properties in the plane of the sheet, characterized by high stampability [47]. Rolling at high temperature produces a texture, where the basal planes are perpendicular to the rolling plane and parallel to the RD (Transverse Texture) (Figure 2.7(b)). Further mixed textures having Basal as well as Transverse part are often observed (Figure 2.7(c)).

Table 2.6 gives the mechanical properties of textural Ti-Al-2Sn-4Zr-6Mo plate in different directions. Different factors that affect texture development are:

- i) Starting Microstructure [39]
- ii) Rolling Temperature [40]
- iii) Rolling Direction [34]
- iv) Reduction in Thickness [40]
- v) Heat Treatment [40]
- vi) Impurity Content [9]
- vii) Alloy Composition [40]

## 2.6 FORMING OF TITANIUM ALLOYS [48]

Titanium and titanium alloy sheet and plate are strain hardened by cold forming. This normally increases tensile and yield strengths, and causes a slight drop in ductility. Titanium metals exhibit a high degree of springback in cold forming. To overcome this characteristics, titanium must be extensively overformed or, as is done most frequently, hot sized after cold forming.

Hot forming does not greatly affect final properties. Forming at temperatures from 595 to 815°C (1100 to 1500°F) allows the material to slip more readily and simultaneously stress

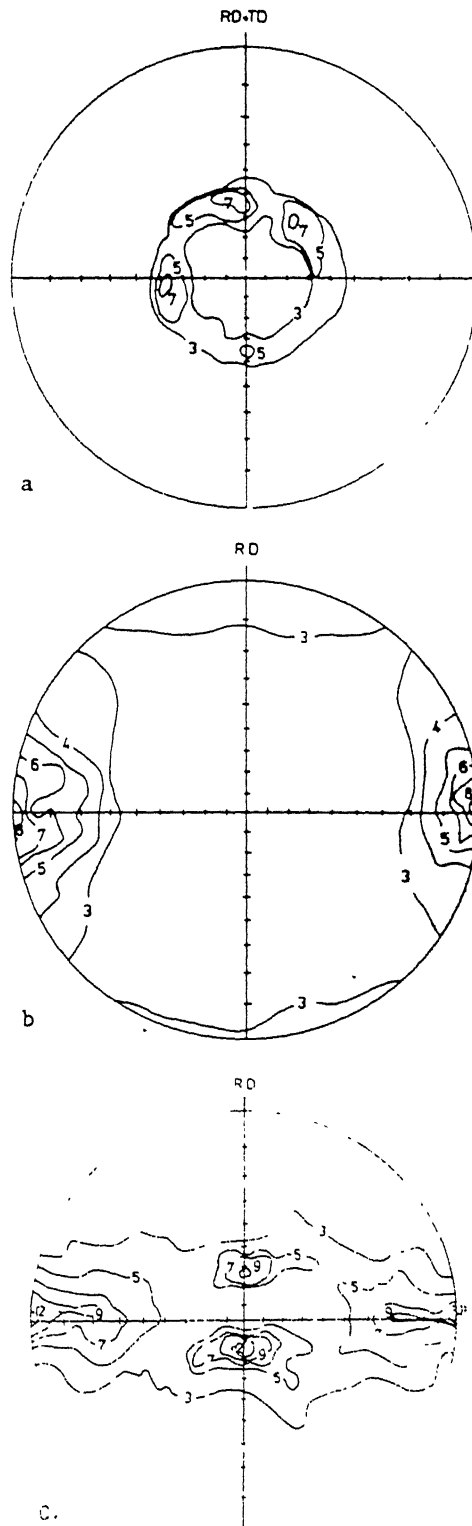


Fig. 2.7 Textures In  $(\alpha+\beta)$  Titanium Alloys.  
 (a) Basal Texture.  
 (b) Transverse Texture.  
 (c) Mixed (Basal+Transverse).

Table 2.5

Properties of Textured Ti Alloy Plate

Test direction (a)	Tensile Strength MPa	Yield Strength MPa	Elongation , %	Reduction in area, %	Elastic modulus GPa	K <sub>IC</sub>		K <sub>IC</sub> Specimen orientation (b)
						MPa <sup>m</sup> <sup>1/2</sup>	ksi.in <sup>1/2</sup> <sup>2</sup>	
L	1027	952	11.5	18.0	107	75	68	L-T
T	1358	1200	11.3	13.5	134	91	83	L-T
S	938	924	6.5	26.0	104	49	45	S-T
(a) High basal pole intensities reported in the transverse direction, 90° from normal, and also intensity nodes in positions. (b) 45° from the longitudinal (rolling) direction and about 40° from the plate normal. L = longitudinal, T = transverse								

relieves the deformed material; it also minimizes the degree of springback. The true net effect in any forming operation depends on total deformation and actual temperature during forming. Titanium metals also tend to creep at elevated temperature; holding under load at the forming temperature (creep forming) is another alternative for achieving the desired shape without having to compensate for extensive springback.

In all forming operations, titanium and its alloys are susceptible to the Bauschinger effect - a drop in compressive yield strength in one loading direction accompanied by an increase in tensile strength in another direction due to strain hardening. The Bauschinger effect is most pronounced at room temperature: plastic deformation (1 to 5% tensile elongation) at room temperature always introduces a significant loss in compressive yield strength, regardless of the initial heat treatment or strength of the alloys. At 2% tensile strain, for instance, the compressive yield strengths of Ti-4Al-3Mo-1V and Ti-6Al-4V drop to less than half the values for solution-treated material. Increasing the temperature reduces the Bauschinger effect; subsequent full thermal stress relieving completely removes it.

Temperatures as low as the aging temperature will remove most of the Bauschinger effect in solution-treated titanium alloys. Heating or plastic deformation at temperatures above the normal aging temperature for solution-treated Ti-6Al-4V will cause overaging to occur and, as a result, all mechanical properties will decrease.

Various methods of forming of ( $\alpha + \beta$ ) alloys include :

1. Press Brake Forming
2. Deep Drawing
3. Superplastic forming
4. Rubber Pad Forming
5. Stretch forming
6. Roll forming
7. Creep forming
8. Vacuum forming
9. Drop Hammer Forming

However, of the above methods superplastic forming is replacing all other conventional methods for it offers unique advantages which are discussed in the next section.

## 2.7 SUPERPLASTIC FORMING OF TITANIUM ALLOYS

Superplastic forming has emerged as a viable manufacturing process over the past decade or so, and is now used to fabricate number of sheet metal components for a range of aerospace systems. More than 200 parts are in production for a number of aircraft and spacecraft vehicles. This process offers unique advantages over the conventional forming operations

1. Low flow stress
2. Reduced machining
3. No springback
4. Uniform metal flow
5. No resultant residual stresses
6. In general no cavitation
7. Formability of shapes not possible by any other approach.

While the alloy Ti6Al4V is quite superplastic as conventionally produced, there are desirable properties of other alloys which form a basis for interest in the superplasticity of those materials as well.

A number of titanium alloys, have been evaluated for superplastic behaviour and a summary of some of these alloys and their related superplastic properties are shown in Table 2.6.

### 2.7.1 Superplasticity

Superplasticity is the ability of certain materials, primarily metals to undergo usually large amounts of uniform plastic deformation before local necking occurs. The remarkable formability of superplastic materials is due to their high strain rate sensitivity, defined by:

$$m = (d \ln \sigma) / (d \ln \dot{\epsilon}) \quad (1) \text{ where } \sigma = \text{true stress and } \dot{\epsilon} = \text{strain rate.}$$



**Table 2.6**

Alloy	Test. Temp. (°C)	Strain Rate (Sec <sup>-1</sup> )	m	Elongation (%)
Ti-6Al-4V	840-870	$1.3 \times 10^{-4} - 10^{-3}$	0.75	750-1170
Ti-6Al-5V	850	$8 \times 10^{-4}$	0.7	700-1100
Ti-6Al-2Sn- 4Zr-2Mo	900	$2 \times 10^{-4}$	0.67	538
Ti-4.5Al-5Mo- 1.5Cr	571	$2 \times 10^{-4}$	0.63 - 0.81	> 510
Ti-6Al-4V-2Ni	815	$2 \times 10^{-4}$	0.85	720
Ti-5Al-4V-2Co	515	$2 \times 10^{-4}$	0.53	670
Ti-15V-3Cr- 3Sn-3Al	515	$2 \times 10^{-4}$	0.54	650
Ti-5Al-2.5Sn	1000	$2 \times 10^{-4}$	0.49	420
Ti-15V-3Cr- 3Sn-3Al	515	$2 \times 10^{-4}$	0.5	229
Ti-13Cr-11V- 3Al	800	-	-	< 150
Ti-5Mn	750	-	0.43	150
Ti-15Mo	800	-	0.6	100
C.M.Ti	850	$1.7 \times 10^{-4}$	-	115

It is generally accepted that material with  $m$  values of 0.5 or higher can be superplastically deformed. The value of strain rate sensitivity index -  $m$  is the primary material parameter indicating the ability of a material to resist plastic instability or necking. The value of  $m$ , however, changes both with a change in formability parameters as well as during the forming operation itself. Thus,  $m$  must be determined as a function of strain, strain rate, temperature and microstructure.

### 2.7.2 Metallurgical Variables

Several metallurgical variables have been shown to affect the superplasticity in titanium alloys.

#### (a) Grain Size

In all superplastic materials, grain size is one of the single most important parameters. Grain size is known to strongly influence the superplasticity of Ti6Al4V alloy [49] and an example is presented in Figure 2.8. As is typically found for most superplastic materials, increasing grain size increases the flow stress and tends to reduce the maximum  $m$  value as well as reducing the strain rate at which maximum  $m$  is observed.

#### (b) Grain Growth Kinetics

Grain growth kinetics affect the superplastic flow in direct relation to the grain size developed. In a systematic study of grain growth effects on Ti6Al4V, Ghosh and Hamillon [49] showed that flow hardening observed during constant strain rate superplastic flow was a direct result of grain growth. In addition it was observed that a superimposed deformation caused an acceleration in the grain growth and that the higher the strain rate, the greater the growth rate.

#### (c) Grain Aspect Ratio

Due to the mechanism of superplasticity, i.e. grain rotation and migration, an equiaxed

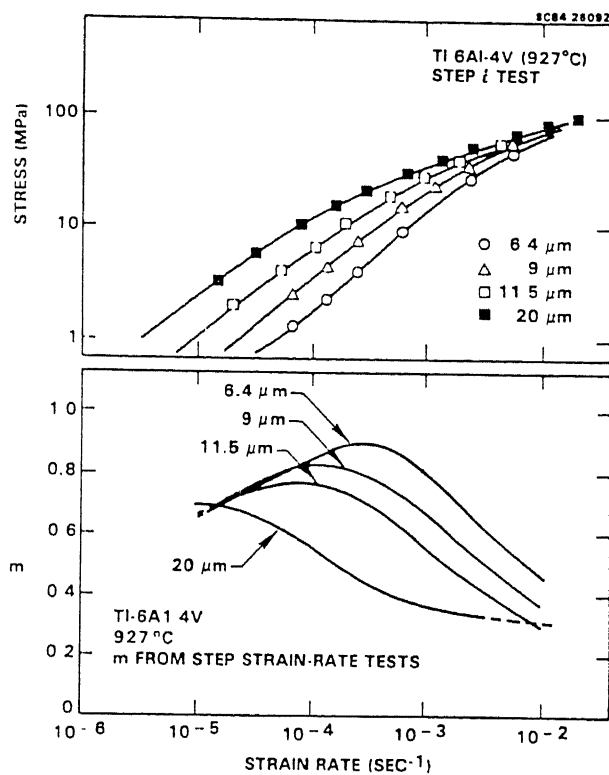


Fig. 2.8

Effect Of Average Grain Size On The Flow Stress And Strain Rate Sensitivity (m) For Ti-6Al-4V At 1200 °K.

structure is preferable for superplastic forming. Thus grain shape, characterized by grain aspect ratio defined as the ratio of the interphase spacing along the major axis, is also a microstructural variable to be considered. Grain aspect ratio close to 1.0 are clearly favoured for optimum superplasticity [50]. Acicular  $\alpha$ , Blocky lamellar  $\alpha$  are detrimental for superplastic deformation, because they make grain boundary sliding very difficult.

#### (d) Texture

A systematic study conducted in the Soviet Union [51] revealed that strongly textured Ti-6Al-5V alloy exhibited significantly higher total elongations than did the weakly textured material particularly for the intermediate temperatures. This effect is illustrated in Fig. 2.9 which shows the pole figures for the alloy evaluated and the total elongation measured in the rolling direction. As much as 200% elongation difference is seen between the two materials. The difference in this behaviour was more pronounced at tensile test directions along the rolling directions and at 45° to the rolling direction, but no noticeable difference was observed normal to the rolling direction.

#### (e) Phase Ratio

In the ( $\alpha + \beta$ ) alloys, the concentration of the  $\beta$  - phase generally increases with temperature until the beta transus temperature is reached, and therefore the phase ratio can change with temperature as well as alloy composition. An example of the variation of  $\alpha$  content with temperature is shown in Fig. 2.10 for three titanium alloys. That such a change might affect the superplasticity was indicated in Figure 2.11 [52] in which the flow stress and strain rate sensitivity were observed to undergo minima and maxima respectively at about 900°C, at which the  $\alpha$  content was also intermediate at about 65%.

#### (f) Diffusivity

It is widely accepted that diffusion is an important process in the superplastic flow of fine grained alloys including the titanium alloys as well. The best indication of this factor is usually the activation energy, which is determined from the change in strain rate with changes in temperature as shown :

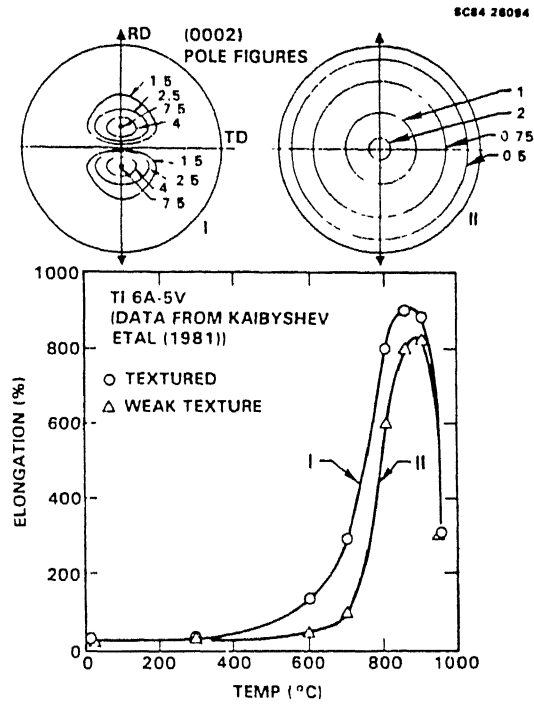


Fig. 2.9 Effect Of Texture On Total Elongation For Ti-6Al-4V.

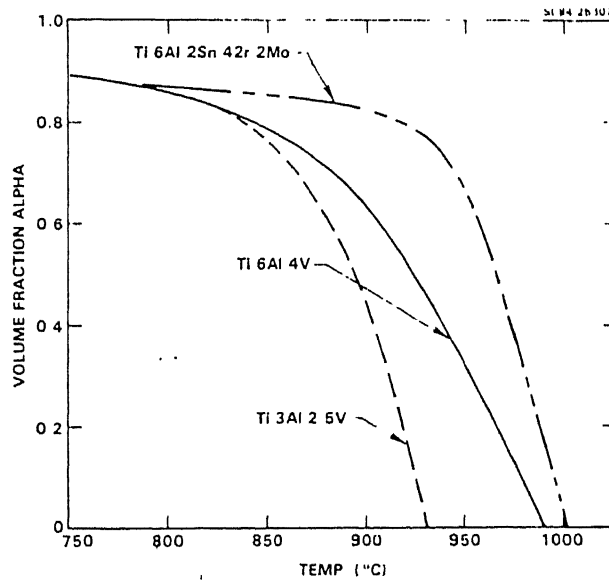


Fig. 2.10 Variation Of  $\alpha$  Volume Fraction With Temperature For Three Ti Alloys.

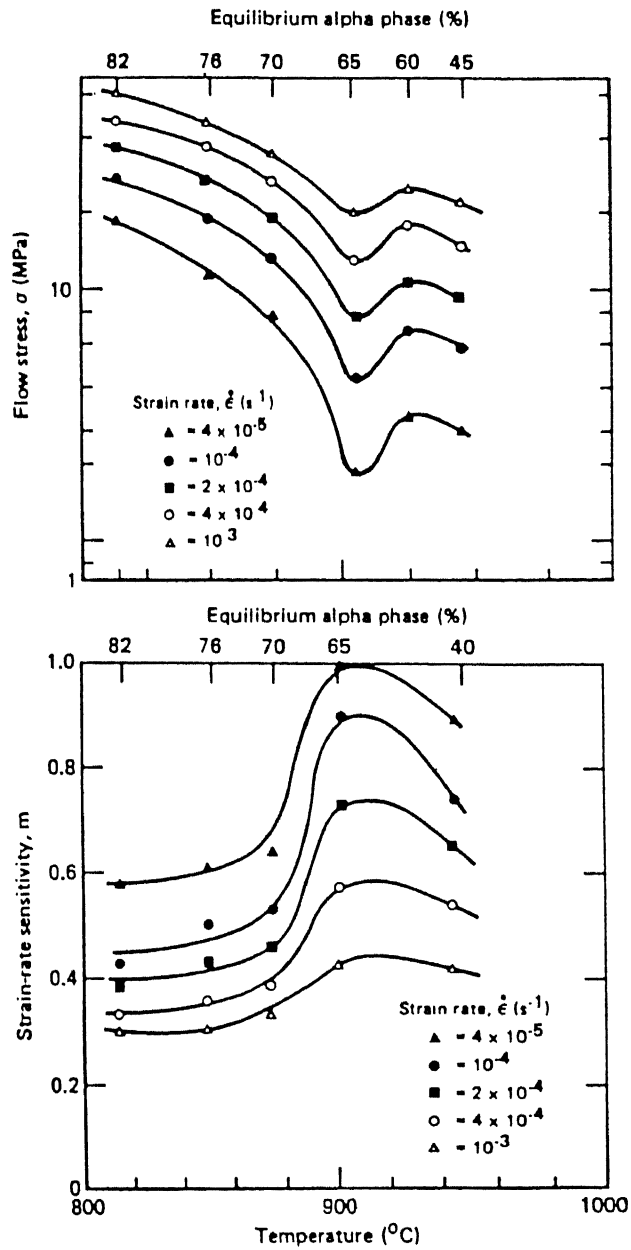


Fig. 2.11 Flow Stress And 'm' As Functions Of Temperature And  $\alpha$  Phase Content For Ti-6Al-4V.

$$Q = [\partial \ln \dot{\epsilon}] / [\partial (-1/RT)]$$

where  $\dot{\epsilon}$  = strain rate, R = gas constant and T = absolute temperature.

There are limited studies reported in which the activation energy has been specifically determined for the titanium alloys, but as summary of such existing data [53,54,55] has been presented in Table 2.7. Also presented for comparison are recent values of the activation energy of  $\alpha$  and  $\beta$  phases. As can be seen from the table, the activation energies determined from superplastic data are consistently higher than those for selfdiffusion. The activation energy for the grain boundary diffusion should be lower yet. It is suggested that the reason that the activation energy is high due to the fact that the microstructure is not constant with the change in temperature as would normally be assumed. And changes as indicated in Figure 2.10.

#### (g) Alloy Composition

Studies on Ti6Al4V [50] have indicated that lower flow stresses and somewhat higher on values were developed by the extra-low interstitial (ELI) grade alloy than by the regular grade alloy, even though the ELI grade material had a somewhat larger grain size. Super temperature can be reduced by adding  $\beta$  stabilizing etc. like Mo, Cr, V etc. in two phase alloys.

#### (h) Temperature

Temperature is a fundamentally important forming parameter for superplasticity, which generally occurs above about 0.5  $T_m$ , where  $T_m$  is the melting point. Depending on the alloy and temperature,  $\alpha$ ,  $\beta$  or  $\alpha+\beta$  phases more exist. This is important because the flow properties of the phases are different and the  $\beta$  phase has a self-diffusivity two orders of magnitude higher than the  $\alpha$ -phase. Changes in elongation with temperature are shown in Fig. 2.12 [51] for fine grained Ti6Al5V. There is a limited temperature range over which superplastic ductility is observed.

Table 2.7

Activation Energies for Superplastic Deformation and Self-diffusion in Titanium Alloys

Alloy	Temperature Range (°C)	Q (Kcal/Mole)
Ti-5Al-2.5Sn	800-950	50-65
Ti-6Al-4V	800-950	45
Ti-6Al-4V	850-910	45-99
Ti-6Al-4V	815-927	45-52
Ti-6Al-2Sn-4Zn-2Mo	843-900	38
Self Diffusion	$\alpha$ -phase	40.4
Self Diffusion	$\beta$ -phase	36.5
Self Diffusion	$\beta$ -phase	31.3



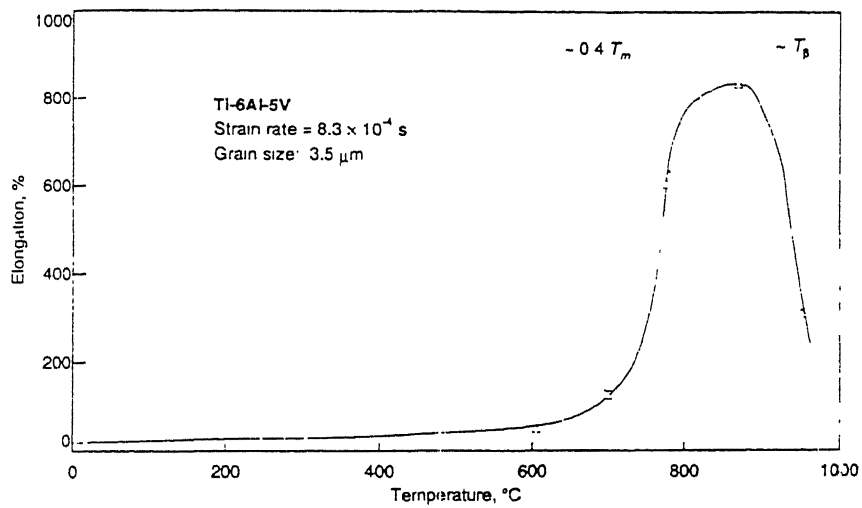
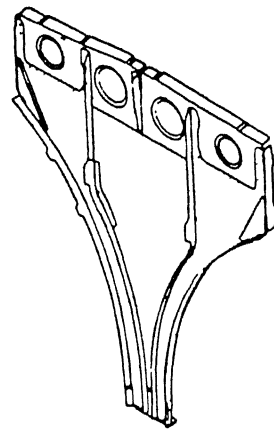


Fig. 2.12 Elongation vs Temperature Of Ti-6Al-5V.

### 2.7.3 Applications of Superplastic Forming

Superplastic forming of titanium alloys has been widely used by the aerospace industry. A well known example of superplastic forming carried out at Rockwell International using a Ti6Al4V alloy is shown in Fig. [2.13]. The component shown is a nacelle centre beam frame (A number of such parts formed a proposed structure of B-1 aircraft). Superplastically formed Ti6Al4V is also used for service doors and panels for airbus aircraft , missile fins , turbofan blades and turbine discs . The lower deck structure of an anionics compartment illustrates the potential application of SPF technology as shown in Fig. 2.14. The conventional fabrication method involves 48 details, 134 tools, and 1009 fasteners, while with SPF technology, the same part can be fabricated with only nine details, requiring eight tools and no fasteners. Other aerospace applications include applications like : beads, sinewares, small bend radii, return flanges with joggles, compound contours, deep formed pockets and multiple hollow parts. Typical engine nacelle frame, ancillary power unit (APU) door, centre caps, windshields, hot airblast nozzles, fairleads for the pressure bulkhead of the Airbus A320 , titanium wheel hubs for high performance passenger cars etc.



**12 DETAILS  
81 FASTENERS**



**ONE PIECE  
SPF/DB**

**COST SAVINGS - 43.5%  
WEIGHT SAVINGS - 40%**

Fig. 2.13 Superplastically Formed Nacelle Frame Showing Savings Potential.

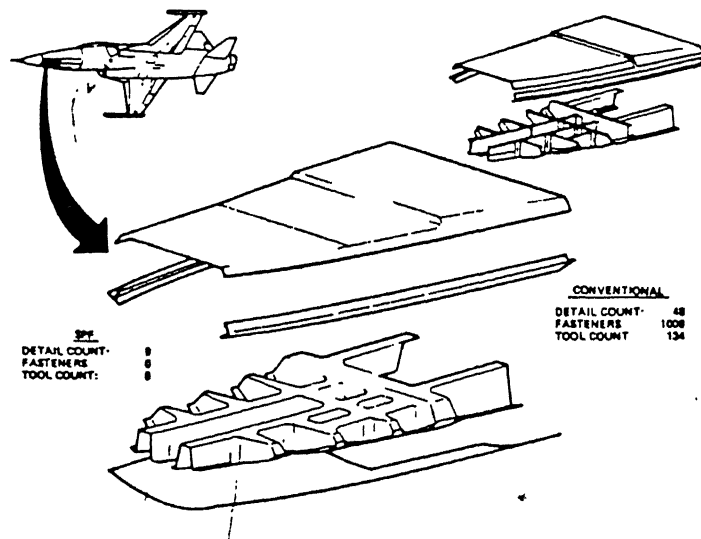


Fig. 2.14 Potential Superplastic Forming Applications In The Avionics Compartment.

## CHAPTER 3

### EXPERIMENTAL PROCEDURE

#### 3.1 STARTING MATERIAL

Ti-6.5Al-3.2Mo-1.8Zr-0.3Si alloy (hence after referred to as Ti-632Si alloy) used in this study was supplied by Mishra Dhatu Nigam Ltd., Hyderabad. The supplied material was in the form of forged bar of square cross-section of 100 x 100 mm<sup>2</sup>. These bars were produced from an ingot which was made from titanium sponge and other masteralloys by the vacuum melting of consumable electrode in the vacuum arc remelting (VAR) furnaces. Double melting method for preparing the ingot was followed. Ingots then produced were surface machined and were substantially forged above the  $\beta$  transus temperature on a hydraulic press of 1500 T capacity. Microstructure of the as received alloy is shown in Figure 3.1. Chemical composition of the supplied material has been shown in Table 3.1

Table 3.1

Alloying Element	Al	Zr	Mo	Si	Fe	O	H	C	N
Amount (wt%)	6.05	1.94	3.44	0.23	0.155	574	21	0.014	12

#### 3.2 THERMOMECHANICAL PROCESSING

Thermomechanical processing done in the present investigation involved homogenizing, hot rolling with or without intermediate annealing treatments.

The coupons for homogenizing or hot rolling were subjected to protective coating with some organic material known as Delta Glaze for prevention of oxygen diffusion.

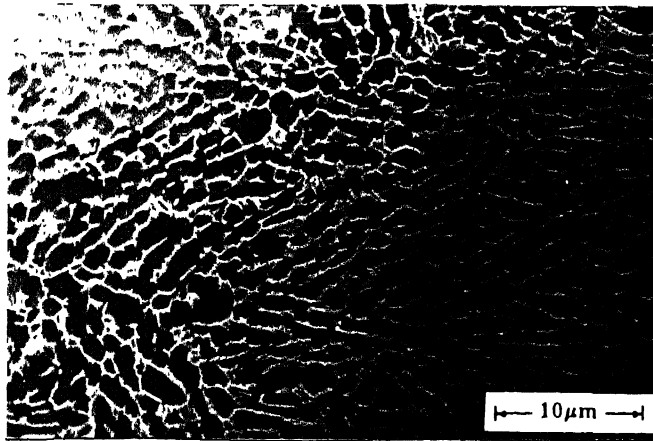


Fig. 3.1      Microstructure of the alloy in the as received condition

### 3.2.1 Equipments for Thermomechanical Processing:

Heating and soaking of the coupons was done in a specially designed high temperature furnace kept very close to the rolling mill. The design of the furnace was done such that it was capable of maintaining protective atmosphere. All the thermal treatments were done under a continuous flow of argon atmosphere. The furnace was having a constant temperature zone of 1500 in length and was heated by silicon carbide rods muffle of the furnace consisted of an inconel tube and was closed from one end. Gas was introduced into the furnace through a 4 mm internal diameter stainless steel tube passing through the closed end of the chamber. The furnace was mounted on wheels so as to bring it very close to the rolling mill.

Hot rolling required was done on a 2 high rolling mill which had 135 mm diameter of the rolls. Speed of rotation for hot rolling mill was kept at 55 rpm in all the experiments. No prior heating of rolls was done before hot rolling of the specimen and they were maintained at room temperature.

Prior to the thermal treatment or hot rolling, the samples were placed on a perforated inconel tray and then pushed carefully into the hot zone of the furnace.

Hot rolling was either single pass or multipass. For hot rolling, the samples were drain out and quickly fed to the feeding end of the rolling mill. There was a very little drop in temperature till the time the sample could get rolled, which may be attributed to the thermally insulating effect of the dettaglaze coating or the quickness of the feeding process. Cooling was kept strictly unidirectional. After the homogenizing treatment or rolling, the samples were water quenched.

The surfaces of the rolled samples were ground and subjected to pickling in 10%  $\text{HNO}_3$  + 5% HF solution for nearly 4 hrs at 50°C to remove the  $\alpha$ -casing layer formed due to oxygen diffusion. These samples were further cleaned on belt grinding and emery polishing before being investigated further.

The final thickness of the sheets for superplastic testing were:

- a. 1 mm from 8 mm thickness raw material (for strain rate jump tests).
- b. 1.8 mm from 12 mm thickness raw material ( for elongation to failure tests).

### 3.2.2 Thermomechanical Processing Schedule

There different processing schedules were used for producing the strips. These processing schedules are shown schematically in Fig. 3.2 and in process sheet in Fig. 3.3

#### ROUTE 3

This was basically a optimization route of the process. Some important processing parameters were selected through this route for obvious reasons discussed later. Rolling in  $\beta$  phase field was single pass (60% reduction) while rolling in  $\alpha + \beta$  phase field was multipass with reduction of 15 % per pass total 60% reduction) (5 passes) the optimized flow sheet for samples by this route polished of  $\beta$  rolling at 1050°C, with 60% reduction, annealing of  $\beta$  phase at 1020°C for 30s, rolling in ( $\alpha + \beta$  phase field at 850°C then annealing at 850°C for 30 min. and 2 hrs. Other details are shown in the flow sheet. Superplastic testing samples were cut from following sheets

1. Rolled in ( $\alpha + \beta$ ) at 850°C followed by w/q.
2. Rolled in ( $\alpha + \beta$ ) at 850°C followed by W/Q and annealing at 800°C (0.5 hrs) followed by W/Q.
3. Rolled in ( $\alpha + \beta$ ) at 850°C followed by W/Q and annealing at 850°C (4 hrs) followed by W/Q.

#### Route 2:

In this route  $\beta$  phase rolling was done but no  $\beta$  phase annealing. The samples were then rolled at 850°C in  $\alpha + \beta$  phase field, with the parameters shown in flow sheet. Superplastic samples were cut from the samples rolled in ( $\alpha + \beta$ ) at 850°C followed by W/Q.

#### ROUTE 1

In this route, the raw material was only homogenized in  $\beta$  phase field at 1050°C ( followed by rolling in ( $\alpha + \beta$ ) phase field at 850°C. Superplastic samples were cut from the samples rolled in ( $\alpha + \beta$ ) at 850°C followed by W/Q. The details of this route are shown in the flow sheet.

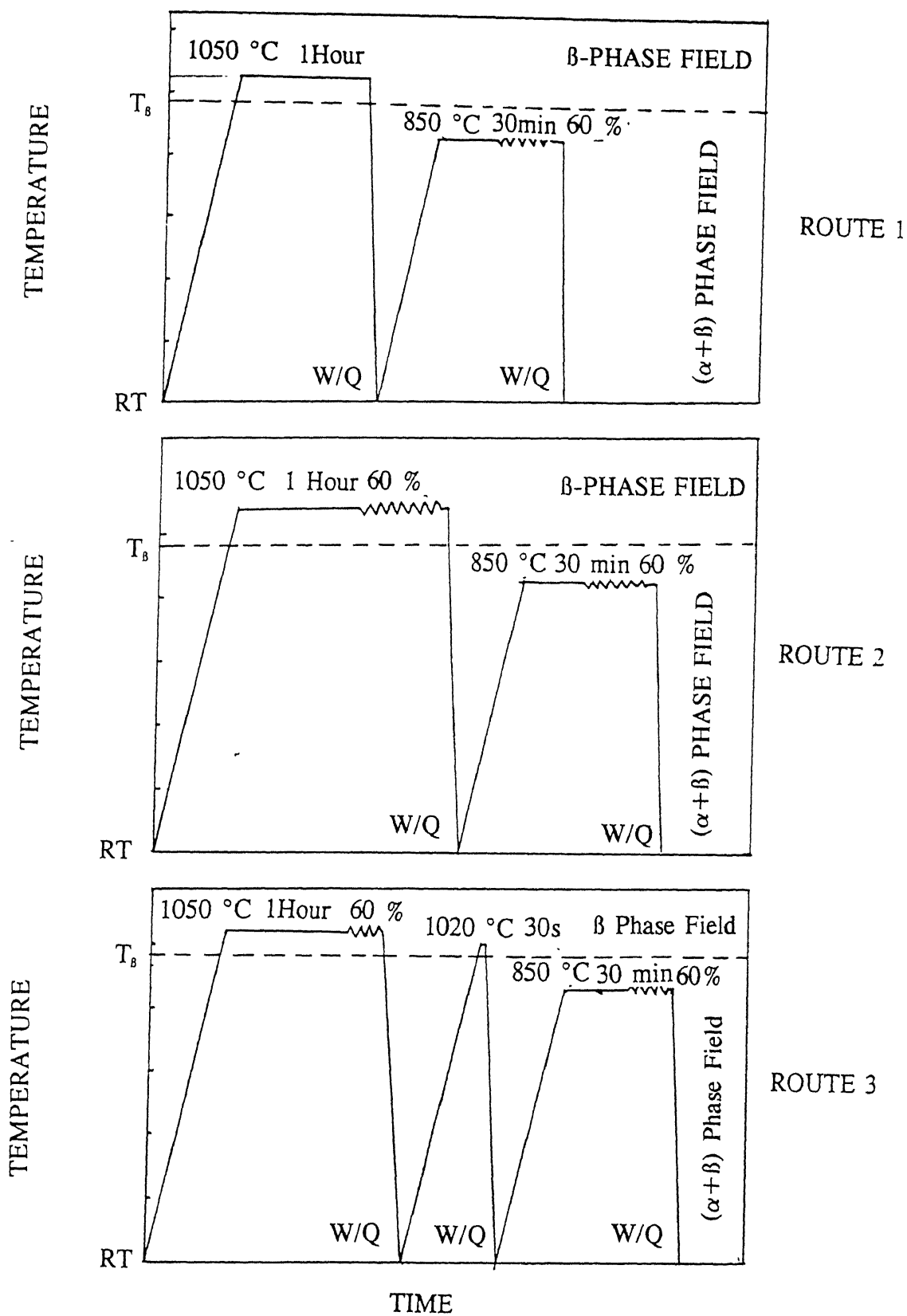


Fig. 3.2 Schemetic Representation Of The Thermomechanical Processes Studied.



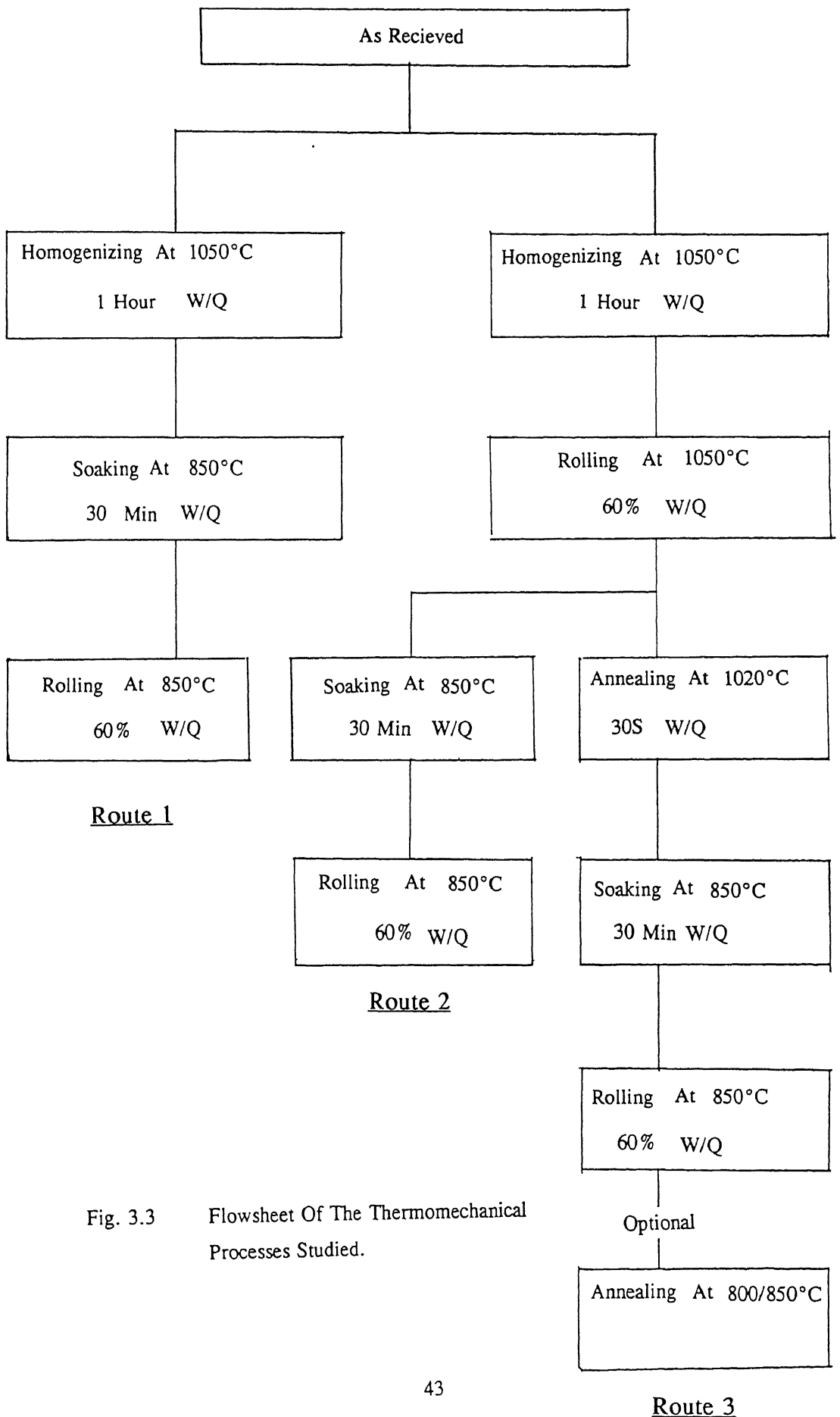


Fig. 3.3 Flowsheet Of The Thermomechanical Processes Studied.

### 3.3 CHARACTERIZATION TECHNIQUES

The characterization techniques used in the present investigation can be classified under three headings, Microstructural characterization, Structural characterization, and Mechanical Testing.

#### 3.3.1 Microstructural Characterization

Microstructures of the as processed specimens were examined by optical and scanning electron microscopy.

- a. Optical Microscopy : The  $\beta$  processed samples were subjected to micro-structural examination under a Leitz Wetzlar Optical Microscope. Prior to this the samples were polished on emery papers (0 to 4 grades) followed by wheel polishing with alumina powders of sizes 1  $\mu\text{m}$ , 0.3  $\mu\text{m}$  and 0.05  $\mu\text{m}$  respectively. The polished samples were etched with Kroll's Etchant (4% HF + 2% HNO<sub>3</sub>). Microstructural observations were, generally, done on longitudinal thickness section of the specimen.
- b. Scanning Electron Microscopy (SEM) : Most of the microstructural characterization in the present investigation was done with scanning electron microscope (JEOL-JSM 840A). For this, the samples were polished and etched as discussed in the section on optical microscopy. The polished and etched samples were observed under the scanning electron microscope operated at 10 KV using secondary electron radiation (SE mode).
- c. Quantitative Microscopy : For determining aspect ratios, length and thickness measurements were made for a number of samples. Aspect ratio which is a measure of shape can be defined as

$$f = l / t.$$

$l$  = length of individual particle.

$t$  = thickness of individual particle.

Average aspect ratio can be given as :

$$f(\text{ave.}) = (1/n) * \sum(l/t).$$

Grain size measurements were also made by measuring the diameters of the individual grains. The grain sizes obtained were average grain sizes.

In the metallographic cross-sections it was not possible to distinguish between width and thickness due to random sectioning of alpha plates. Hence the reported values of aspect ratios and grain sizes are all averages.

### 3.3.2 Structural Characterization:

Structural characterization done was basically X-ray characterization to detect the phases formed after quenching from different temperatures during processing. The processed samples were subjected to x-ray examination using normal bragg scan. Normal Bragg Scan was recorded from polished surface of the sheet plane of the specimens on a Seifert Deby X-ray Diffractometer operated at 30 KV using  $\text{CuK}_\alpha$  radiation and scanning speed was kept at 1.2 °/min in  $2\theta$ . The X-ray diffraction patterns obtained were indexed and identification of the phases was done by matching the 'd' values corresponding to each of the peak position of the diffraction pattern with 'd' values of all possible phases obtained from literature. In order to have a consistency, all the experiments were performed using a fixed beam dimension.

### 3.3.3 Mechanical Testing

#### a. Microhardness Testing.

Microhardness of the  $\beta$  processed samples were measured using the Leitz Miniload Microhardness Tester under a load of 25g. At least three indentations were made on each sample and the average value of microhardness was calculated.

#### b. Superplastic Testing:

Superplastic Testing of the processed sheets was done on the MTS machine model: 810.12 .

The furnace used had a heating rate of 800°C/1hr. The samples were homogenized for 15 min at the desired temperature before deformation starts.

Heating and deformation was carried out in air. The specimens used were machined and further ground, pickled and polished to remove the  $\alpha'$  casing formed due to oxygen diffusion. Two types of tests were carried on the polished samples at different temperatures

(i) **Strain Rate Jump Tests** : In this test the strain rate was increased in successive steps from  $10^{-4}/s$  to  $5.5 \times 10^{-1}/s$  (8 different strain rates were used) and the corresponding flow stress was measured. The samples used here had the following dimensions :

Grip length and width	=	23 mm, 18 mm
Gauge length	=	10 mm
Gauge width	=	5.5 mm
Gauge thickness	=	0.9 mm
Hole diameter	=	6.5 mm
Total length	=	61 mm

This testing was done at three different temperatures 850°C, 900°C and 925°C. Utmost care was taken to prevent necking of the sample throughout the testing history. From the stapes of the log-log plots of stress v/s strain rate, the value of strain rate sensitivity (m) was determined for a range of strain rates and temperatures.

ii. **Elongation t Failure Testing** : In this testing the samples were strained to failure under constant strain rate of  $5.5 \times 10^{-3}/s$  at 900°C and 925°C. The samples used here had the following dimensions:

Grip length	=	23 mm
Grip width	=	18 mm
Hole diameter	=	6.5 mm
Gauge length	=	6.5 mm
Gauge width	=	5 mm
Gauge thickness	=	1.8 mm
Total length	=	55 mm

After failure of the sample, the sample was allowed to furnace cool and then measured for its maximum elongation. The furnace cooled and deformed samples were cut into different sections and microscopically (SEM) examined.

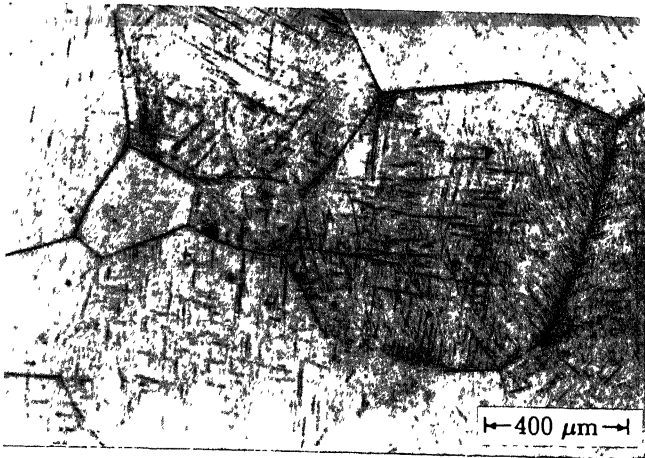
## Chapter 4

### RESULTS AND DISCUSSION

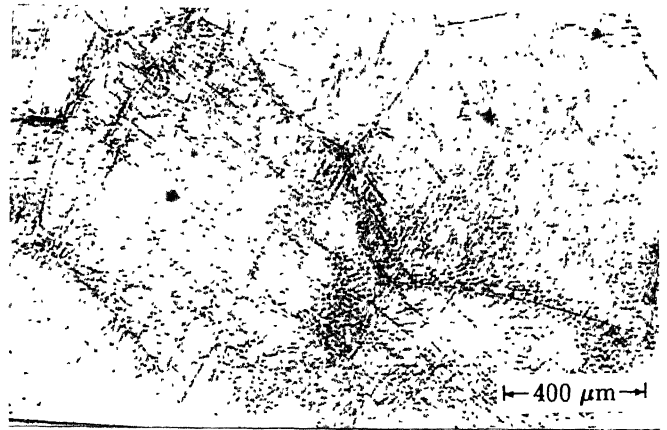
As discussed in Chapter 2, Ti-6.8Al-3.2Mo-1.8Zr-0.3Si (Ti-632Si) alloy belongs to the family of two-phase ( $\alpha+\beta$ ) titanium alloys with both  $\beta$  (bcc) as well as  $\alpha$  (hcp) phases stabilized at room temperature. Control of the  $\alpha$  phase morphology is vital if the alloy is to be subjected to superplastic forming. An equiaxed primary  $\alpha$  morphology with grain size  $< 10 - 15 \mu\text{m}$  is generally considered essential for such applications. Transformation of the lamellar or Widmanstätten primary  $\alpha$  morphology to an equiaxed primary  $\alpha$  morphology necessarily requires hot working of the material in the ( $\alpha+\beta$ ) phase field during which the lamellar  $\alpha$  structure breaks down and results into nearly-equiaxed  $\alpha$  structure either during working itself or during post-deformation recrystallization annealing.

The conventional thermo-mechanical processing of ( $\alpha+\beta$ ) titanium alloys, therefore, involves with forging/rolling/extrusion through the  $\beta$ -transus temperature of the alloy with a minimum specified reduction in the two-phase field. In general, the conventional processing is carried out by (a) giving  $> 30\%$  reduction at a temperature of at least  $50 - 60^\circ\text{C}$  below the  $\beta$ -transus temperature of the alloy and (b) post-deformation mill-annealing at a temperature lower than the hot-working temperature. Such a processing does transform the lamellar  $\alpha$  structure to the equiaxed  $\alpha$  structure with  $\alpha$  grain size varying generally between  $10-50 \mu\text{m}$ .

The  $\alpha$  grain size in the equiaxed structure, however, depends on the plate thickness of the lamellar structure which in turn, depends on the condition of  $\beta$  grains from which it transforms. The present work was undertaken to study the effect of thermo-mechanical processing parameters on (i) the conditioning of  $\beta$  grains and (ii) conditioning of lamellar  $\alpha$  prior to working in the ( $\alpha+\beta$ ) phase-field and influence on the superplastic behaviour of Ti-632Si alloy.



(a)



(b)

Fig. 4.1 Micrographs Showing The Martensitic Structure With Prior  $\beta$  Grain Boundaries After Solutionising And Quenching From different temperatures.  
(a) 1050 °C (b) 1150 °C.



Fig. 4.2 Micrograph Showing Martensitic Structure Consisting Of Partially Disordered Array Of Individual Platelets Of Acicular  $\alpha$  Martensite After Quenching From 1050 °C.

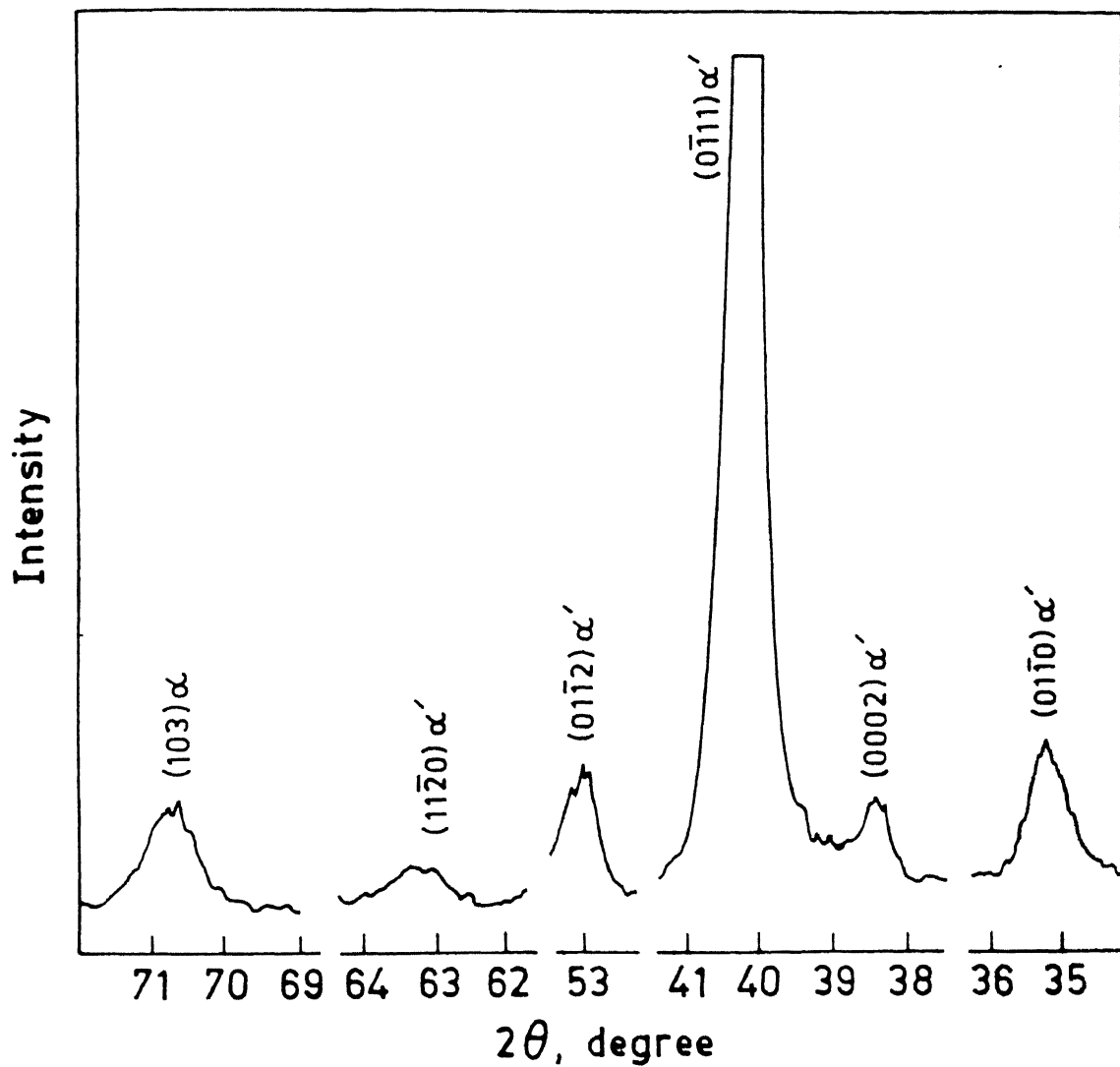


Fig. 4.3 X-Ray Diffraction Pattern For As Solutionised Sample Quenched From 1050 °C.

## 4.2 EFFECT OF THERMO-MECHANICAL PROCESSING VARIABLES ON CONDITIONING OF $\beta$ GRAINS OF Ti-632Si ALLOY

Details of processing variables employed for altering the condition of  $\beta$ -grains are given in Chapter 3. To summarize, the processing of Ti-632Si alloy consisted of the following three alternative approaches;

- i. Preserving coarse recrystallized  $\beta$  grains obtained by recrystallization annealing carried out at about 50°C above the  $\beta$ -transus temperature;
- ii. Obtaining pancaked unrecrystallized  $\beta$  grains of different size and aspect ratio by rolling the alloy for different thickness reductions in the single phase  $\beta$  field at temperatures of  $\sim$  50°C, 150°C and 250°C respectively above the  $\beta$ -transus temperature;
- iii. Obtaining fine recrystallized  $\beta$  grains by subjecting pancaked  $\beta$  grains by a recrystallization annealing treatment at a temperature of 10-20°C above the  $\beta$ -transus temperature;

and are schematically shown in Figures 4.4 and 4.5.

### 4.2.1 Effect of Recrystallization Temperature on $\beta$ Grain Size:

As shown in Figure 4.1, soaking of Ti-632Si alloy in the  $\beta$  phase field results in recrystallized equiaxed  $\beta$  grains. The figure also shows effect of soaking temperature on  $\beta$  grain size. It was observed that as the soaking temperature increased from 1050 °C to 1150 °C, the  $\beta$  grain size increased from 560  $\mu\text{m}$  to 760  $\mu\text{m}$ . It was thus seen that the grains of  $\beta$  in Ti-632Si alloy undergo a rapid grain growth when heated above the  $\beta$ -transus temperature. Such observations are also made for other ( $\alpha+\beta$ ) titanium alloys.

### 4.2.2 Effect of Rolling Temperature and Thickness Reduction on the Characteristics of $\beta$ Grains :

Through high-temperature stress-strain curves of Ti-632Si alloy for its deformation in the



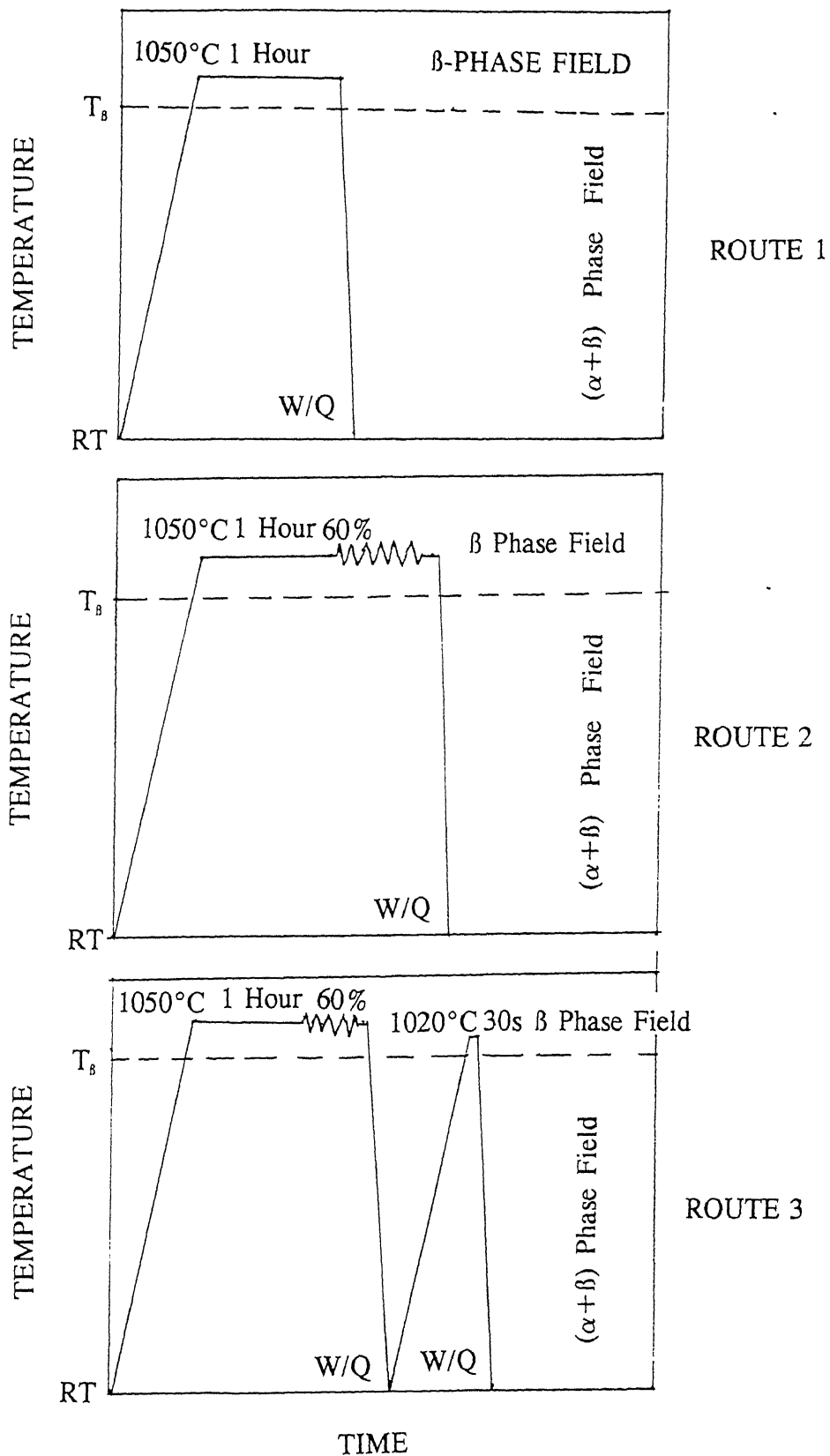


Fig. 4.4 Schematic Representation Of The  $\beta$ -Processes Studied.

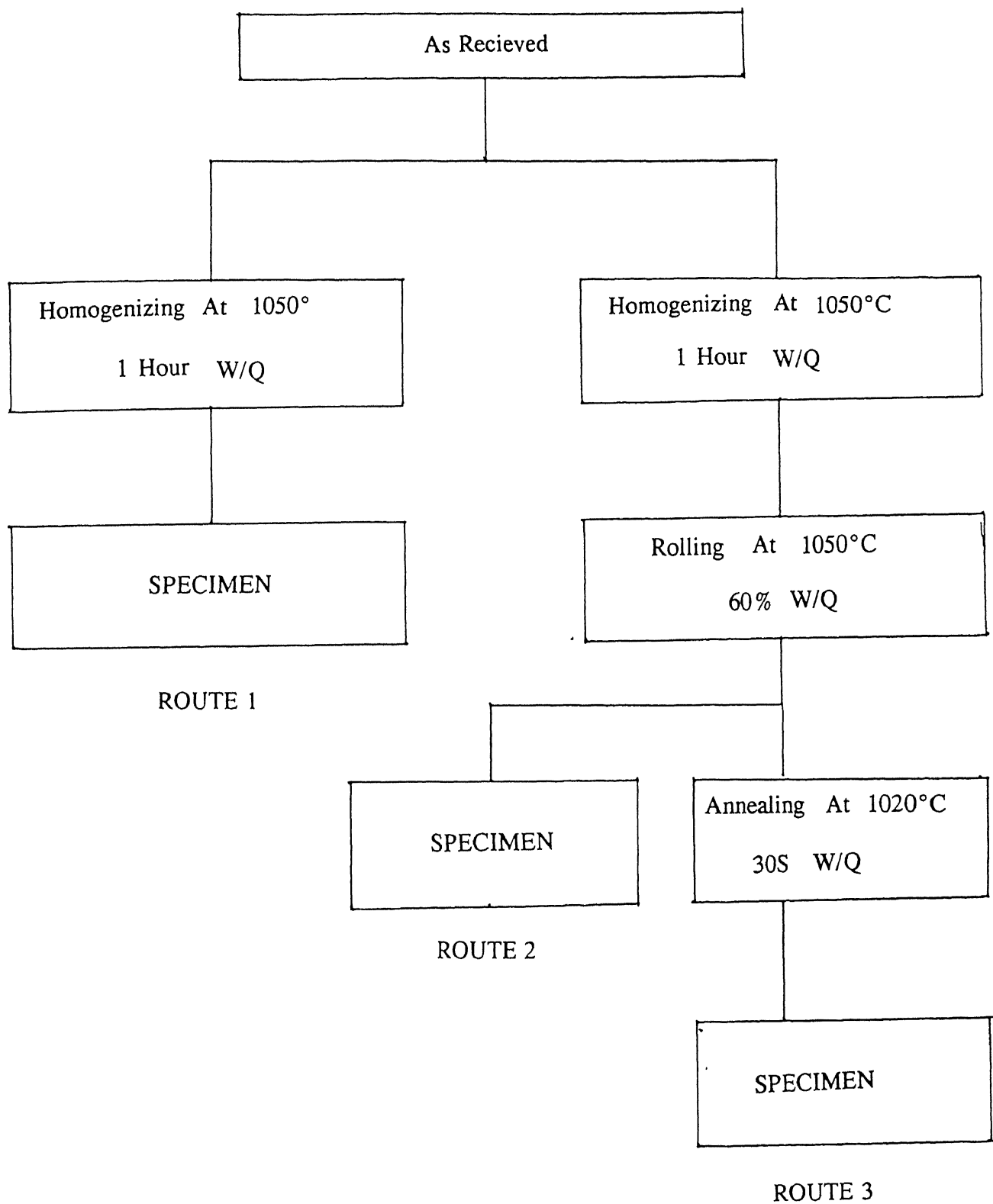
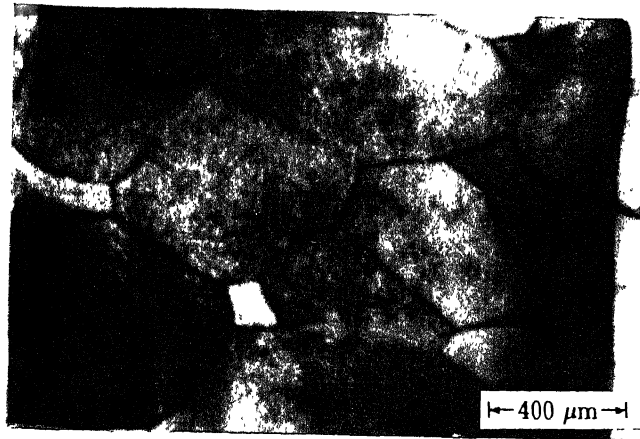


Fig. 4.5 Flowsheet Of The  $\beta$ -Processes Used.

$\beta$  phase field are not available in the open literature, such curves for Ti-6242Si, Ti-64Al-4V, Ti-4Al-4Mo-2Sn-0.5Si alloy clearly indicate that the  $\beta$  phase during its deformation does not undergo dynamic recrystallization upto about 150°C above the  $\beta$ -transus temperature. Microstructures of Ti-632Si alloy rolled at 1050°C and 1150°C respectively for 20 %, 40% and 60% thickness reduction are shown in Figures 4.6 - 4.7. Similar results were also obtained for strips rolled at 1250°C. Pancaked grains of  $\beta$  phase can be readily seen in all the cases which clearly indicate that like other ( $\alpha+\beta$ ) titanium alloys of its kind, Ti-632Si alloy also does not undergo dynamic recrystallization during its high-temperature deformation of strain rate of  $10^{-1} \text{ s}^{-1}$  which is typical of rolling conditions prevailing under the present study. The fact that the pancaked grains of  $\beta$  were observed in the material rolled at even 1250°C indicates that dynamic recrystallization does not occur in Ti-632Si alloy at a temperature as high as ~250°C above the  $\beta$ -transus temperature even after 60% thickness reduction. Variation in the aspect ratio of pancaked unrecrystallized  $\beta$  grains with % thickness reduction at the rolling temperature of 1050°C, 1150°C and 1250°C is shown in Figure 4.8. It is readily seen from these curves that the  $\beta$  grains became increasingly pancaked as the % thickness reduction increased at any given hot rolling temperature. The aspect ratio also increased by increasing the hot rolling temperature. The variation of aspect ratio with rolling temperature can be understood in terms of decreased flow stress of  $\beta$  phase with (a) increase in rolling temperature and (b) increase in grain size of  $\beta$  due to grain growth occurring in the material during its preheating.

A closer examination of pancaked  $\beta$  grains revealed that they often contained deformation bands comprising of hair-like structure and regions undergoing deformation by shear. The occurrence of such features increased with increase in thickness reduction and decrease in rolling temperature. Figure 4.9 shows the occurrence of such deformation features in samples rolled at 1050° by a thickness reduction of 60%. Such microstructural features are associated with unstable flow occurring in materials and the flow in  $\beta$  phase at a temperature of about 10-50°C above the  $\beta$ -transus temperature indeed indicates characteristics of unstable flow in ( $\alpha+\beta$ ) titanium alloys .

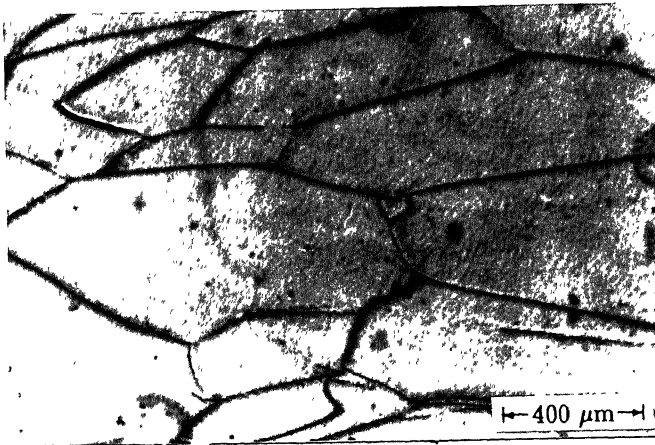
Another set of features associated with deformed  $\beta$ -grains was the occurrence of fine equiaxed grains in a few regions [Figure 4.10]. The fraction of such grains was, however, too



(a)



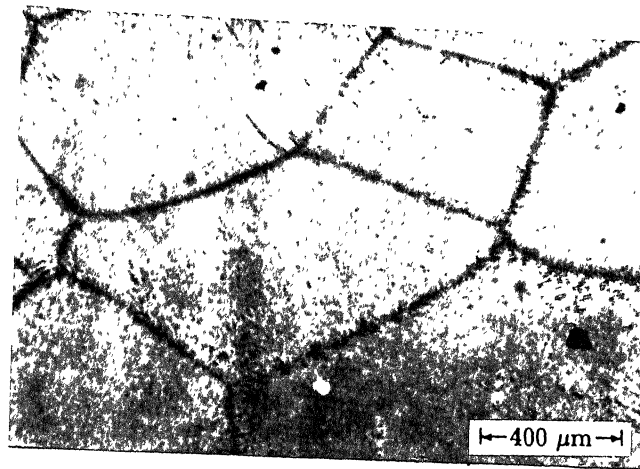
(b)



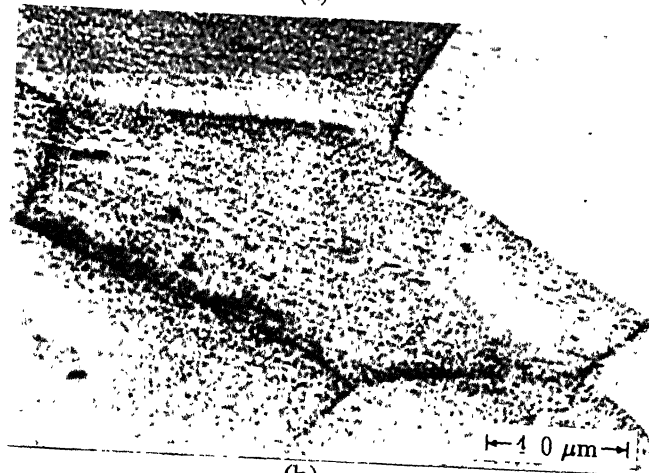
(c)

Fig. 4.6

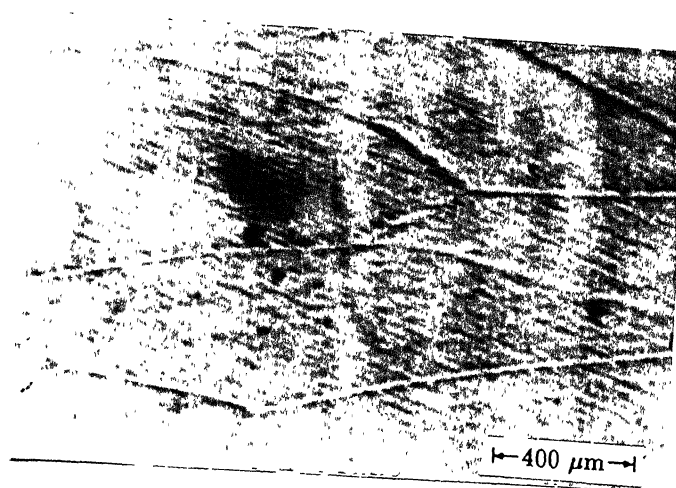
Microstructures Of Ti-632Si Rolled At 1050 °C , W/Q.  
(a) 20 %    (b) 40 %    (c) 60 %.



(a)



(b)



(c)

Fig. 4.7

Microstructures Of Ti-632Si Rolled At 1150 °C , W/Q.  
(a) 20 % (b) 40 % (c) 60 %.

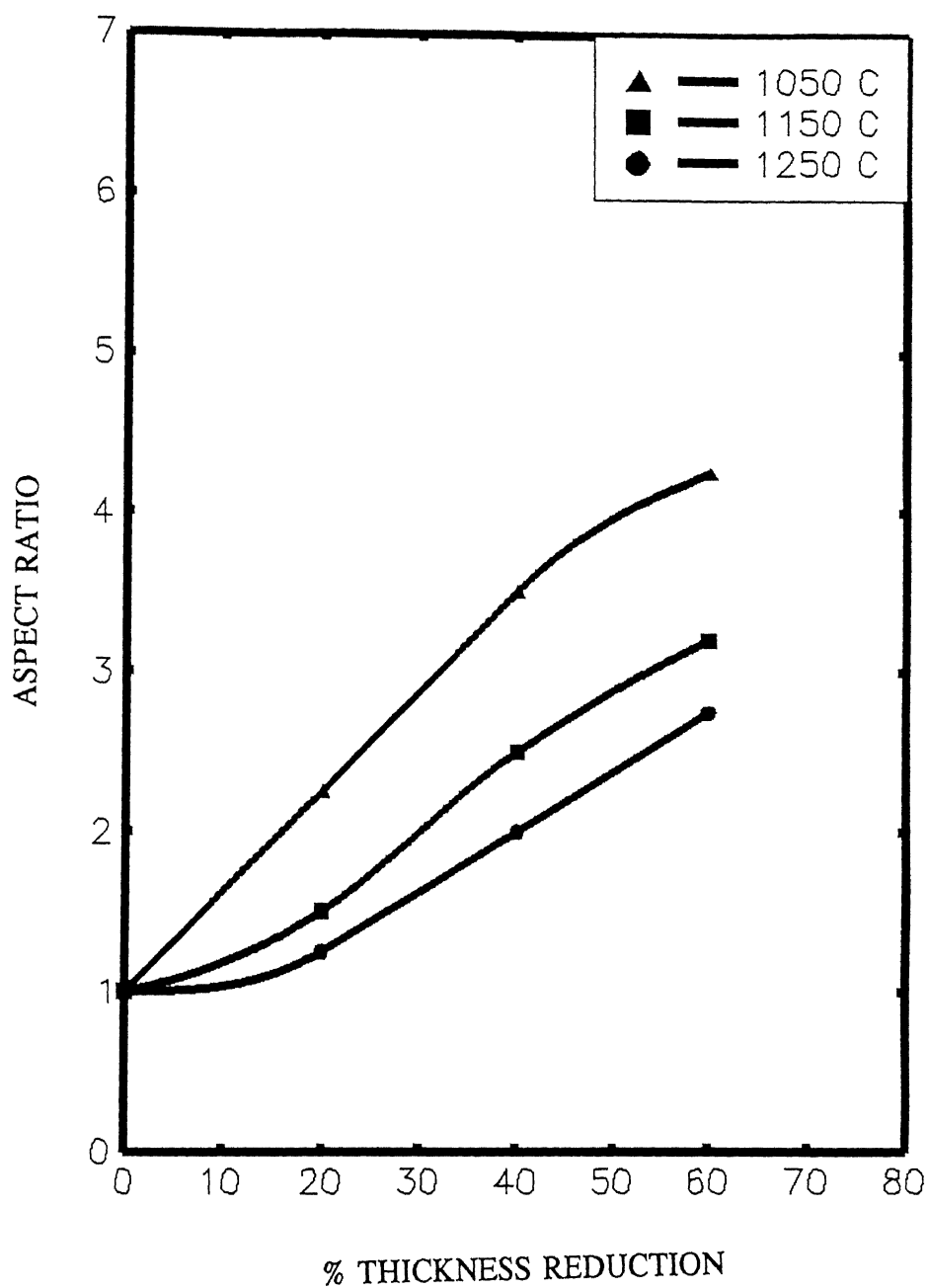


Fig. 4.8 Variation In The Aspect Ratio Of Pancaked Unrecrystallised  $\beta$  Grains With % Thickness Reduction At The Rolling Temperatures Of 1050 °C, 1150 °C and 1250 °C.

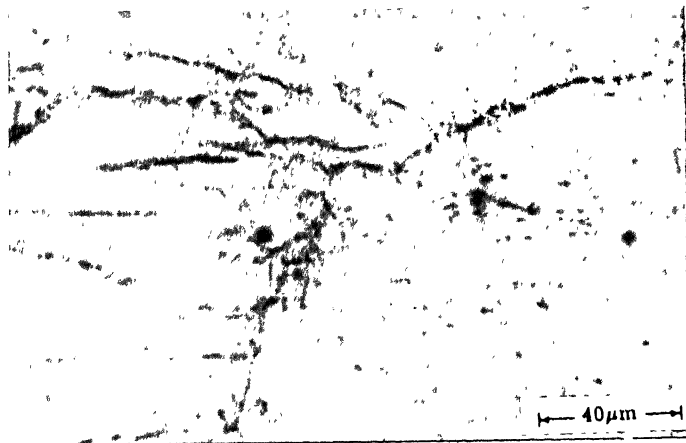
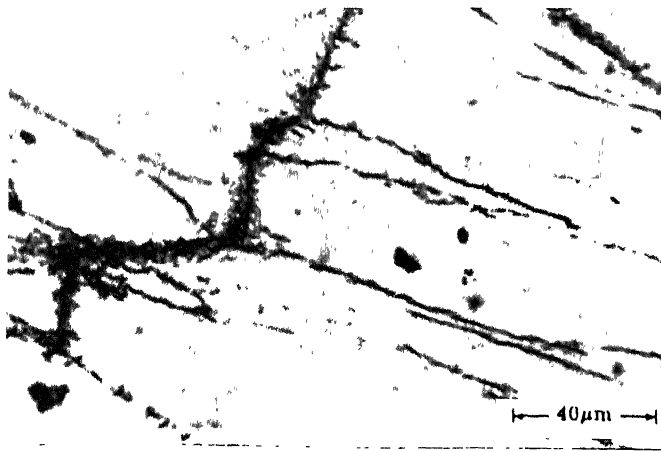


Fig. 4.9 Hair Like Structures Indicating Presence Of Shear Bands In The Heavily Deformed Samples (Rolled At 1050 °C, 60% Thickness Reduction, W/Q).

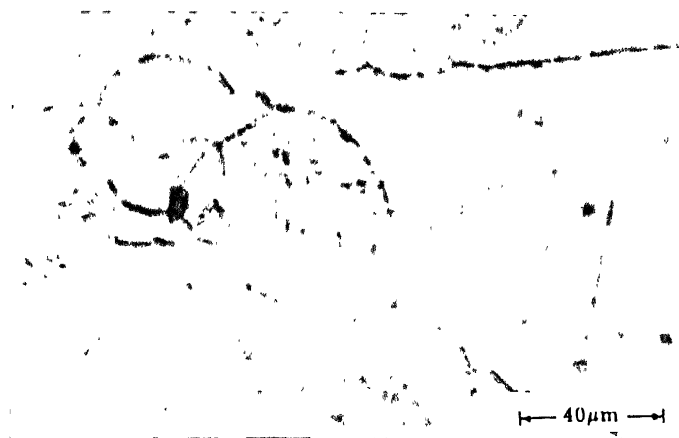
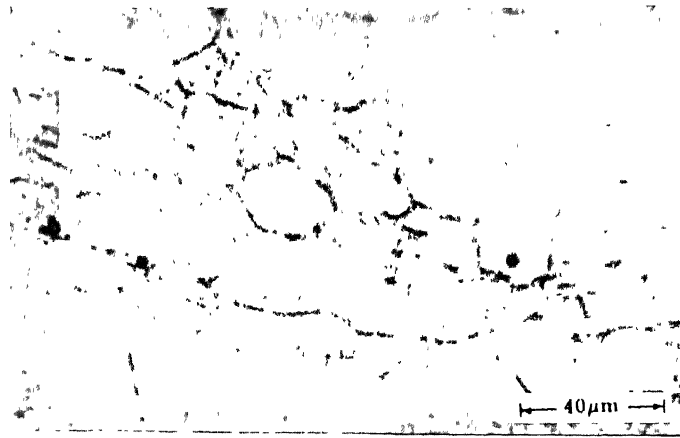


Fig 4.10 Presence Of Fine Equiaxed Grains In The As Rolled Samples(1050°C, 60 % Thickness Reduction, W/Q).



small and the occurrence of equiaxed grains is not indicative of deformation characteristic of  $\beta$  phase. While the  $\beta$  phase is not expected to undergo dynamic recrystallization during its deformation, it readily undergoes static recrystallisation during the course of cooling from the hot rolling temperature. The presence of some regions of fine equiaxed  $\beta$  grains therefore indicates that these regions did not cool sufficiently fast and gave rise to nearly equiaxed grains by static recrystallization.

#### **4.2.3 Effect of $\beta$ Rolling Temperature and Thickness Reduction on the Characteristic Features of As-Quenched Structure**

It has already been shown that the  $\beta$  phase in Ti-632Si alloy does not undergo dynamic recrystallization during its rolling at temperatures upto 1250°C. It, therefore, softens by dynamic recovery. Flow curves of the  $\beta$  phase of ( $\alpha + \beta$ ) titanium alloys also are indicative of the same. However, since the  $\beta$  phase is not stable at room temperature even after water-quenching, the development of cell boundaries and sub-structure can not be directly seen by the examination of the micro-structure of the alloy being deformed. The morphology of the transformation product from the  $\beta$  phase, i.e.  $\alpha'$  (martensite), on the other hand, is expected to be influenced by the sub-structure of deformed  $\beta$  grains.

Though, the morphology of  $\alpha'$ , formed by the transformation of  $\beta$  was not studied by the transmission electron microscopy, characteristics of  $\alpha'$  platelets were studied under high magnification (X500 and X1000) optical microscope and their widths and lengths were measured. The variation of the aspect ratio of martensitic platelets in  $\beta$ -rolled and water-quenched structure of the alloy is shown in Figure 4.11. It can be seen that the aspect ratio of martensitic platelets continuously decreased with increasing thickness reduction. Also, in samples rolled for a given thickness reduction at 1150°C and 1050°C, it was found to be higher at the higher rolling temperature. Since the development of sub-grains in non-recrystallizing structure occurs with increasing strain and the size of sub-grains decreases with increasing strain and lowering of the deformation temperature, the aspect ratio of martensitic platelets, as shown in Figure 4.11, seems to be correlated with the development of sub-grains in the pancaked  $\beta$  grains. Such observations have also been made in the case of steels.

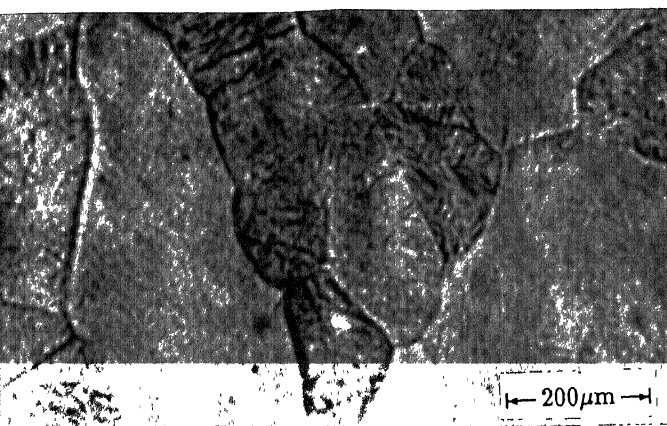
#### 4.2.4 Effect of $\beta$ -Annealing on the Structure of Hot Rolled Alloy:

It has already been stated that the objective of changing the condition of  $\beta$  grains, as followed in the present study, was to recrystallize pancaked  $\beta$  grains. For this purpose, a set of sheets of Ti-632Si alloys were hot rolled by giving 60% thickness reduction in single pass at 1050°C and were annealed at 1020 °C, i.e.  $\sim 20^\circ\text{C}$  above the  $\beta$ -transus temperature. Annealed specimens were then water-quenched to retain  $\beta$  grain boundaries for their subsequent microstructural examination.

Microstructures of partially and fully recrystallized specimens have been shown in Figure 4.12 (a) - (d). Volume fraction of recrystallized  $\beta$  grains,  $f$ , was obtained metallographically. The variation of  $f$  as a function of recrystallization annealing time has been shown in Figure 4.13. These results show that recrystallization kinetics of pancaked  $\beta$  grains is very fast at as low temperature as  $20^\circ\text{C}$  above the  $\beta$  transus temperature. The mean  $\beta$  grain size after full recrystallization was found to be  $300\ \mu\text{m}$  which is found to be much smaller than the initial grain size which were  $600\ \mu\text{m}$ .

Softening of pancaked  $\beta$  grains during the course of their annealing at  $1020^\circ\text{C}$  was also monitored by the microhardness measurement. In view of the fact that the separation of  $\alpha$  and  $\beta$  phases is suppressed by water quenching and the microstructure consists of  $\alpha'$ , the hardness measurements were made by micro-hardness indenter. Variation of the hardness as a function of annealing time is shown in Figure 4.14 and is found to have trends similar to that of microstructural changes. The drop of microhardness is steep in the initial stages of annealing which indicates that the major stress relief is by recovery process than the actual recrystallisation.

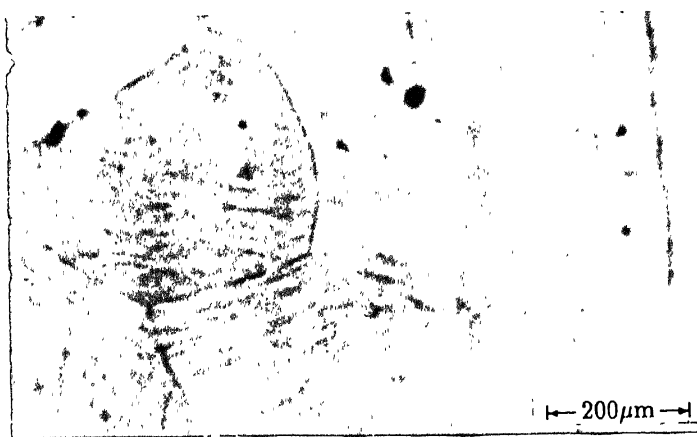
Metallographic measurements on the aspect ratio of martensitic platelets were also made. Platelets of  $\alpha'$  were found to have a mean value of 30.



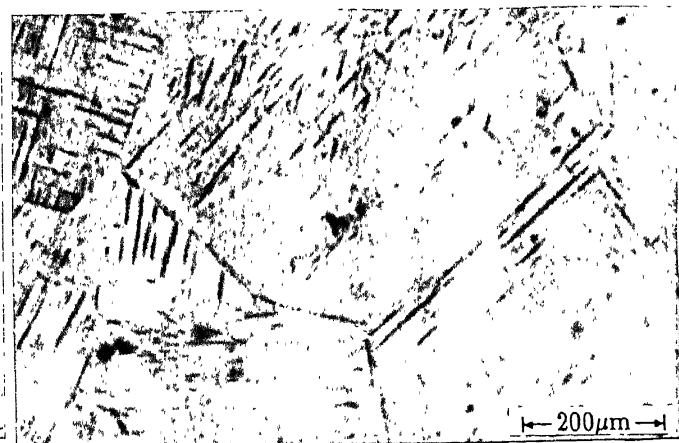
(a)



(b)



(c)



(d)

Fig. 4.12 Microstructures Of The Samples Showing Partial And Full Recrystallisation After Annealing At 1020 °C (W/Q).  
 (a) 10 s (b) 15 s (c) 20 s (d) 30 s

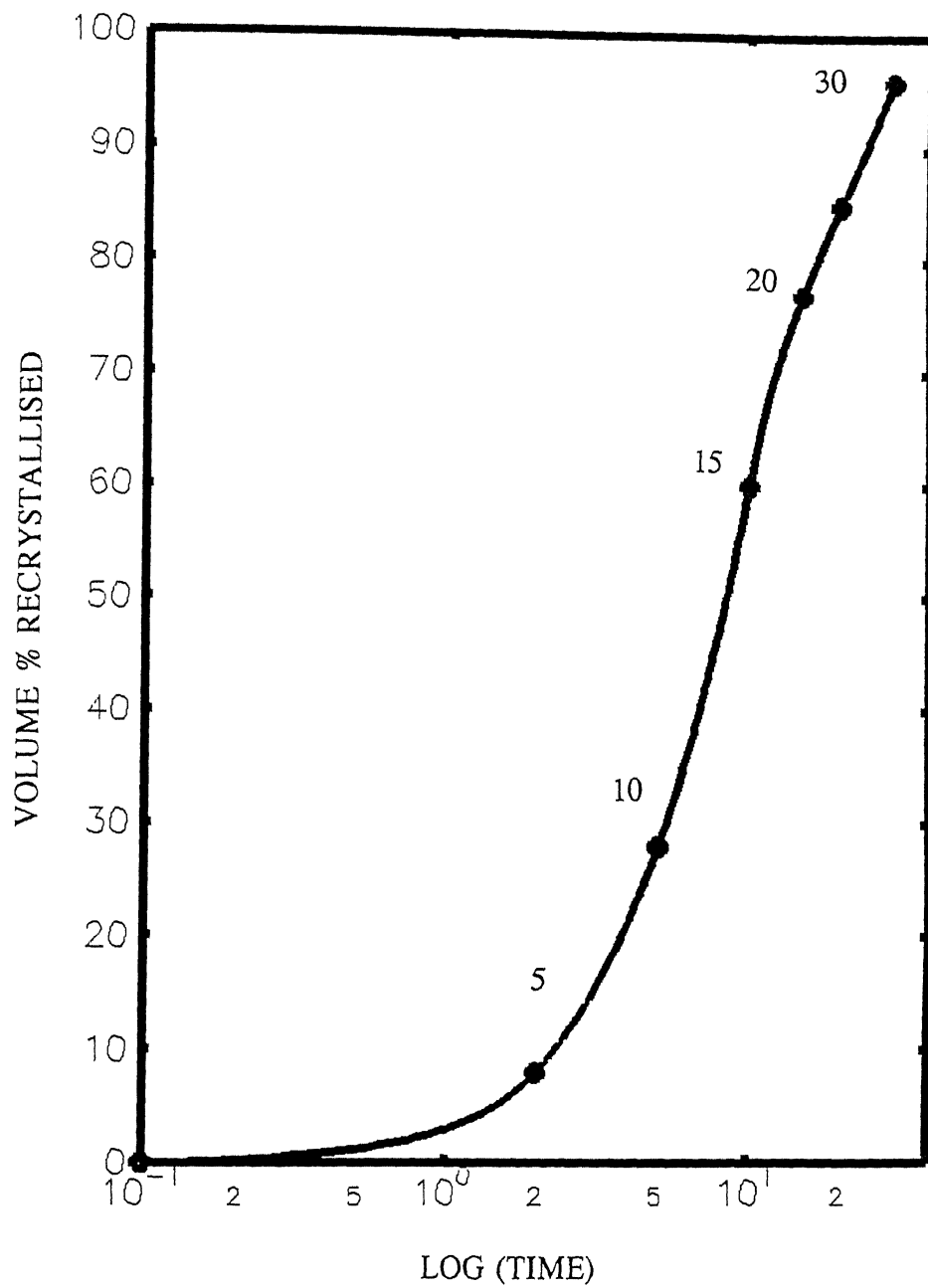


Fig. 4.13 Volume Fraction Of Recrystallised  $\beta$  Grains As A Function Of Annealing Time (Annealed At 1020 °C)

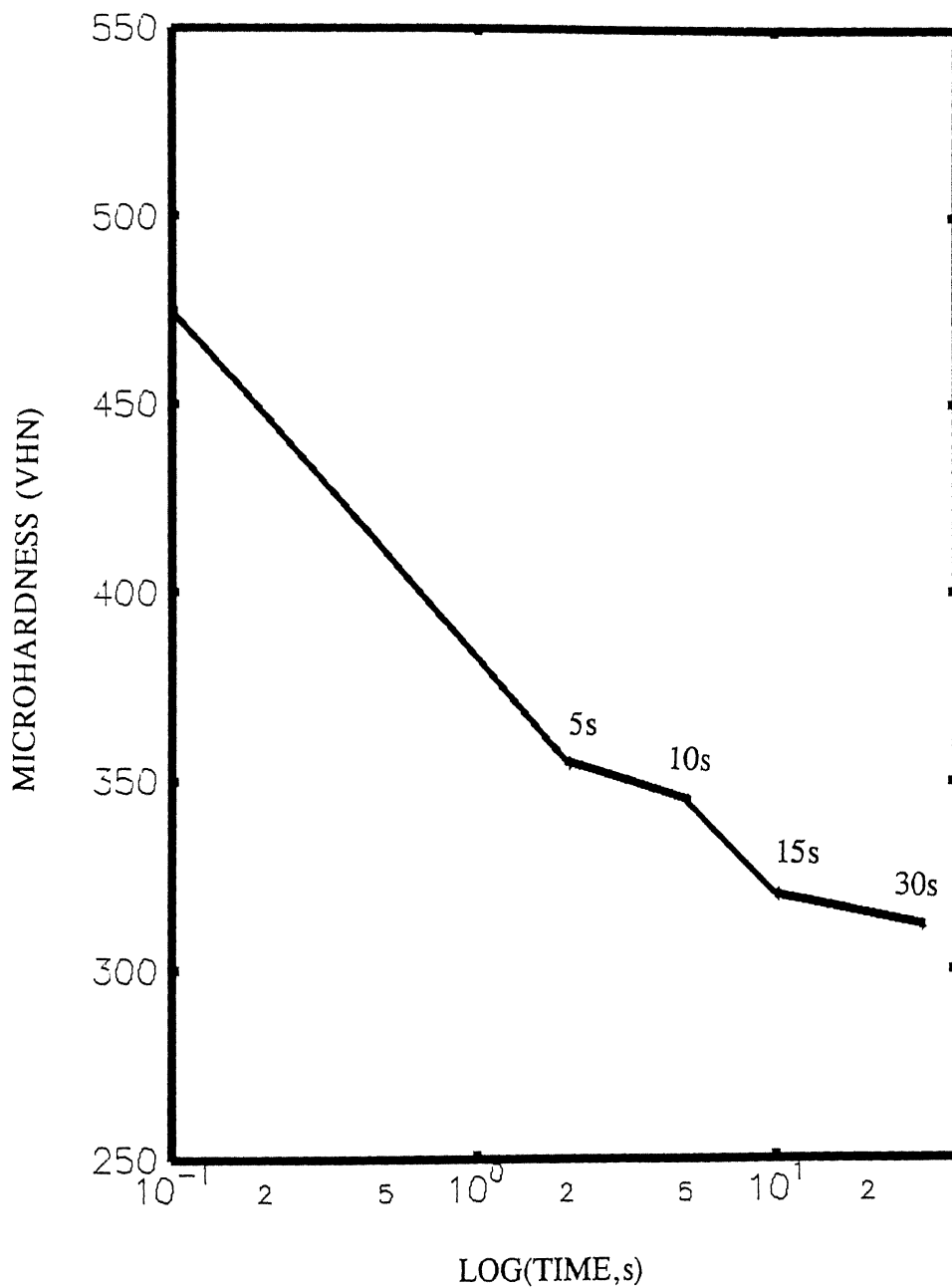


Fig. 4.14 Graph Showing Reduction In Vicker's Microhardness (VHN) With ln (Annealing Time,s) After Annealing At 1020°C(W/Q).

#### **4.2.5 Comparison Between Conditions of Water-Quenched $\beta$ Grains as Obtained by Varying the Thermo-mechanical Processing of Ti-632Si Alloy in the $\beta$ Phase Field:**

The previous sections have discussed the microstructural evolution of  $\beta$  grains during the three  $\beta$  processing routes followed. Considerable refinement of  $\beta$  grains were achieved by the processing Route 3. The martensitic structure obtained is important in the comparison of the three processing routes followed. The aspect ratio measurements on the  $\alpha'$  martensitic plates were done and the results obtained are shown in Figure 4.15. It is observed that lowest aspect ratio of martensitic plates are found in specimens processed by Route 2, While the aspect ratio slightly increased for Route 1 specimens but a large increase in aspect ratio in the Route 3 specimen is also seen. Refinement of martensitic plates occur in the as rolled specimens obtained by Route 2 as discussed in the section 4.2.3. While, the martensite plates thickened in the fine grains after annealing the specimens obtained by Route 3. This was also shown in Figure 4.12. The refinement of martensite plates in the as  $\beta$  rolled and water quenched structure is due to the formation of  $\beta$  subgrains during the heavy deformation above the  $\beta$ -transus temperature. These fine subgrains provide a number of nucleation sites during water quenching and so the occurrence of fine martensitic plates.

#### **4.3 EFFECT OF THERMO-MECHANICAL PROCESSING VARIABLES IN $(\alpha + \beta)$ PHASE FIELD ON MICROSTRUCTURAL REFINEMENT IN Ti-632Si ALLOY:**

Refinement of equiaxed primary  $\alpha$  in the structure of  $(\alpha + \beta)$  titanium alloys is essential for their improved superplastic behaviour. As suggested earlier, conditioning of primary  $\alpha$  plates/lamellae in the starting microstructure prior to hot rolling in  $(\alpha + \beta)$  phase field is of utmost importance. Since primary  $\alpha$  plates/lamellae form as a consequence of transformation of the  $\beta$  phase, their conditioning, in turn, depends on (a) conditioning of  $\beta$  grains, (b) cooling rate during  $\beta$  to  $\alpha$  transformation and (c) heating rate and temperature of transformation in case of  $\beta$  is transformed to  $\alpha'$  (martensite) and  $\alpha'$  then transforms to  $\alpha$ . Effect of thermo-mechanical processing in altering characteristics of  $\beta$  grains in Ti-632Si alloy has already been described and discussed in section 4.2. Conventional thermo-mechanical processing routes involving deformation in the two-phase field for  $(\alpha + \beta)$  titanium alloys generated involve the

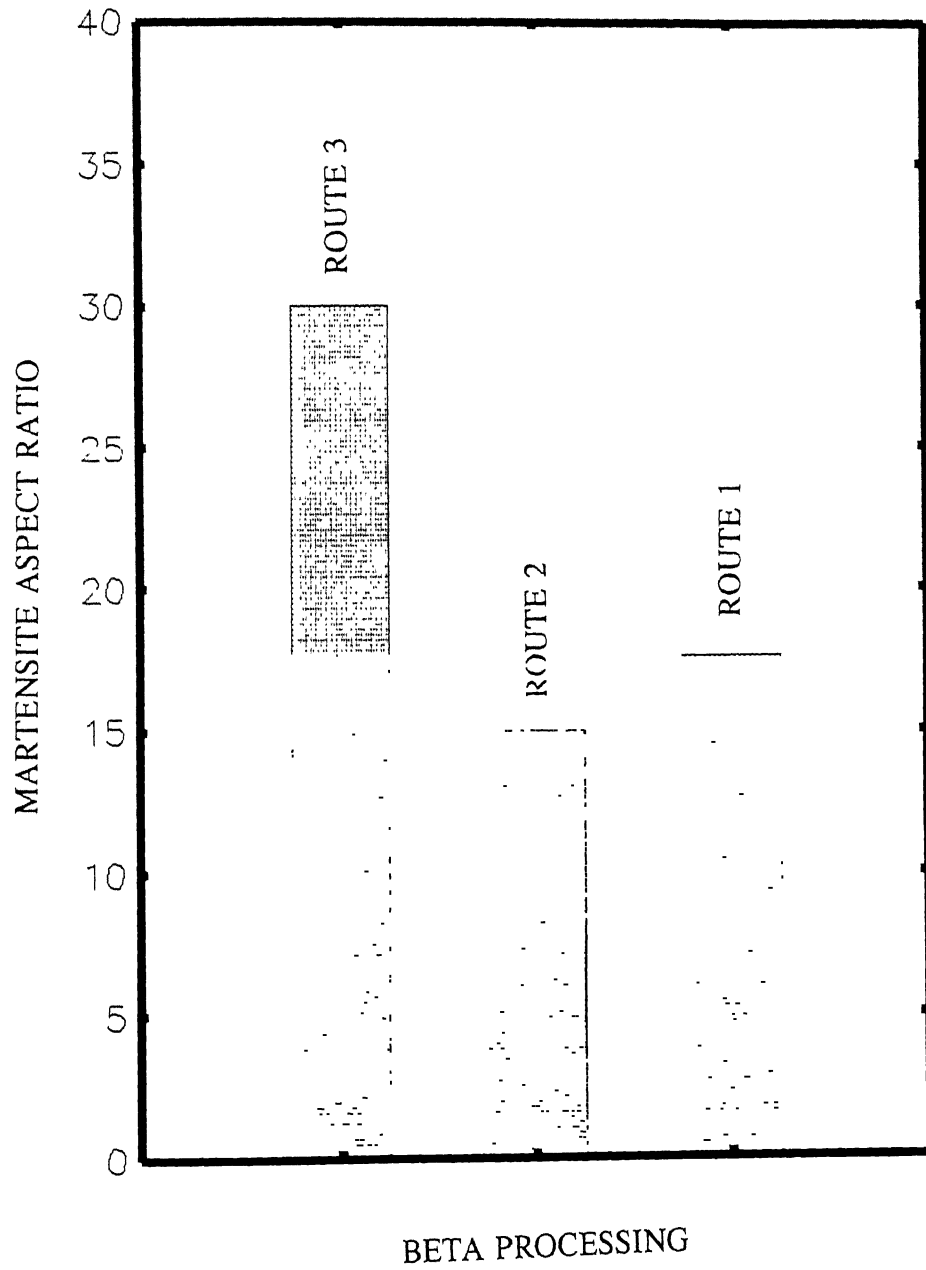


Fig. 4.15 Variation Of Martensite Aspect Ratios With Different  $\beta$  Processing Routes.

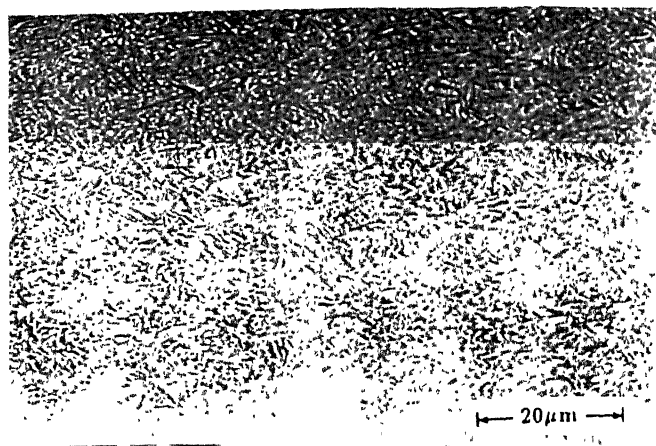
transformation of  $\beta$  to  $\alpha$  by air-cooling. In view of the formation of relatively thick primary  $\alpha$  plates/lamellae under such a condition this approach was not considered in the present study. In contrast, acicular morphology of primary  $\alpha$ , which can be obtained by the transformation of  $\alpha'$  to  $\alpha$  during preheating to hot-rolling temperature, is well known to be of considerably lower thickness and a higher aspect ratio [56]. However, specific morphological features of acicular  $\alpha$  are expected to depend on morphological features of  $\alpha'$  which, in turn, depends on conditioning of  $\beta$  grains. The effect of conditioning of  $\beta$  grains on morphological features of  $\alpha'$  is already shown in Section 4.2. Thus, the acicular  $\alpha$  structure obtained during preheating for hot rolling in specimens differently processed in the  $\beta$  phase field, i.e., by Route 1, Route 2 and Route 3, was hot rolled in the  $(\alpha+\beta)$  phase field. The effect of thermo-mechanical processing variables in the  $(\alpha+\beta)$  phase field on the refinement of structure in Ti-632Si alloy is described and discussed in the present section.

#### 4.3.1 Effect of the Hot Rolling Temperature on the Morphology of Primary $\alpha$ :

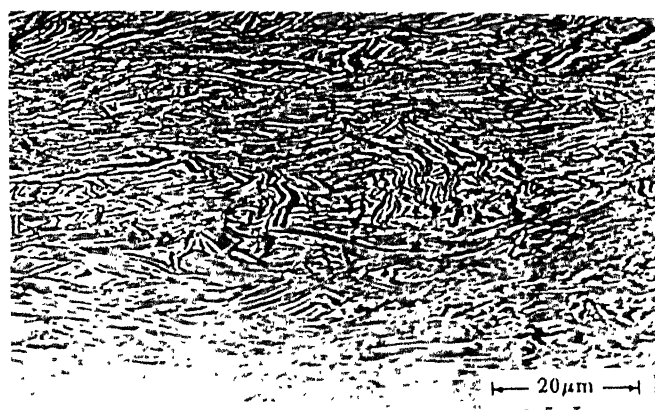
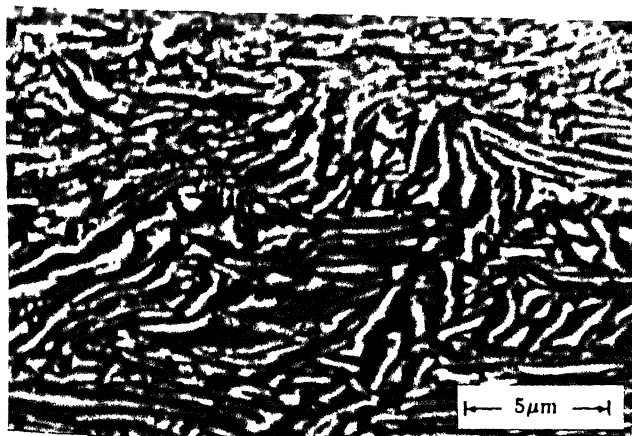
The temperature of hot rolling of  $(\alpha+\beta)$  titanium alloys in the two-phase field manifests itself in several ways. Firstly, the volume fractions of equilibrium  $\alpha$  and  $\beta$  phases in the alloy change with temperature, with volume fraction of  $\beta$  phase increasing with increasing the temperature. Secondly, since the present study was concerned with thermo-mechanical working of acicular  $\alpha$  morphology, which is obtained by the transformation from  $\alpha'$ , the mean width of acicular  $\alpha$  plates changes with the transformation temperature. It is expected that the mean width of acicular plates increases with increasing the pre-heating or hot rolling temperature. Finally, the deformation resistance and plasticity of individual phases, i.e.  $\alpha$  and  $\beta$  phases, change with temperature, with the deformation resistance decreasing and plasticity increasing with increasing the temperature. Since the plate/lamellar/acicular  $\alpha$  morphology in  $(\alpha+\beta)$  titanium alloys undergo changes during working in  $(\alpha+\beta)$  phase field, all the above three factors play important role in fragmentation and/or refinement of the  $\alpha$  phase.

Specimens subjected to  $\beta$  working followed by  $\beta$  recrystallization annealing(those obtained by Route 3) were hot rolled at 850°C, 950° and 950°C respectively, ie., at about 150°C, 100°C and 50°C below the  $\beta$ -transus temperature by giving about 60% thickness reduction in

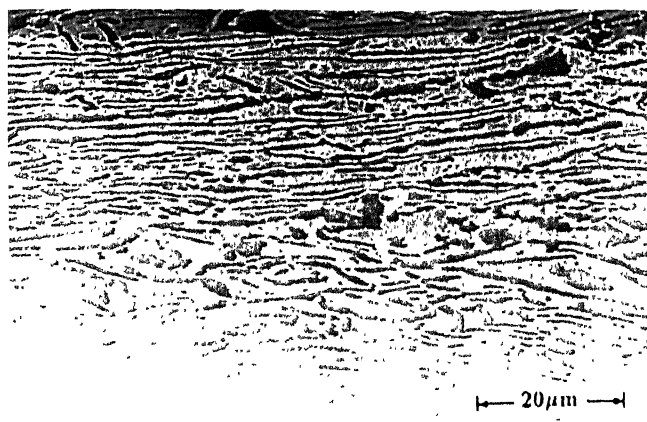
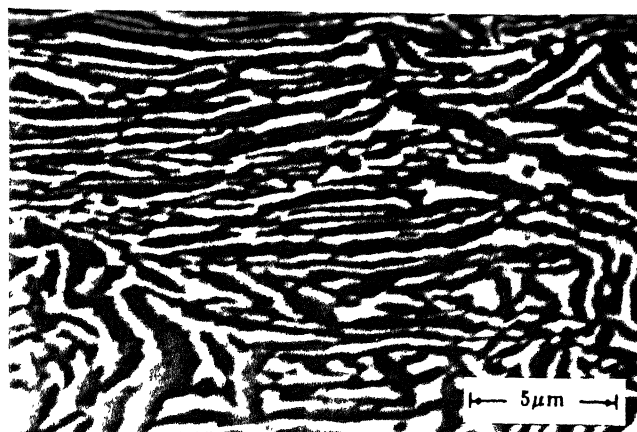




(a)



(b)



(c)

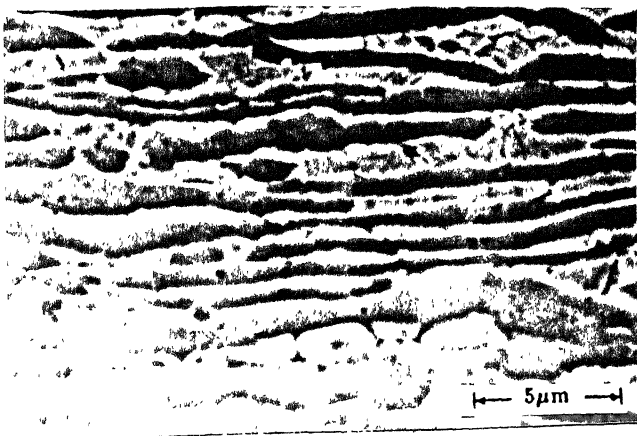


Fig. 4.16 Microstructures Of The Specimens Deformed In The  $(\alpha + \beta)$  Phase Field at Different Temperatures.  
 (a) 850 °C (b) 900 °C (c) 950 °C

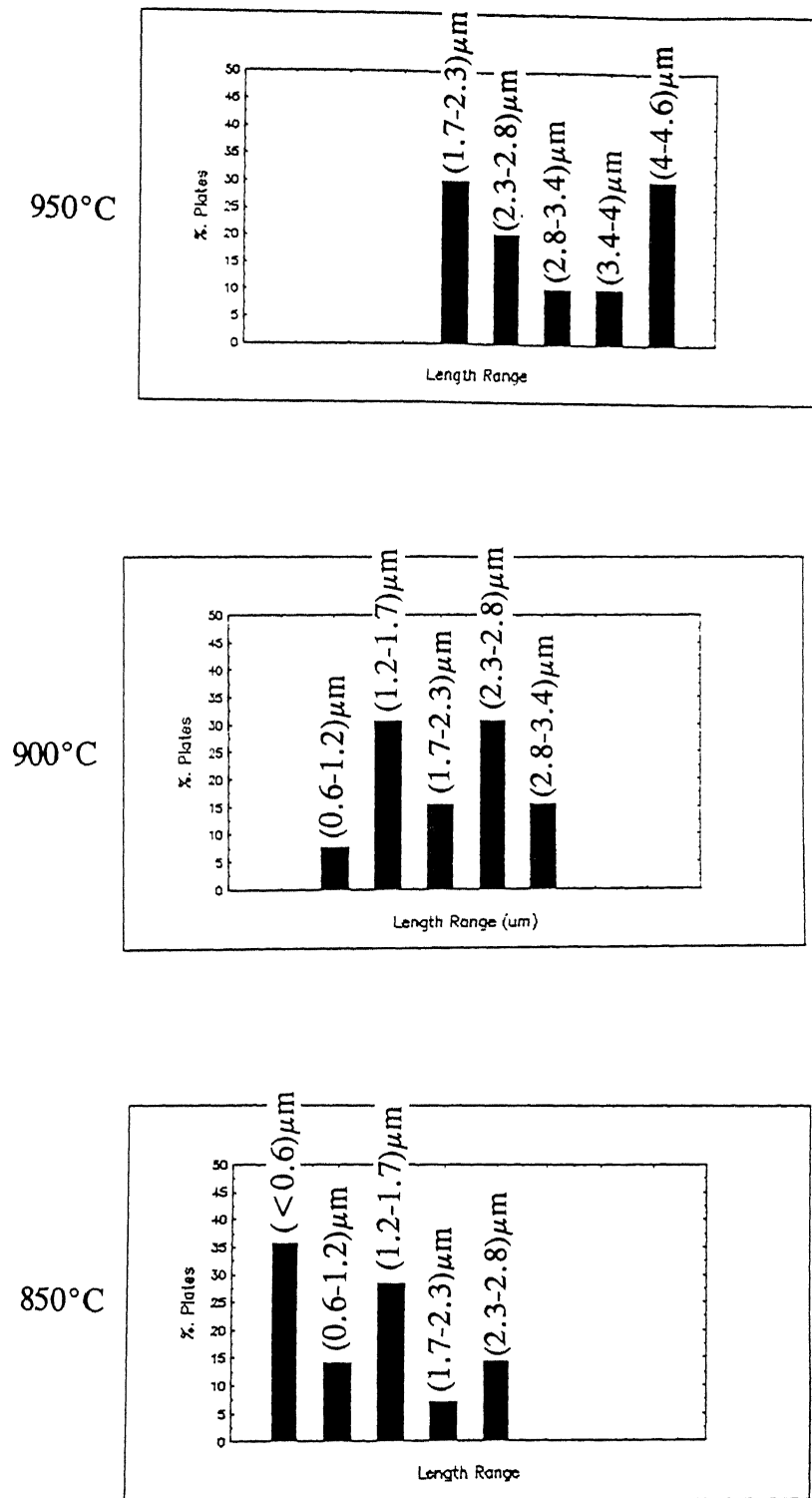
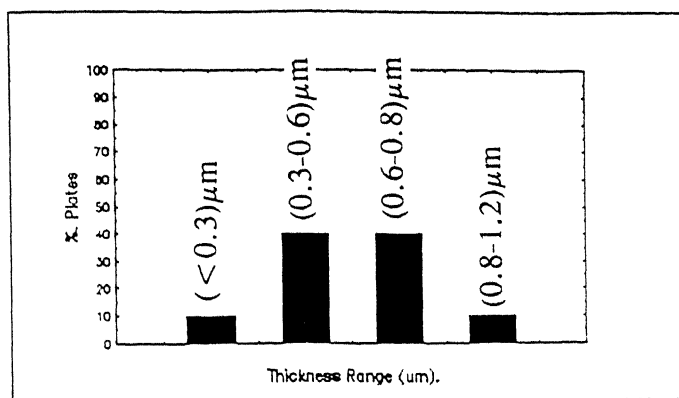
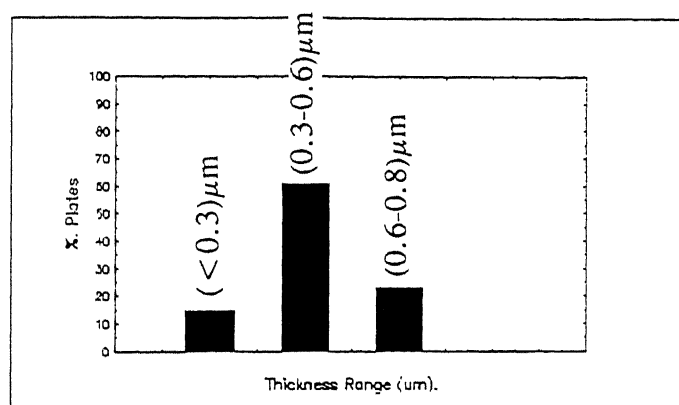


Fig. 4.17 Length Distribution Of The  $\alpha$  Plates In Specimens Rolled In ( $\alpha + \beta$ ) Field At Different Temperatures.

950°C



900°C



850°C

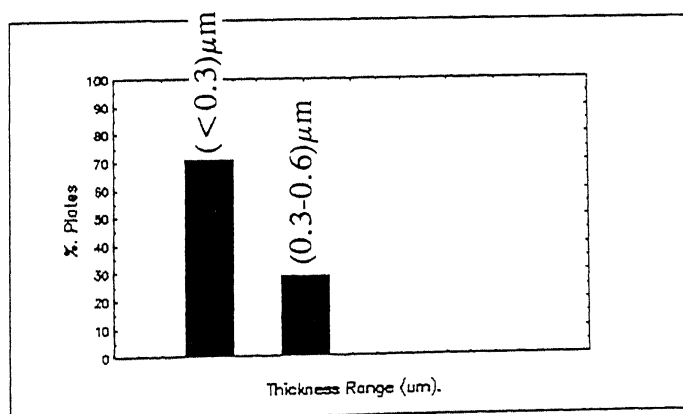


Fig. 4.18 Thickness Distribution Of The  $\alpha$  Plates In The Specimens Rolled In  $(\alpha+\beta)$  Field At Different Temperatures.

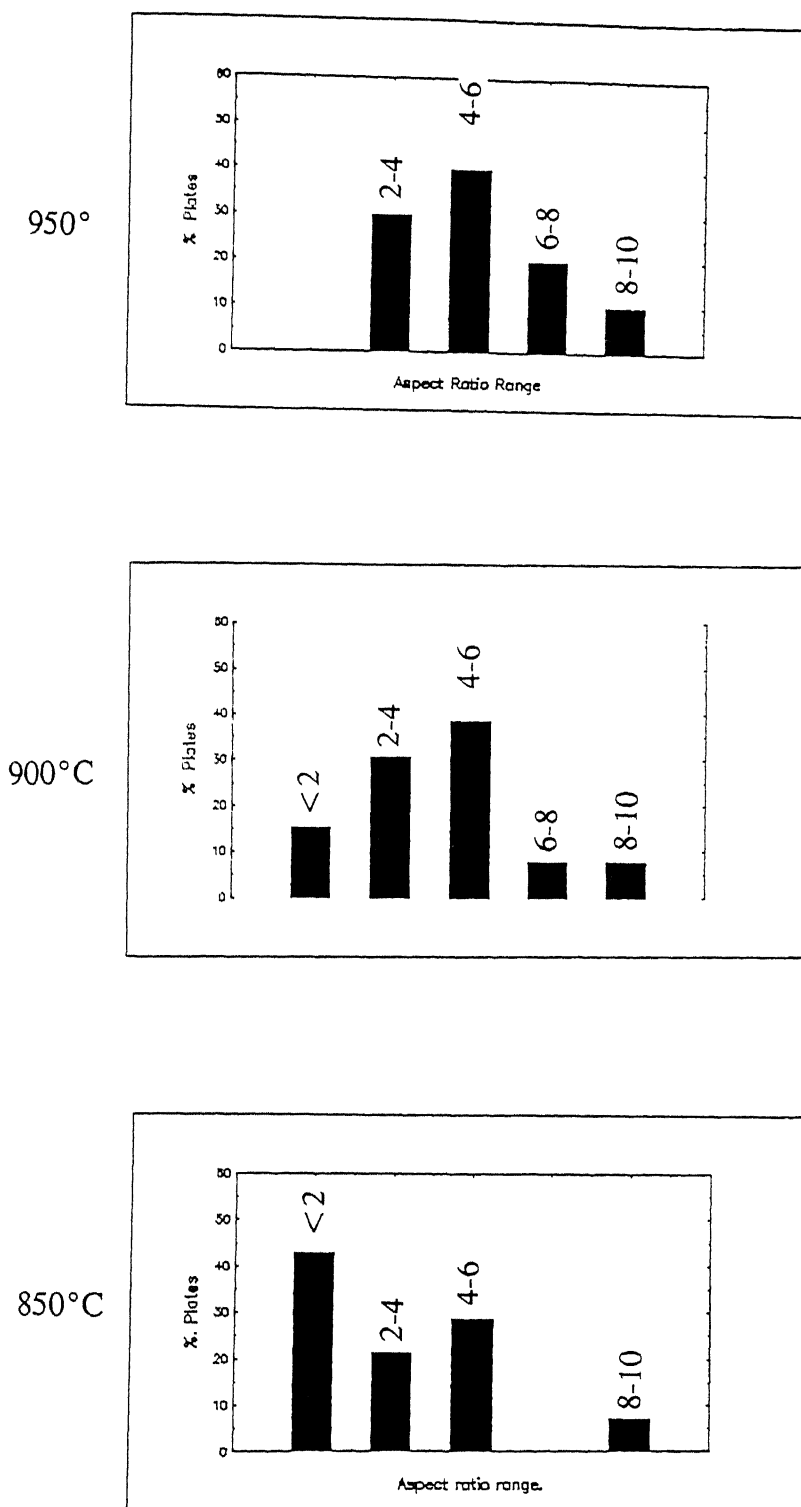


Fig. 4.19 Aspect Ratio Distribution Of The  $\alpha$  Plates In The Specimens Rolled In  $(\alpha+\beta)$  Field At Different Temperatures.

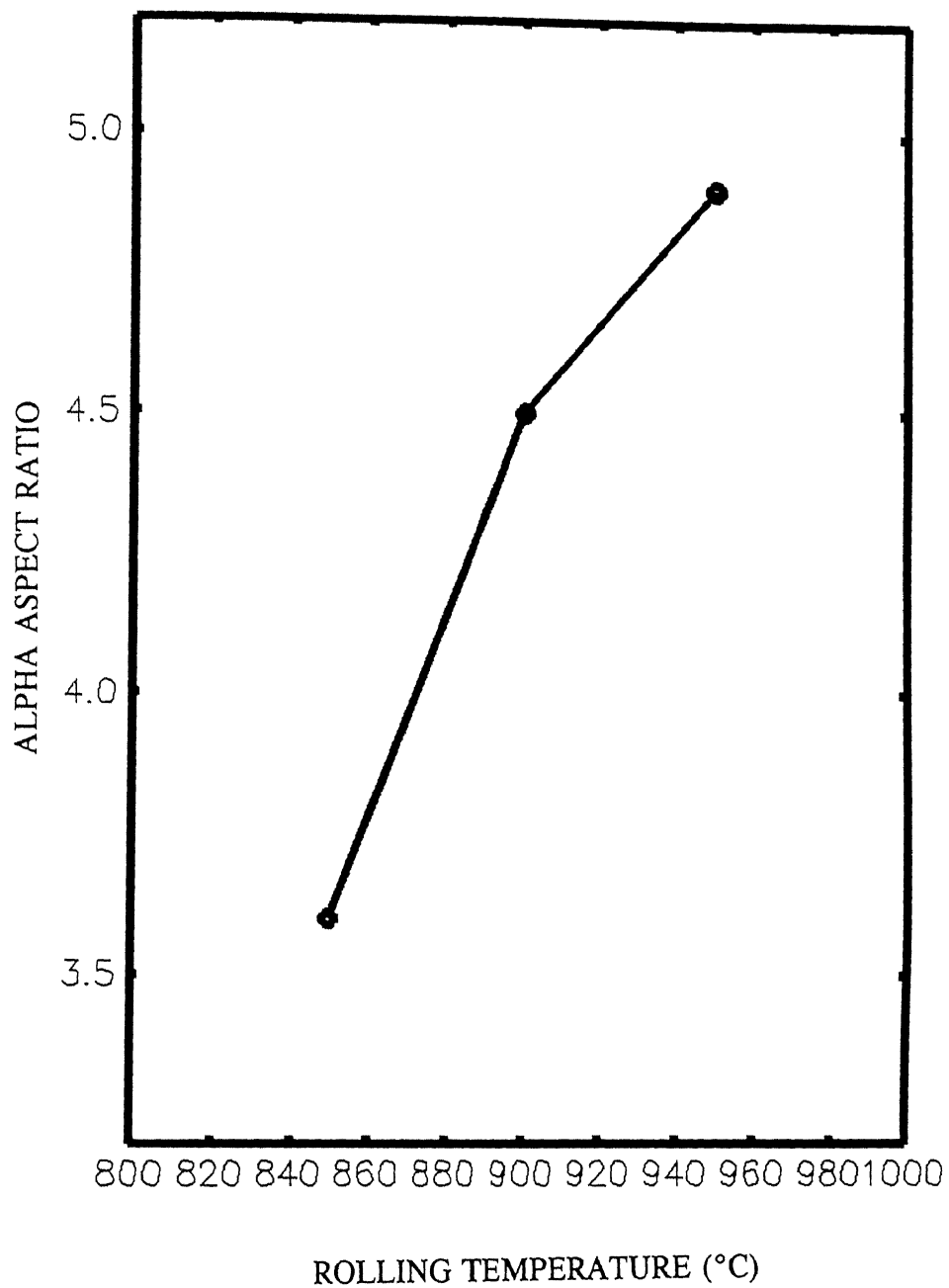


Fig. 4.20 Variation In  $\alpha$  Aspect Ratio As A Function Of Rolling Temperature.

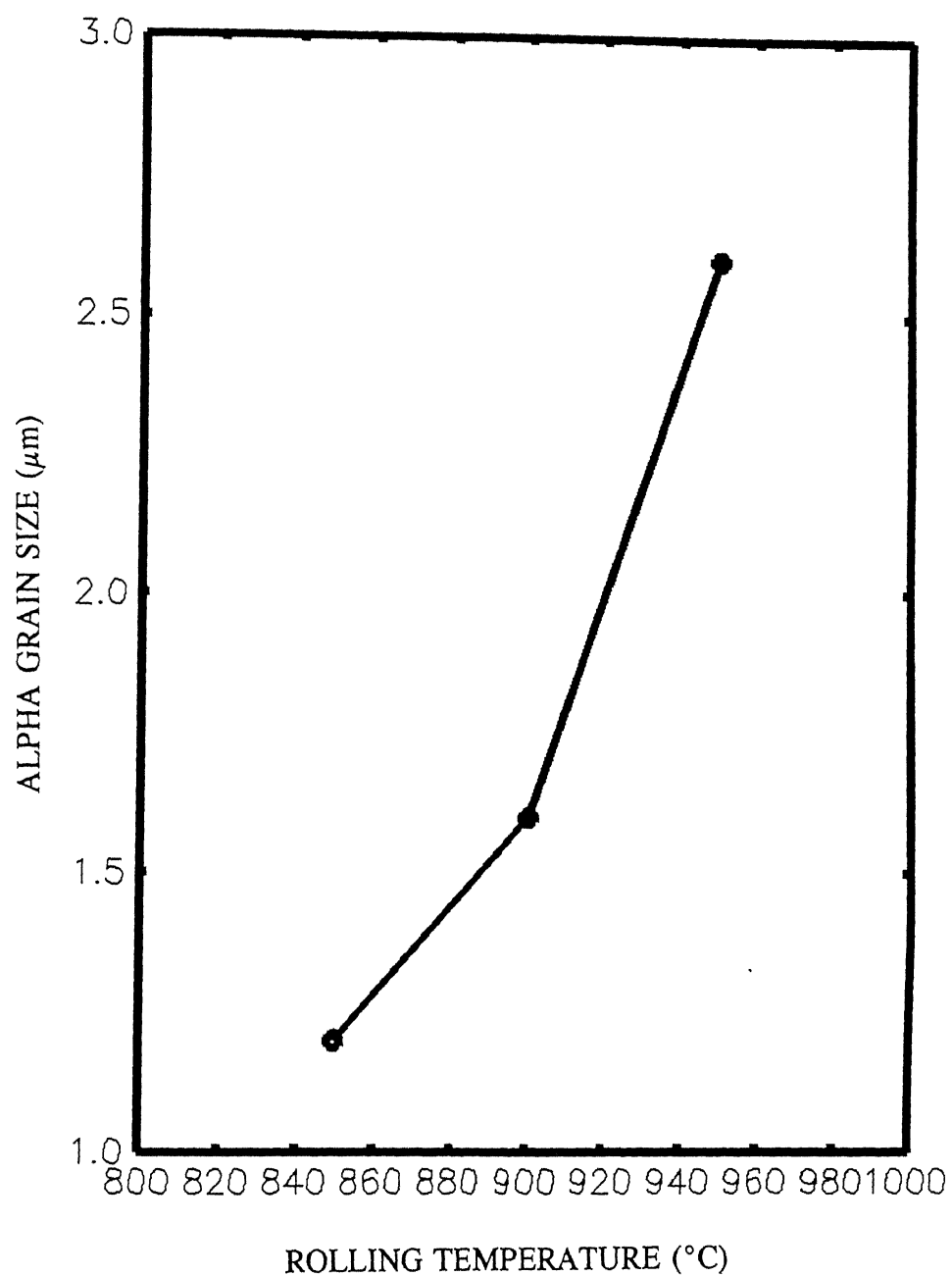


Fig. 4.21 Variation Of Mean  $\alpha$  Grain Size As A Function Of Rolling Temperature.

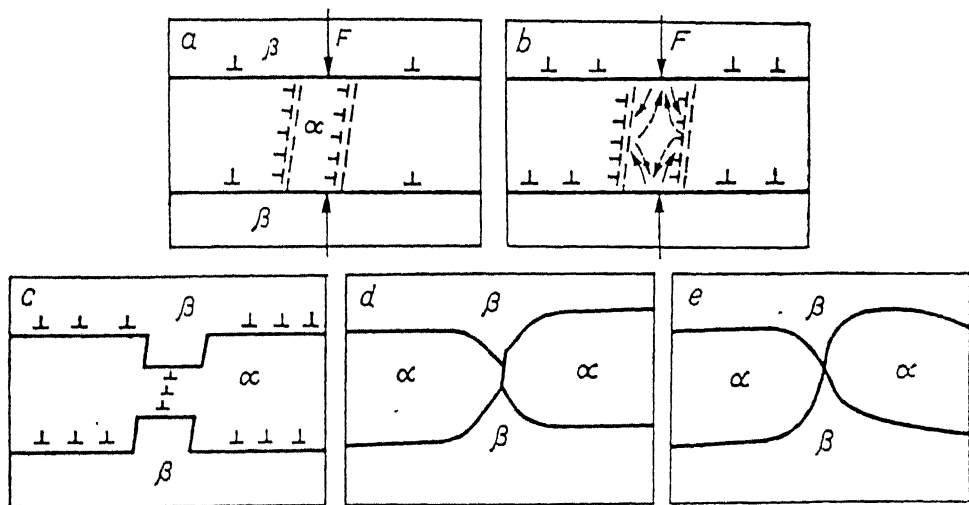


Fig. 4.22 Scheme Of Division Of  $\alpha$ -Phase Plate During Deformation In The  $(\alpha+\beta)$  Field.  $\longrightarrow$ : Direction Of Flux Of Al Atoms,  $-\ - \rightarrow$ : Direction Of Vacancy Flux.

The depletion of Al from the surface of the compressed part of  $\alpha$  plate results in its transformation to  $\beta$  phase and forms groove on the  $\alpha/\beta$  interface (Figure 4.22(c)). Under the continued operation of stresses such a groove penetrates into the  $\alpha$  phase (Figure 4.22(d)). In the presence of high dislocation density, this process gets intensified and complete penetration of the  $\beta$  phase, i.e. fully developed  $\beta$  cusps at the  $\alpha/\beta$  interface, occurs during hot deformation in the  $(\alpha + \beta)$  phase field. The frequency of occurrence of these cusps increases with the decrease in deformation temperature. Microstructures of typical breakups of the  $\alpha$  lamellae by the  $\beta$  penetration as occurring in the specimen rolled at 950 °C is shown in Figure 4.23. Further, due to the activation of diffusion processes, the breaking of  $\alpha$  plates is likely to be assisted by change in the interface from that of low angle to one of high angle configuration. As, low angle grain boundaries are formed with the increase in degree of deformation and the increase in grain misorientation, the grain boundary sliding is also likely to occur. This mechanism is schematically depicted in Figure 4.22(e).

Therefore, the model as proposed by Kaibyshev [58] for the microstructural refinement of  $\alpha$  platelets explains explicitly the observations of the present investigation, in particular, the decrease in aspect ratio of  $\alpha$  platelets with deformation.

#### 4.3.2 Effect of Conditioning of $\beta$ Grains on Microstructural Refinements in Ti-632Si Alloy After Rolling In $(\alpha + \beta)$ Phase Field :

Effect of hot rolling temperature in the  $(\alpha + \beta)$  phase field has already been described in Section 4.3.1 and it was concluded that the degree of refinement of the microstructure improves as the rolling temperature goes down. Ti-632Si alloy in other  $\beta$  conditioned states was therefore rolled at 850 °C for a total of 60 % thickness reduction in 3-4 passes.

Microstructures of  $(\alpha + \beta)$  hot rolled specimens obtained from (a) coarse recrystallised water quenched  $\beta$  grains, i.e  $\beta$  processing Route 1, (b) pancaked unrecrystallised water quenched  $\beta$  grains, i.e  $\beta$  processing Route 2, and (c) fine recrystallised water quenched  $\beta$  grains, i.e Route 3 are shown in Figure 4.24. The microstructure show nevertheless very fine  $\alpha$  homogenously distributed in the  $\beta$  matrix. The specimen obtained from Route 2 shows the much finer nearly-



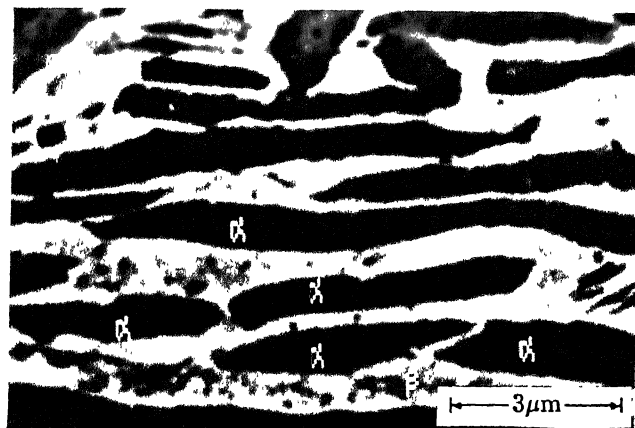
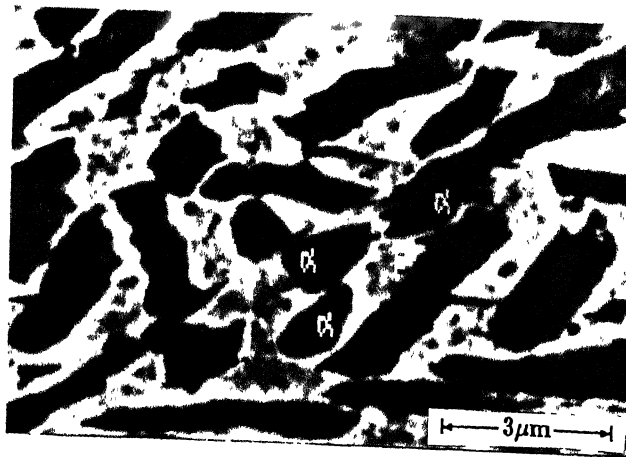


Fig. 4.23 Microstructures Of Typical Breakups Of  $\alpha$  Lamellae By The  $\beta$  Penetration As Occurring In The Specimen Rolled At 950 °C.

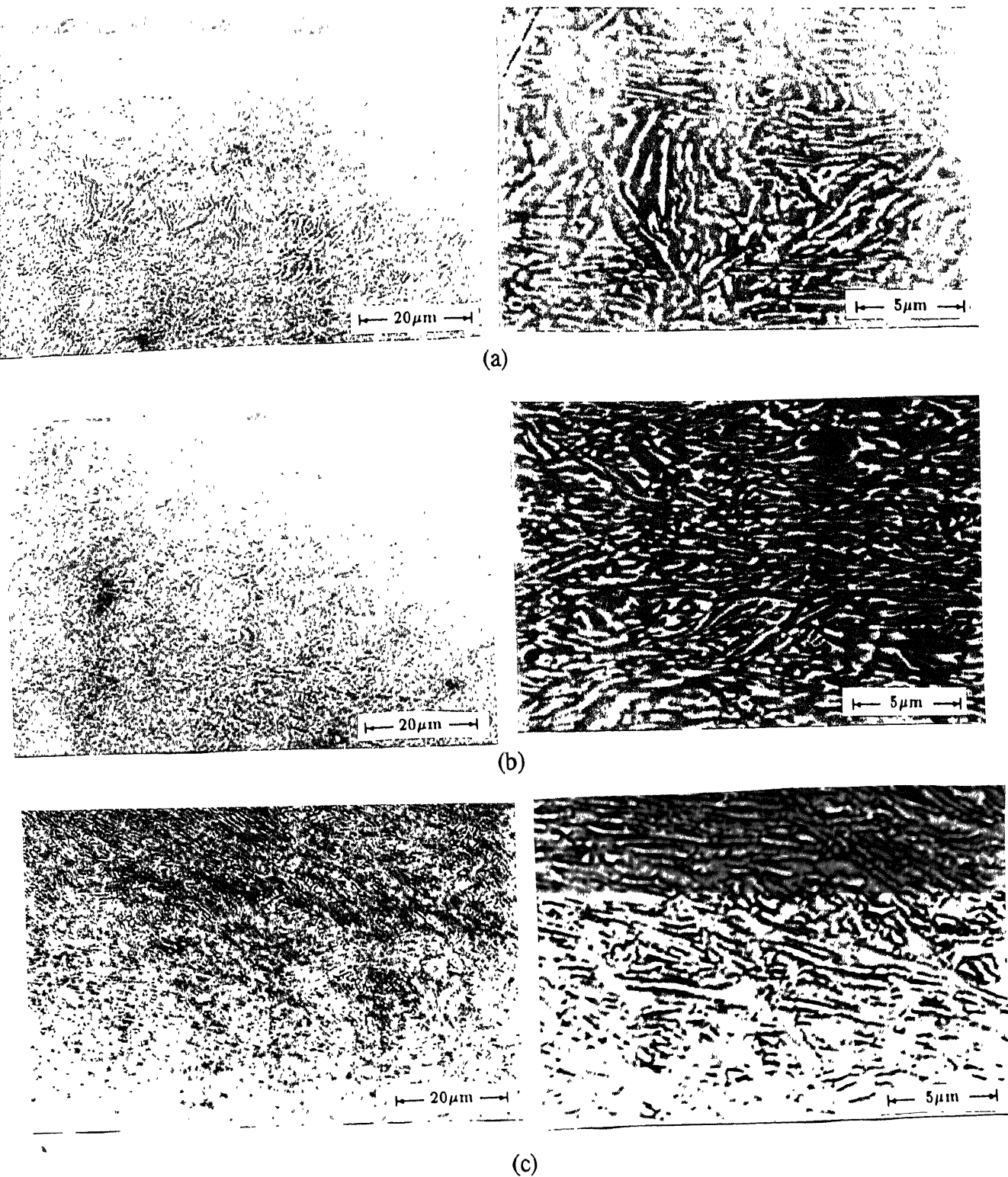


Fig. 4.24 Micrographs Of Specimens Rolled At 850 °C Following Different Thermomechanical Processing Routes.  
 (a) Route 1 (b) Route 2 (c) Route 3

equiaxed  $\alpha$  homogenously distributed while specimens obtained from Route 1 and Route 3 show partial refinement with  $\alpha$  platelets bending and  $\beta$  phase pinching the elongated  $\alpha$  phase.

Of the specimens obtained by following three different processing routes, the specimen obtained from Route 2 showed the highest degree of  $\alpha$  refinement (mean grain size =  $0.9\mu\text{m}$  & a mean aspect ratio = 2) while the specimen obtained from Route 3 showed a comparatively lower degree of  $\alpha$  refinement (mean grain size =  $1.2\mu\text{m}$  and a mean aspect ratio = 3.7). Figure 4.25 and Figure 4.26 show the mean  $\alpha$  aspect ratio variation and the mean  $\alpha$  grain size with the processing routes. The extensive refinement of the  $\alpha$  phase in specimens obtained from Route 2 might be due to the formation of very fine beta sub-grains with very fine martensite needles after the  $\beta$  rolling which provide a large number of nucleation sites for the  $\alpha$  nucleation during reheating prior to the  $(\alpha+\beta)$  rolling. While as the other specimens (Route 1 and Route 3) didn't have such a  $\beta$  sub-grain structure filled with fine martensitic needles and distributed in it before rolling in the  $(\alpha+\beta)$  field, significant  $\alpha$  refinement could not be obtained. If we compare specimens of Route 1 and Route 3, it is observed that the specimens obtained from Route 1 showed finer  $\alpha$  grains than those of Route 3. This is quite likely because of thicker and higher aspect ratio of martensite plates in the specimens which were obtained by Route 3 prior to their  $(\alpha+\beta)$  rolling (Figure 4.15). Therefore, it was concluded here that  $\beta$  conditioning had a marked effect on the control of the  $\alpha$  refinement during  $(\alpha+\beta)$  rolling.

#### **4.4 EFFECT OF RECRYSTALLISATION ANNEALING IN $(\alpha+\beta)$ PHASE FIELD ON THE $(\alpha+\beta)$ HOT ROLLED Ti-632Si ALLOY**

The metallographic analysis of specimens rolled in the  $(\alpha+\beta)$  phase field showed that though the aspect ratio of  $\alpha$  plates was drastically reduced but did not produce nearly equiaxed  $\alpha$  grains. Conventional thermomechanical processing of  $(\alpha+\beta)$  Ti alloys generally involves with recrystallization annealing in  $(\alpha+\beta)$  phase field. Therefore a limited number of specimens were also subjected to a subsequent recrystallization annealing in the  $(\alpha+\beta)$  phase field. In this section the results obtained in the study of effect of  $\alpha$  plate thickness prior to annealing treatments on  $\alpha$  plate refinement are also discussed.

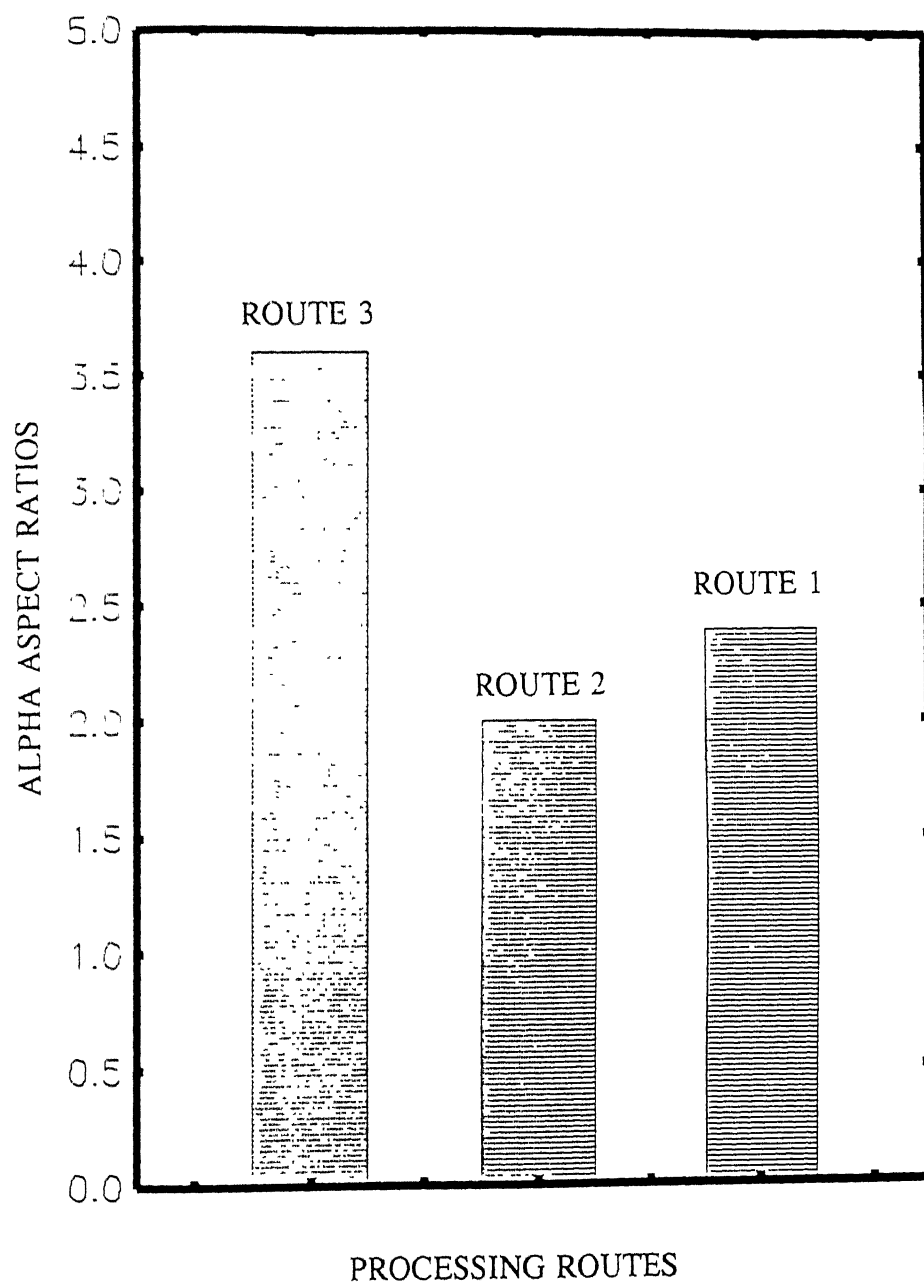


Fig. 4.25 Comparison Of Values Of  $\alpha$  Aspect Ratios In The Thermomechanically Processed Specimens.

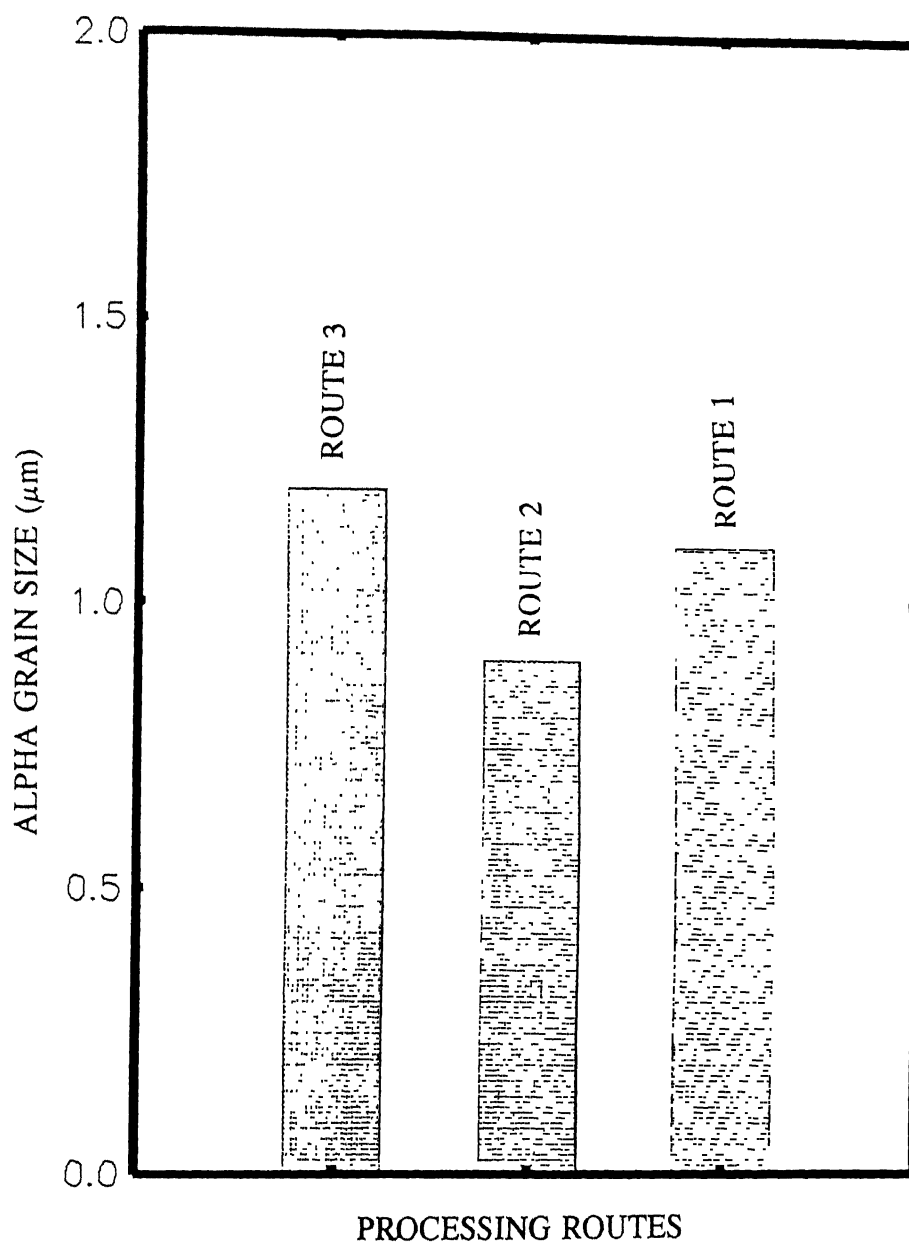


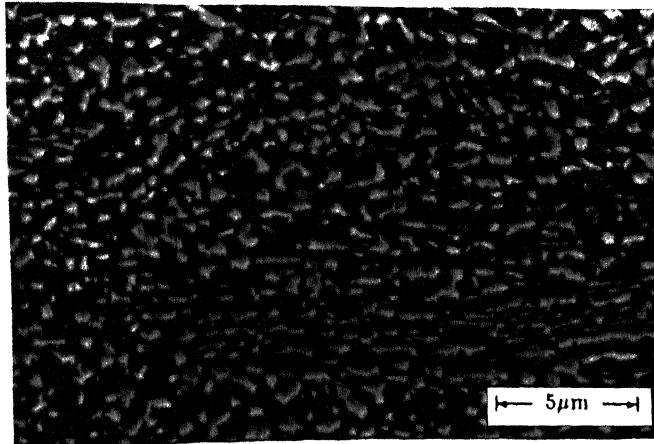
Fig. 4.26 Comparison Of The Mean  $\alpha$  Grain sizes In The Thermomechanically Processed Specimens.

#### 4.4.1 Effect of Recrystallization Temperature and Time on the Annealing Behaviour.

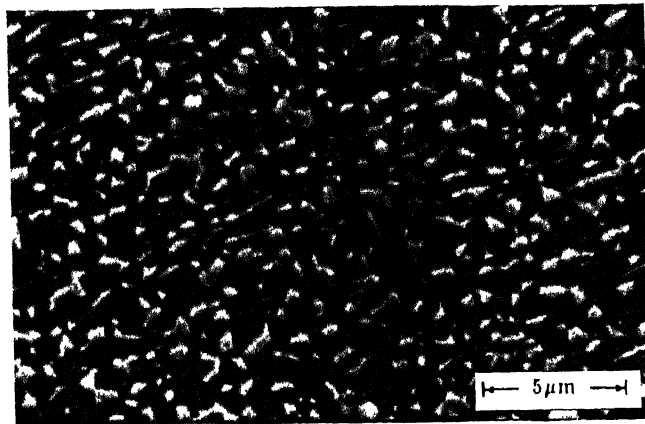
Specimens obtained by Route 3 were subjected for the annealing treatments at 800°C and 850°C for 0.5, 1, 2 and 4 hours. The microstructures of these specimens are shown in Figure 4.27 and Figure 4.28. It is seen that the  $\alpha$  plates significantly got equiaxed and refined after the annealing treatment. Results of  $\alpha$  aspect ratio and  $\alpha$  grain size as obtained by the quantitative metallographic examination are summarised in Figure 4.29 and Figure 4.30. A critical examination of the microstructural features indicate that the  $\alpha$  plates become nearly equiaxed when annealed at 800°C for 2 hours or 850°C for 0.5 hours. It is seen that with an increase in the annealing temperature and time, the extent of equiaxial nature of  $\alpha$  increased, however, with a deleterious effect of  $\alpha$  grain growth.

The actual process of recrystallization is difficult to detect and to measure. However, a few studies were made to describe the physical events which occur and evolve into the new microstructure. The transformation process of lamellar alpha (Figure 4.31,a) to an equiaxed structure has been studied by Margolin and Cohen[41] and is described in the following two paragraphs.

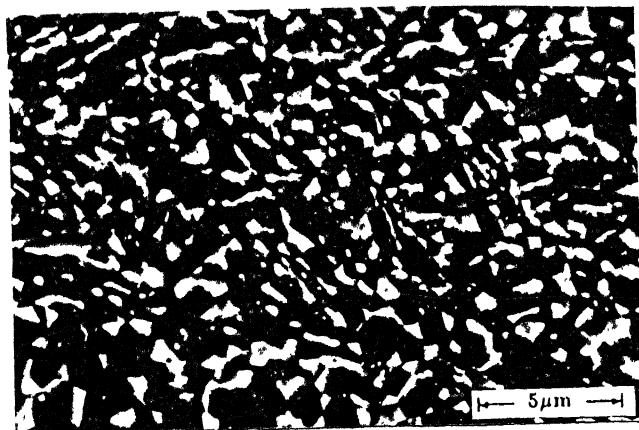
It is generally agreed that  $\alpha$  grains initially nucleate at  $\alpha/\beta$  interfaces . This can be seen in material which has been partially recrystallized wherein the  $\alpha$  nucleates in the high strain boundaries between dissimilarly oriented lamellar  $\alpha$ - $\beta$  colonies . These recrystallised  $\alpha$  grains,  $\alpha_R$ , grow through the grain boundary  $\alpha$  until the boundary of the recrystallised  $\alpha$  crosses the width of the original grain boundary  $\alpha$  platelet (Figure 4.31,b). At this point the rounded  $\alpha_R$  impinges on the surrounding unrecrystallised  $\beta$  platelets, which are forced to part and reshape due to surface energy considerations (Figure 4.31,c). This allows to the  $\alpha_R$  to make contact with the unrecrystallised  $\alpha$  on the far sides of the  $\beta$  platelets.  $\beta$  phase also moves across the prior  $\alpha$  platelets into the new boundaries between  $\alpha_R$  grains. The  $\alpha_R$  thus becomes wider than the original  $\alpha$  platelet (Figure 4.31,d) and can consume the unrecrystallised  $\alpha$  in the adjoining  $\alpha$  platelet. This model of the post-deformation recrystallisation annealing satisfactorily explains the microstructural evolution during recrystallization in the present investigation (Figure 4.27 and Figure 4.28).



(a)

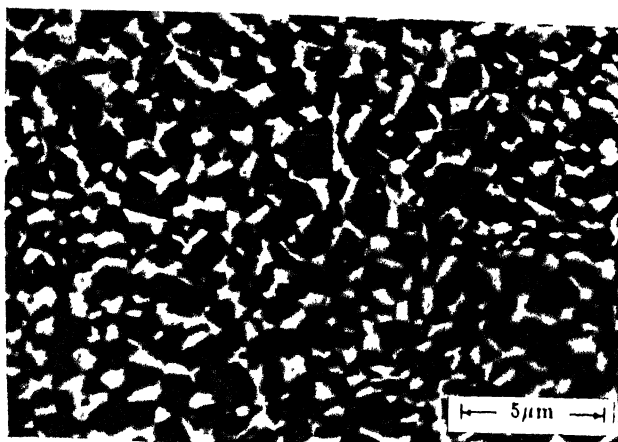


(b)

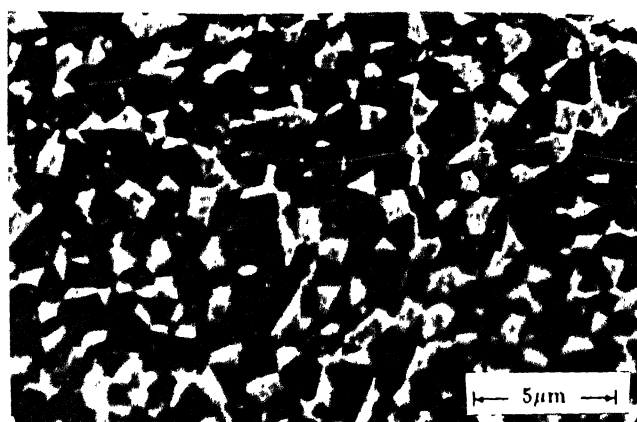


(c)

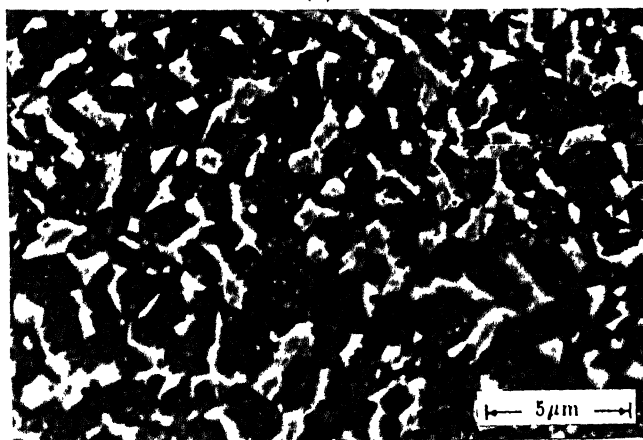
Fig. 4.27 Micrographs Of The Specimens Annealed At 800 °C At Different Times After Rolling In The  $(\alpha+\beta)$  Phase Field At 850 °C Following Route 3.  
 (a) 0.5 hr (b) 2 hrs (c) 4 hrs



(a)



(b)



(c)

Fig. 4.28

Micrographs Of The Specimens Annealed At 850 °C At Different Times After Rolling In The ( $\alpha+\beta$ ) Phase Field At 850 °C Following Route 3.

(a) 0.5 hr

(b) 2 hrs

(c) 4 hrs



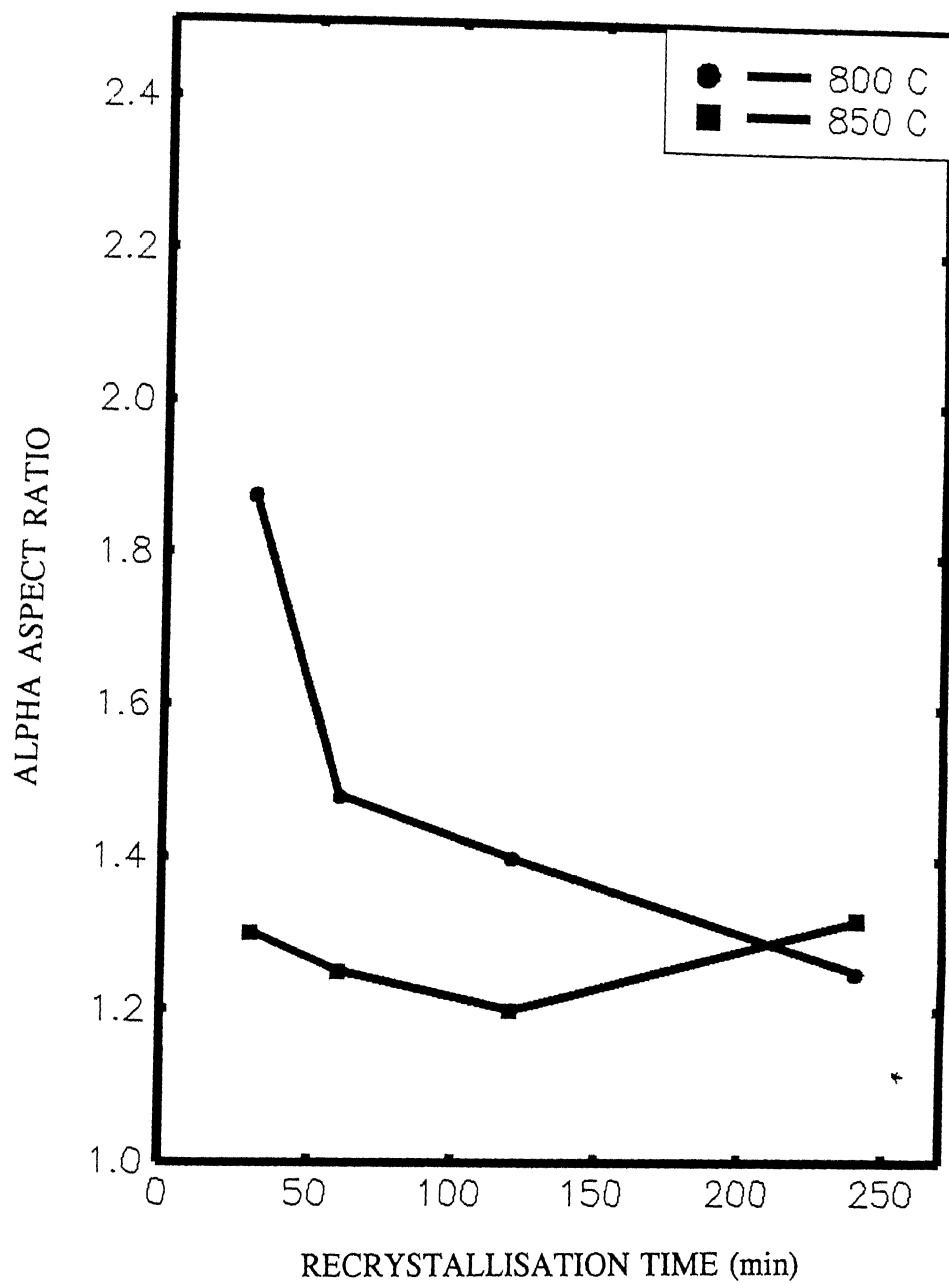


Fig. 4.29 Graph Of  $\alpha$  Platelet Aspect Ratio As a Function Of Annealing Time.

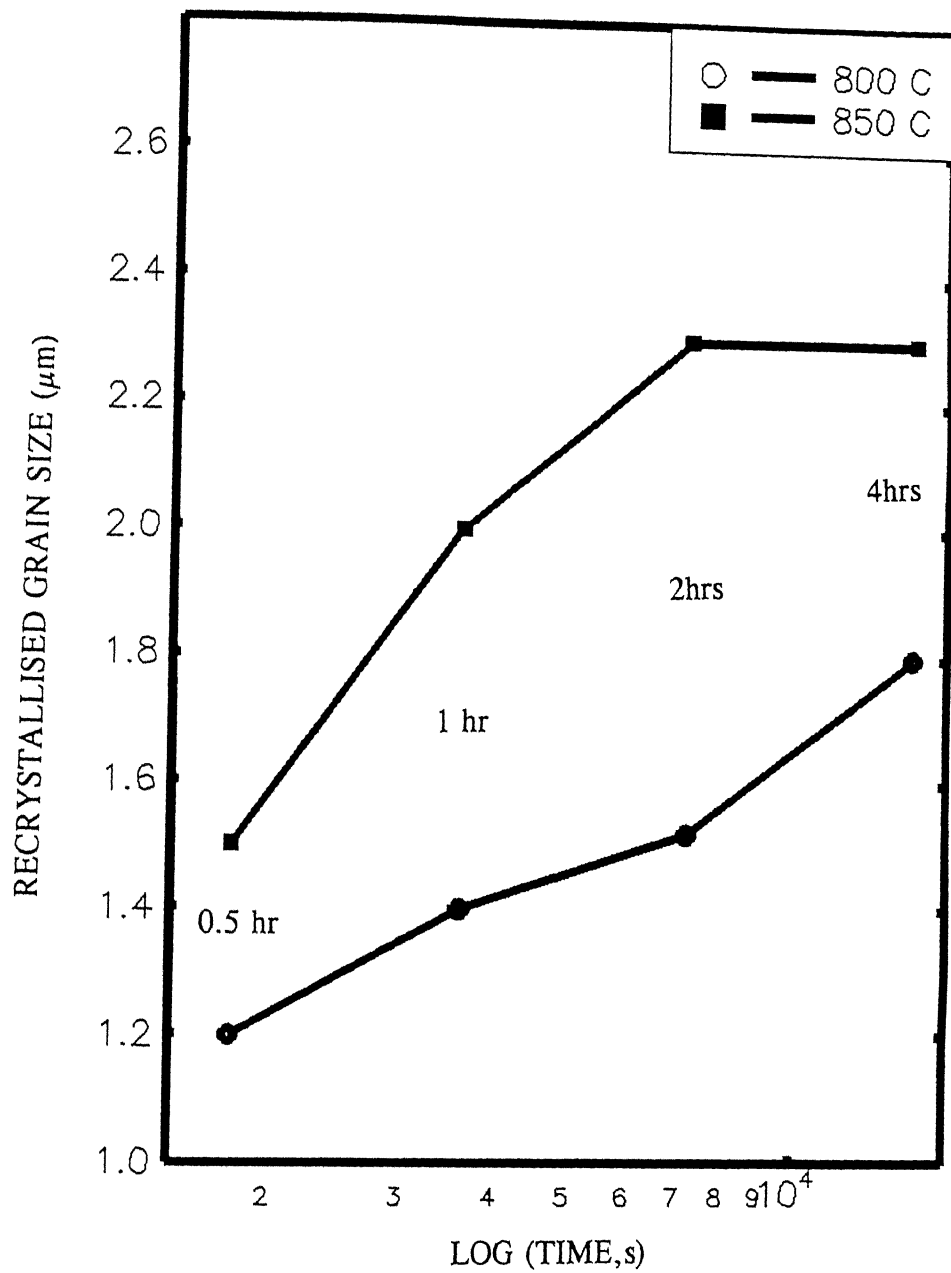


Fig. 4.30 Graph Of Mean  $\alpha$  Grain Size As A Function Of Annealing Time.

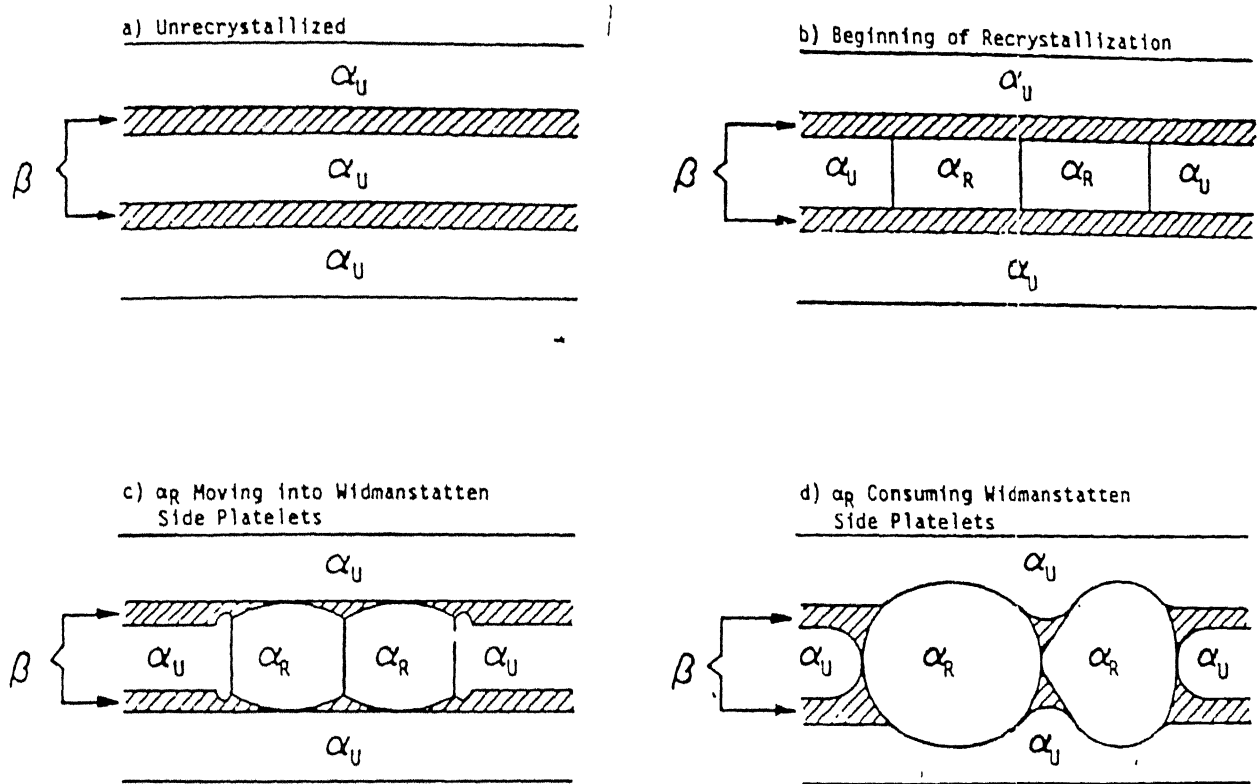


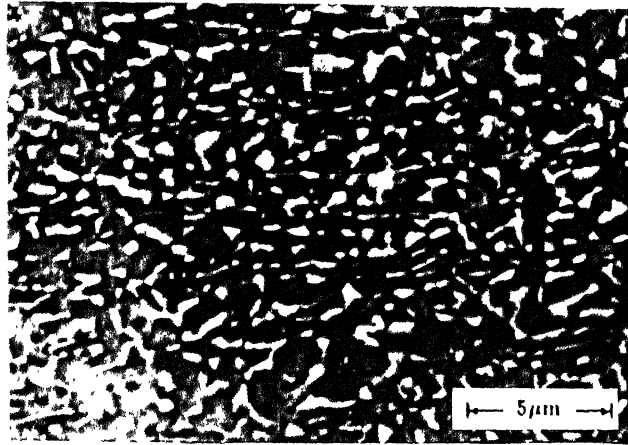
Fig. 4.31 Schematic Representation Of The Conversion Of  $\alpha$  Platellike Structure To Equiaxed Structure During Post Deformation Annealing.

As  $\alpha$  grains recrystallised and begin to separate interlamellar  $\beta$ , surface tension between the  $\alpha$  and  $\beta$  phases causes the  $\beta$  phase to become larger and more rounded than adjacent  $\beta$ . This process leads to equiaxed  $\beta$ . When  $\beta$  recrystallises, surface tension  $\alpha$  and  $\beta$  can cause the  $\alpha$ - $\beta$  interface to appear "scalloped" as the  $\beta$  impinges on the  $\alpha$ .

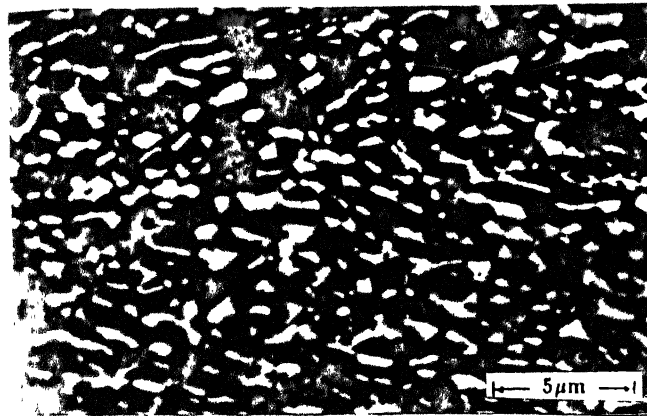
#### 4.4.2 Effect of $\alpha$ Platelet Thickness on the Post-Deformation Recrystallization Behaviour

In this part of recrystallisation studies effect of initial ( $\alpha+\beta$ ) rolled microstructures on the evolution of microstructure during post deformation recrystallisation is presented. For these studies, specimens obtained from Route 3 and rolled at 850°C, 900°C and 950°C with 60% thickness reduction followed by water quenching were used. The microstructures of the as rolled specimens are shown in Figure 4.16. Samples rolled at 950°C had a higher thickness  $\alpha$  platelet (0.7 $\mu$ ) than the specimens rolled at 900°C (0.5  $\mu$ m) and 850°C (0.4  $\mu$ m). These samples were annealed at 800°C and 850°C respectively for 1 hour and were examined for grain size and aspect ratio measurements. Microstructures of the specimens after the annealing treatment are shown in Figure 4.32 and Figure 4.33. The mean aspect ratios and grain sizes are shown in Figure 4.34 and Fig 4.35. It was inferred from these results that with prior rolling in the higher temperature range in the ( $\alpha+\beta$ ) phase field and annealing at higher temperatures in the ( $\alpha+\beta$ ) field, the mean grain size was maximum while, with increasing the temperature of rolling and lowering the annealing temperature, the mean aspect ratio of the  $\alpha$  grains increased. Rolling prior to annealing at lower temperatures followed by lower annealing temperature showed nearly equiaxed  $\alpha$  grains with finer grain sizes. This indicates that the material initially with coarser and higher aspect ratio  $\alpha$  platelet structure revealed a lamellar structure on annealing which was absent in the samples with initial fine lamellar structure.

This behaviour can be explained on the basis of work of Weiss et.al [56]. They have observed that if the  $\alpha$  plate width is larger, i.e more than two times the penetration depth of the  $\beta$  cusps, the separation of  $\alpha$  platelets does not occur readily. For thicker  $\alpha$  platelets, lamellar microstructures prevail even after annealing leading to aggregates of necklace like structure.



(a)



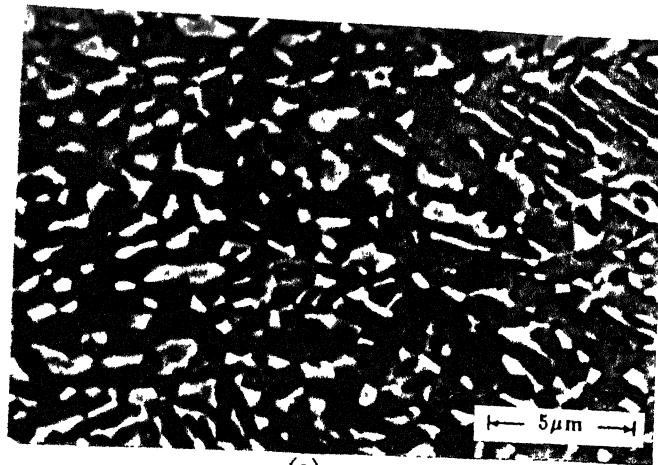
(b)



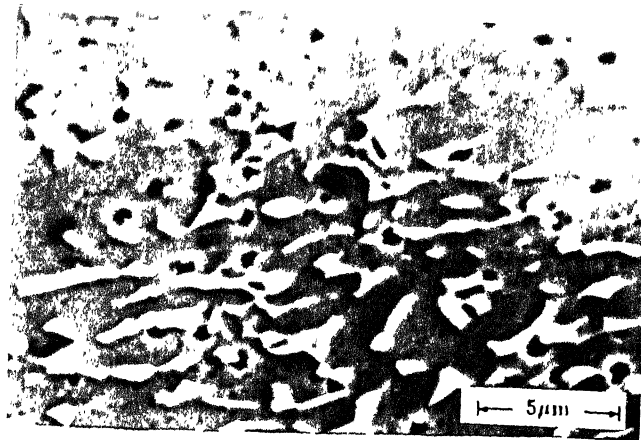
(c)

Fig. 4.32

Micrographs Of The Specimens Annealed At 800 °C For 1 Hour Following 60 % Thickness Reductions In ( $\alpha+\beta$ ) Rolling At Different Temperatures.  
 (a) 850 °C    (b) 900 °C    (c) 950 °C



(a)



(b)



(c)

Fig. 4.33

Micrographs Of The Specimens Annealed At 850 °C For 1 Hour Following 60 % Thickness Reductions In ( $\alpha+\beta$ ) Rolling At Different Temperatures.

(a) 850 °C    (b) 900 °C    (c) 950 °C

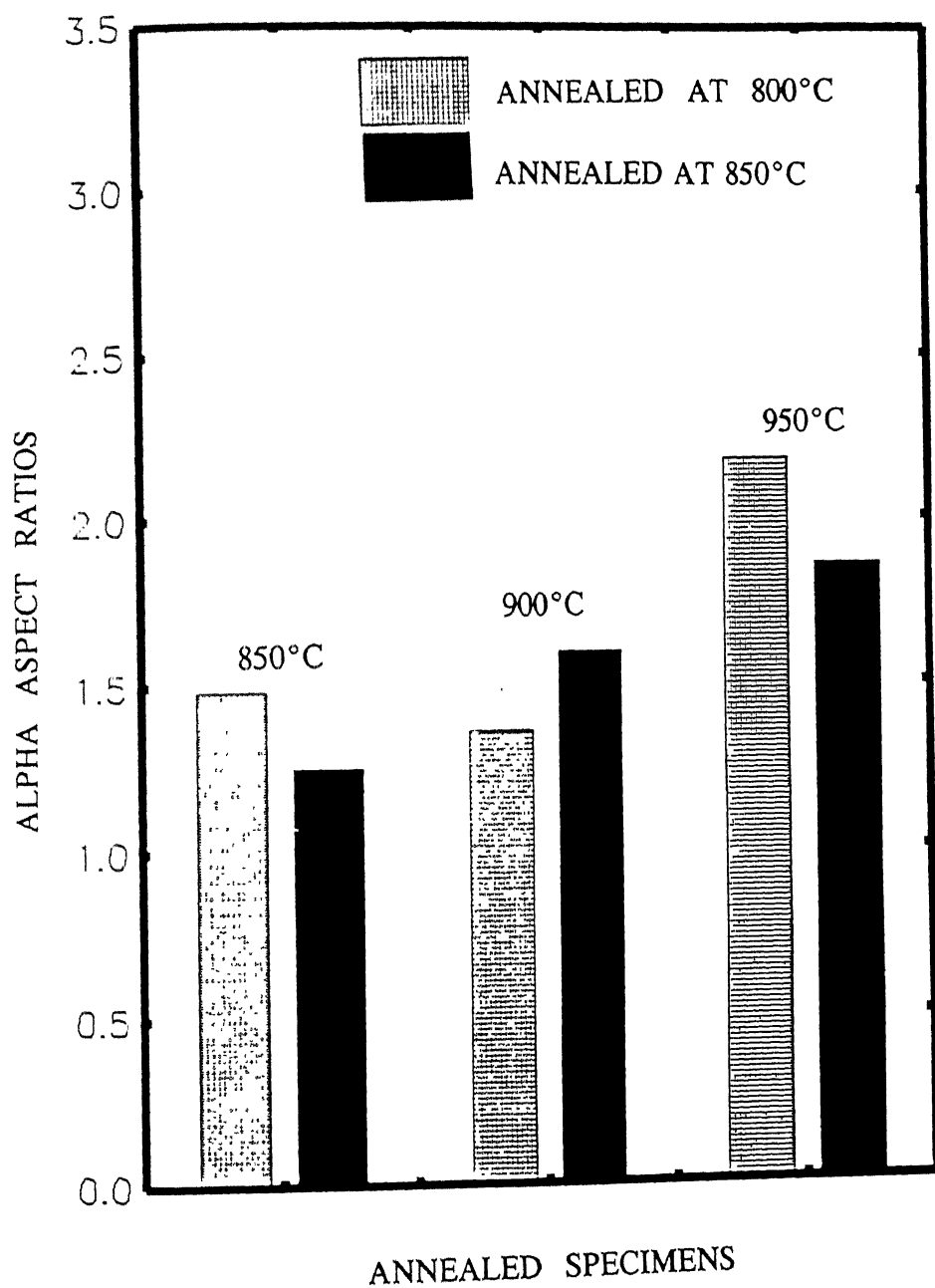


Fig. 4.34 Bar Graph Illustrating Variation In Alpha Grain Aspect Ratios After Annealing At 800 °C and 850 °C For 1 Hour Of The Samples Rolled At Three Different ( $\alpha + \beta$ ) Temperatures.

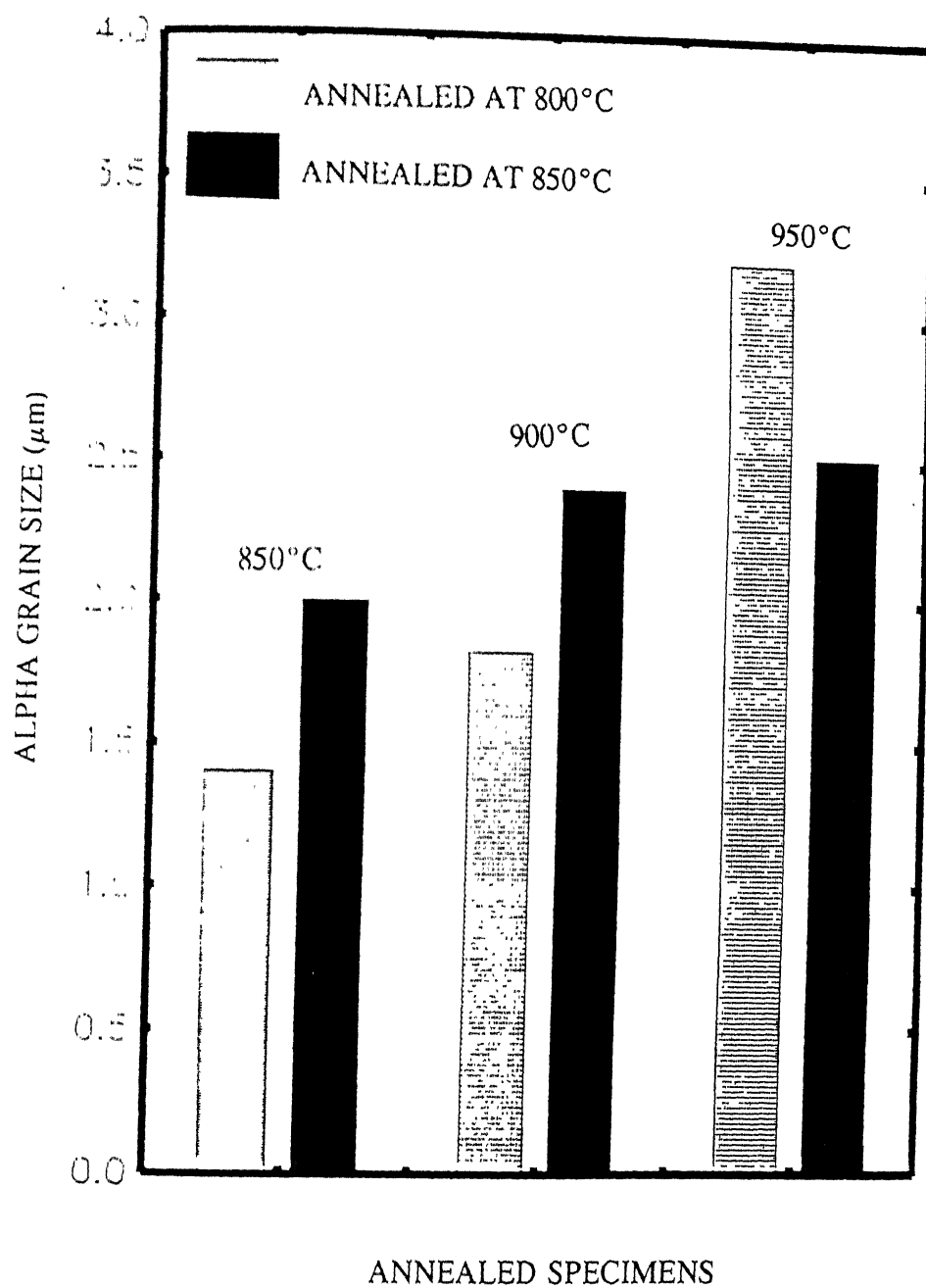


Fig. 4.35 Bar Graph Illustrating Variation In Mean Alpha Grain Sizes After Annealing At 800  $^{\circ}\text{C}$  and 850  $^{\circ}\text{C}$  For 1 Hour Of The Samples Rolled At Three Different ( $\alpha + \beta$ ) Temperatures.



#### 4.5 SUPERPLASTIC BEHAVIOUR OF THERMO-MECHANICALLY PROCESSED Ti-632Si ALLOY:

Control of both primary as well as secondary  $\alpha$  phase morphology in  $(\alpha+\beta)$  titanium alloys through thermo-mechanical processing is of great importance in achieving improved superplastic properties in titanium alloys. Under thermal processing the  $\beta$  phase either is retained at room temperature or transforms to a Widmanstatten structure after air cooling. In the latter case, the material loses the basic prerequisites of equiaxed grains for superplasticity. Slowing down the cooling rate during  $\beta$  transformation results in coarse plates of  $\alpha$ . Thus, the deformation processing of  $(\alpha+\beta)$  titanium alloys is generally carried out by rolling or extrusion followed by an annealing treatment, which transforms as-worked inhomogenously elongated grains of  $\alpha$  into nearly equiaxed  $\alpha$ . It has been pointed out [59] that, not only the deformation mechanism, but also the dynamics of grain boundary dislocation activity are altered, if grains are elongated rather than equiaxed. This means that elongated microstructures reduce superplastic deformation.

It has already been stated earlier that the thermo-mechanical processing of Ti-632Si alloy was carried out with the objectives of

- a. Conditioning of  $\beta$  grains prior to hot rolling of the alloy in  $(\alpha+\beta)$  phase field;
- b. Conditioning of  $\alpha$  platelets/lamellae prior to hot rolling of the alloy in  $(\alpha+\beta)$  phase field so that the transformation of platelet/lamellar primary  $\alpha$  to equiaxed primary  $\alpha$  leads to a refined microstructure.

A few specimens of Ti-632Si alloy, after their hot rolling in the  $(\alpha+\beta)$  phase field were also subjected to recrystallization annealing in the  $(\alpha+\beta)$  phase field. These objectives were achieved by processing Ti-632Si alloy through the following microstructural states in different processing routes.

Route 1 : Coarse recrystallized  $\beta$  grains water quenching  
Packets of  $\alpha'$  (martensite) reheating  
Acicular  $\alpha$  in the matrix of  $\beta$   $(\alpha+\beta)$  hot rolling  
Acicular-Equiaxed  $\alpha$  in the matrix of  $\beta$  water quenching  
Acicular equiaxed  $\alpha$  in the matrix of  $\alpha'$

Route 2 : Coarse recrystallized  $\beta$  grains  $\beta$  hot rolling  
 Pancaked  $\beta$  grains water quenching  
 Packets of  $\alpha'$  (martensite) reheating  
 Acicular  $\alpha$  in the matrix of  $\beta$   $(\alpha+\beta)$  hot rolling  
 Acicular-Equiaxed  $\alpha$  in the matrix of  $\beta$  water quenching  
 Acicular-Equiaxed  $\alpha$  in the matrix of martensite  $\alpha'$

Route 3 : Coarse recrystallized  $\beta$  grains  $\beta$  hot rolling  
 Pancaked  $\beta$  grains water quenching  
 Packets of martensite  $\alpha'$   $\beta$  annealing  
 Fine recrystallized  $\beta$  grains water quenching  
 Packets of martensitic  $\alpha'$  reheating  
 Acicular  $\alpha$  in the matrix of  $\beta$   $(\alpha+\beta)$  hot rolling  
 Acicular - Equiaxed  $\alpha$  in the matrix of  $\beta$  water quenching  
 Acicular-equiaxed  $\alpha$  in the matrix of martensitic  $\alpha'$ .

Characteristics of the microstructural features of Ti-632Si alloy processed through the above routes have already been discussed. Some of the above specimens were subjected to tests pertaining to the study of their superplastic behaviour. Results obtained from these tests are discussed in the present section.

#### 4.5.1 Effect of Temperature and Strain Rate on Strain Rate Sensitivity of Therm-Mechanically Processed Ti-632Si Alloy

The evaluation of the strain rate sensitivity was done on the material processed through Route 3. For this purpose strain rate jump tests were carried out 850°C, 900°C and 925°C. Tests could not be carried out at higher temperatures due to the limitations of the set-up. The strain rates for these tests were varied from  $10^{-4}\text{s}^{-1}$  to  $5.5 \times 10^{-1}\text{s}^{-1}$ . Figures 4.36(a) - (c) show the load vs elongation curves for the samples tested at 850°C, 900°C, 925°C respectively. From these curves  $\log(\text{true stress})$  vs  $\log(\text{strain rates})$  were plotted for all the three conditions. These plots are shown in Figure 4.37. Comparison of these graphs indicates that the flow stress of thermo-

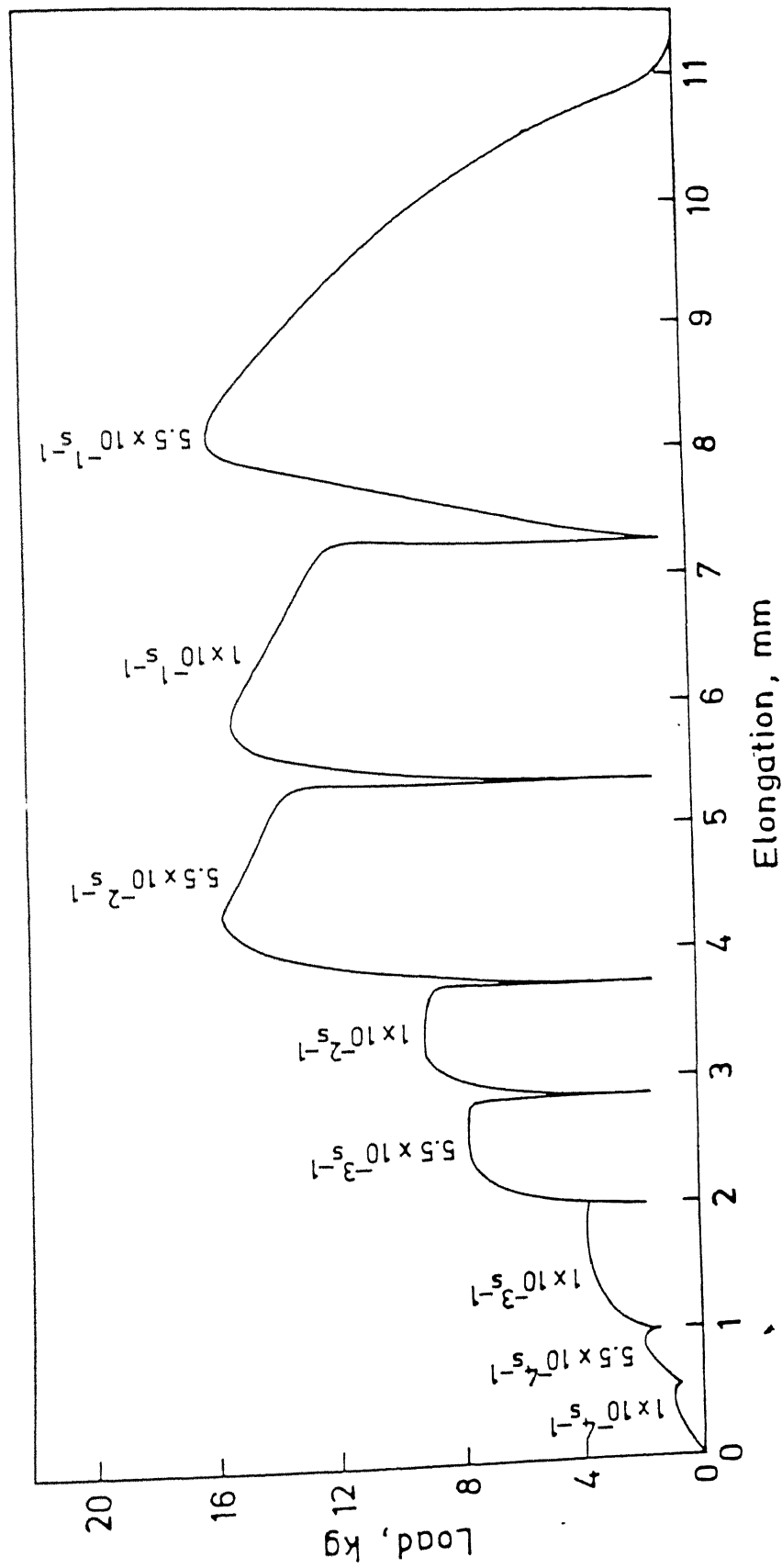


Fig. 4.36 (a) Load vs Elongation Curve For Route 3 Sample Tested At 850°C.

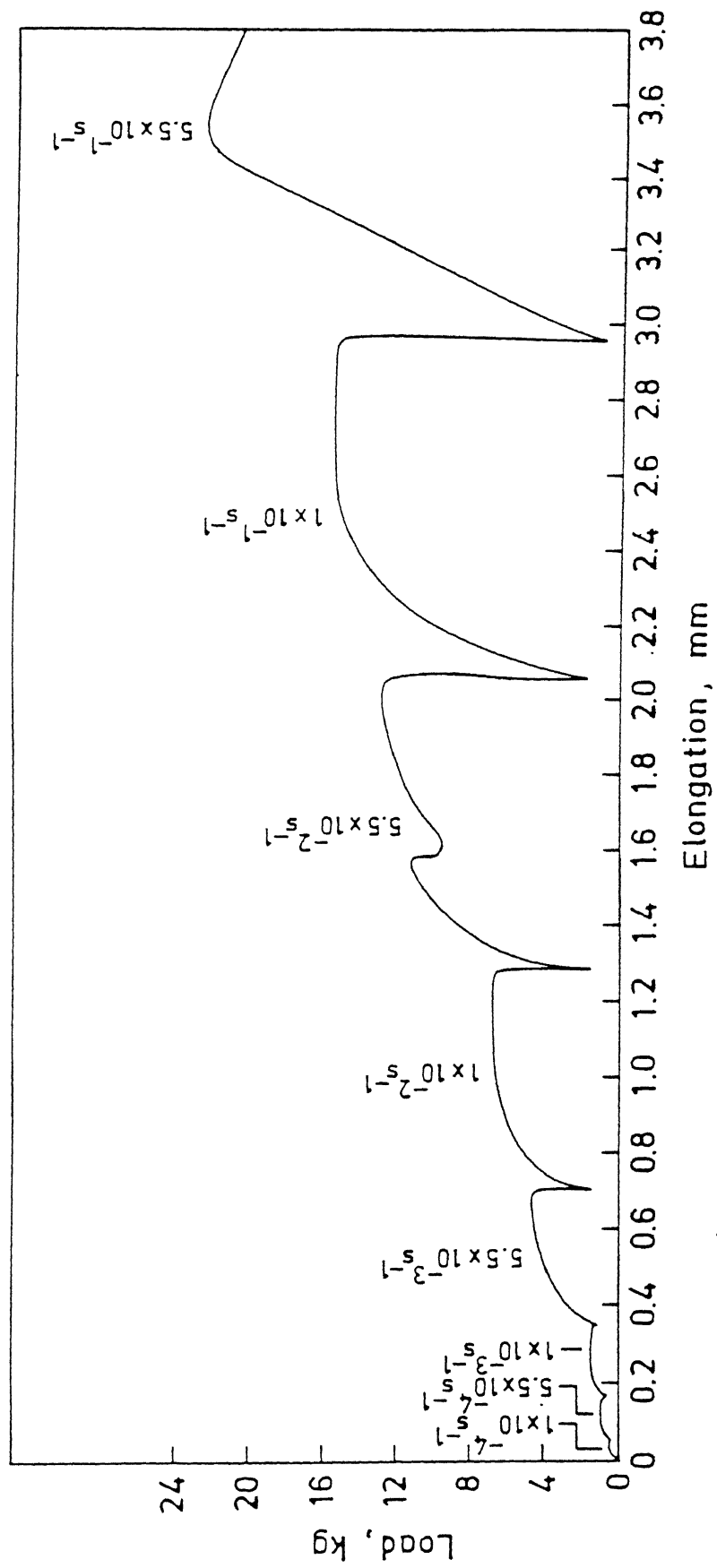


Fig. 4.36 (b) Load vs Elongation Curve For Route 3 Sample Tested At 900°C.

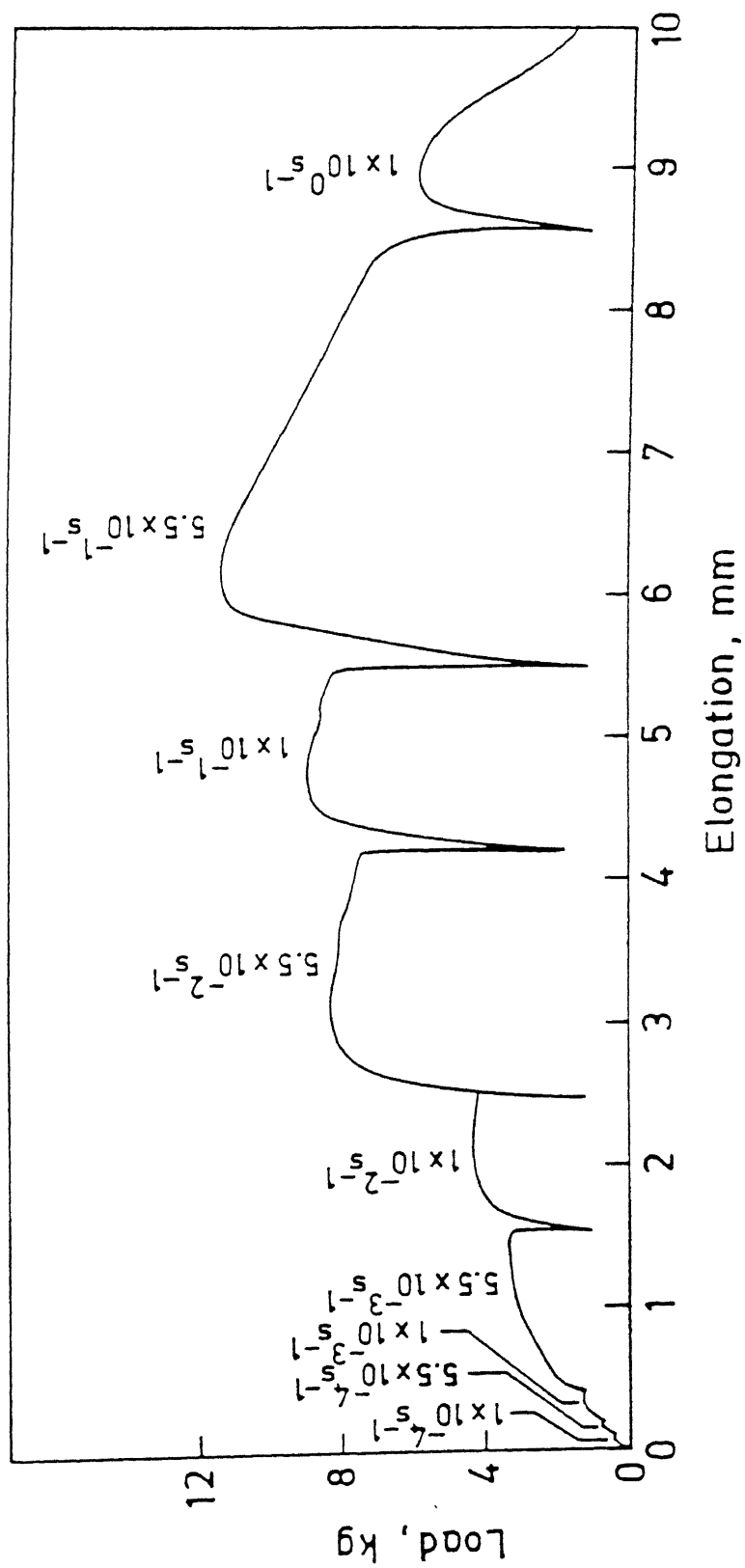


Fig. 4.36 (c) Load vs Elongation Curve For Route 3 Sample Tested At 925°C.

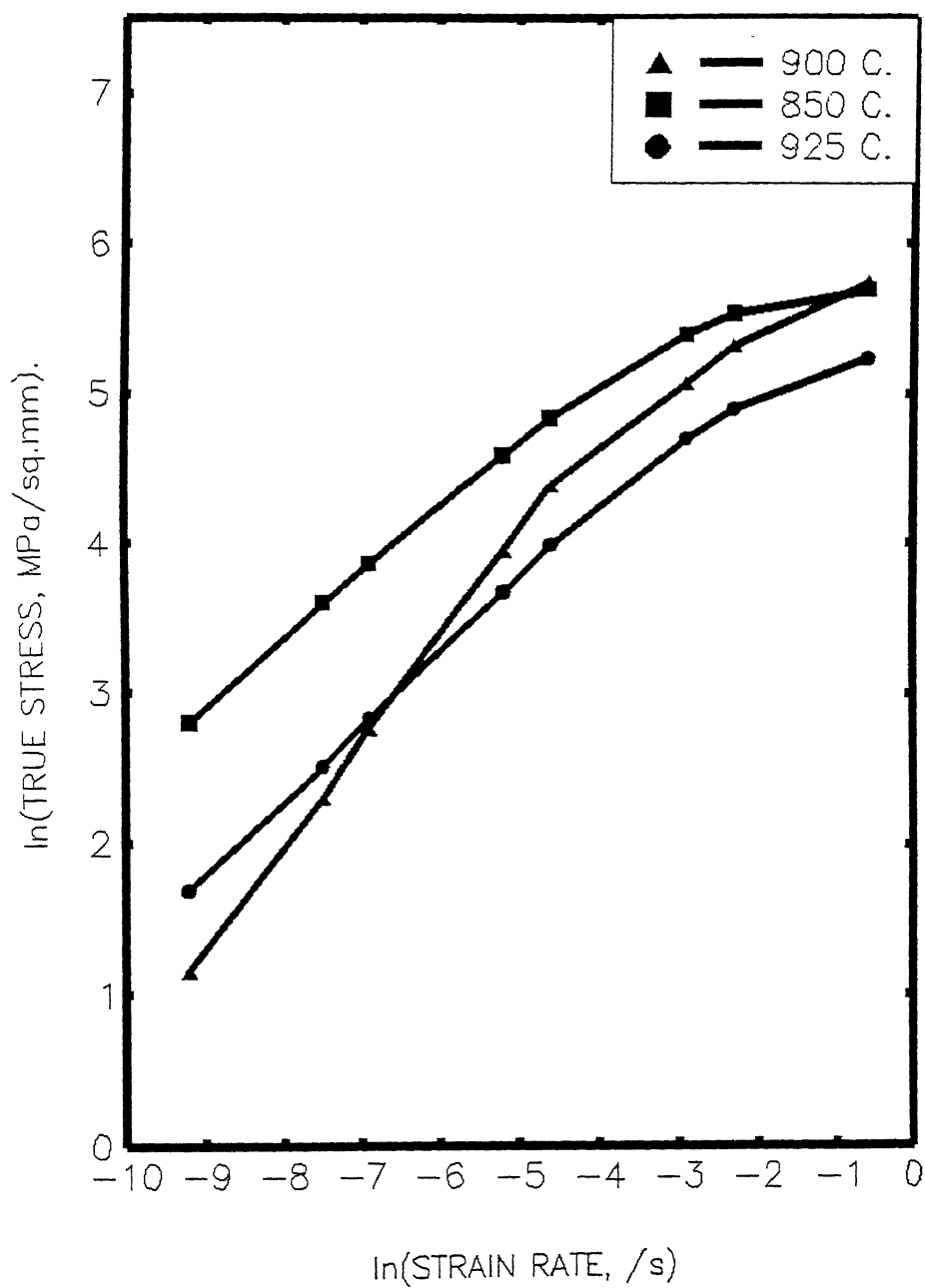


Fig. 4.37 ln(Flow Stress) vs ln(Strain Rate) Plots For Route 3 Samples Tested At 850,900 and 925°C.

mechanically treated Ti-632Si alloy processed through Route 3 increased with decreasing the temperature of deformation. This is speculated to be due to (i) the increase of hcp  $\alpha$  phase content with decrease in temperature which has lower diffusivity and deformability and (ii) higher resistance to deformation of both  $\alpha$  as well as  $\beta$  phases at lower deformation temperature.

From the slopes of the log (stress) vs. log (strain rate) curves at different temperatures, strain rate sensitivity,  $m$ , values were obtained at different strain rates and were plotted as a function of strain rate. The variation of  $m$  with strain rate at different temperatures is shown in Figure 4.38. It can be observed from this figure that a maximum  $m$  of 0.76 was exhibited by sample tested at 900°C with strain rate  $10^{-3}\text{s}^{-1}$ . and with increasing or decreasing strain rates, the  $m$  value decreased. The sample tested at 925°C showed maximum  $m$  value of 0.6 at  $10^{-3}\text{s}^{-1}$ . On the other hand, at 850°C a maximum  $m$  value of 0.46 only was obtained at the strain rate of  $5.5 \times 10^{-4}\text{s}^{-1}$ .

It can be seen that the log (true stress) vs. log (strain rate) curves (Figure 4.37) show a sigmoidal behaviour with three different regimes of deformation : Region I and Region III at low and high stress, where the value of  $m$  is low, and an intermediate Region II.

#### 4.5.2 Effect of Temperature on Elongation till Failure

It is well known that the temperature is a fundamentally important forming parameter for superplasticity which occurs above  $0.5 T_m$ . In addition, it has a significant role on the phase stability of the present alloy. In ( $\alpha+\beta$ ) titanium alloys depending upon the temperature of deformation  $\alpha$ , ( $\alpha+\beta$ ) or  $\beta$  phases may exist. The physical and mechanical properties of  $\alpha$  and  $\beta$  phases are significantly different. For example, the flow properties of the  $\alpha$  and  $\beta$  phases are quite different and also the self diffusivity of the  $\beta$  phase differs with two orders of magnitude than that of the  $\alpha$  phase.

For the material processed through Route 3 the elongation-to-failure tests were done at 900°C and 925°C respectively with a strain rate of  $5.5 \times 10^{-3}$ . The load elongation curves for these are shown in Figures 4.39(a) and 4.39(b) respectively. It was observed that flow stress was lower

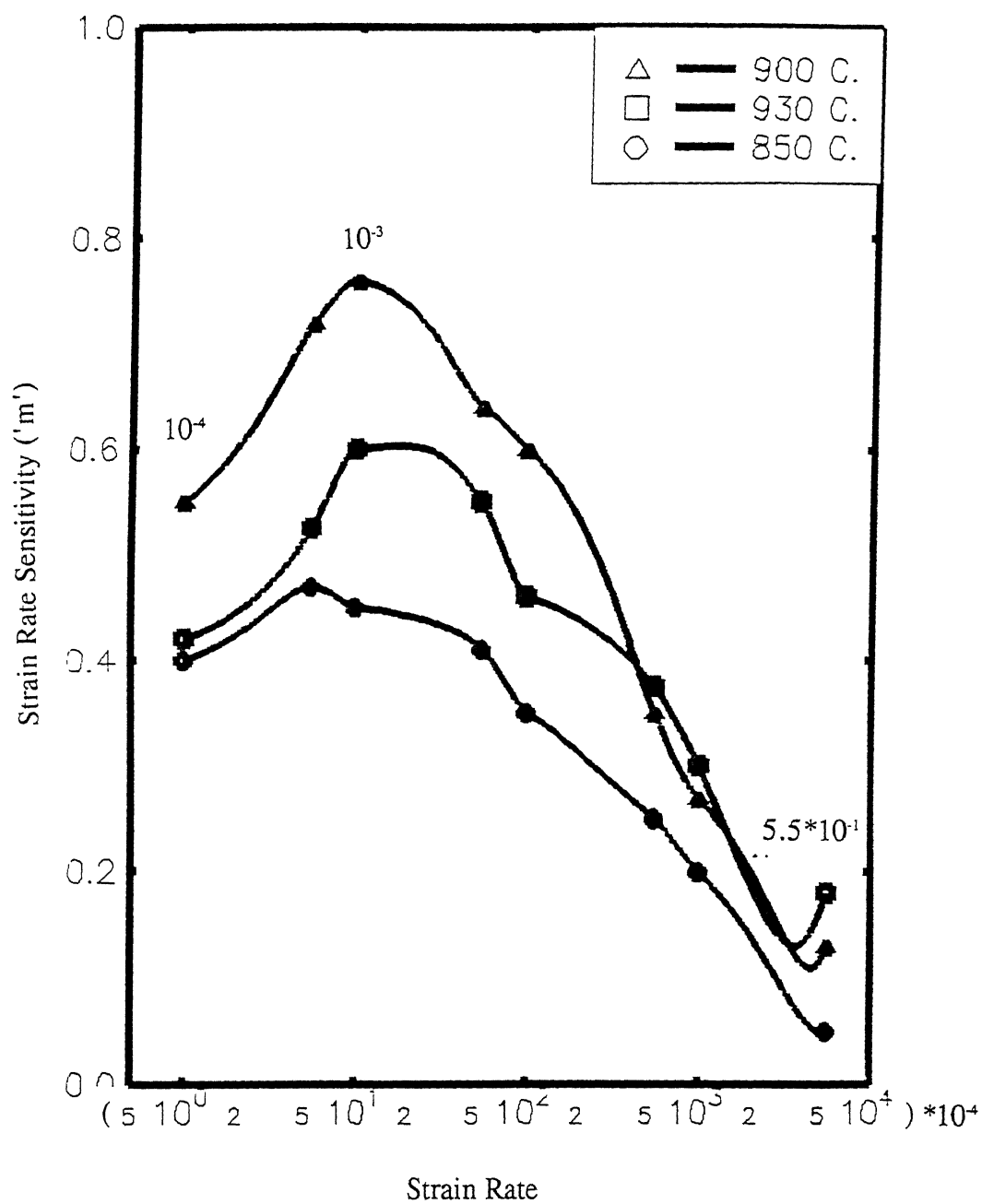


Fig. 4.38 Variation Of Strain Rate Sensitivity ( $m'$ ) With Strain Rate At Different Temperatures.



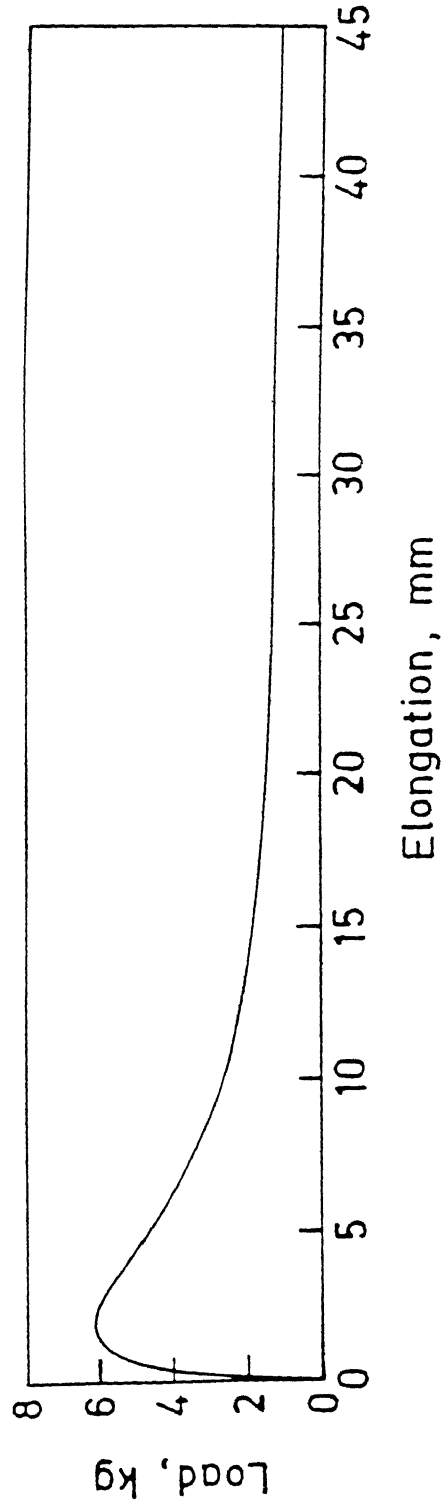


Fig. 4.39 (a) Load vs elongation Curve For Route 3 Sample Tested At 900°C and Strain Rate :  $5.5 \times 10^{-3}$ .

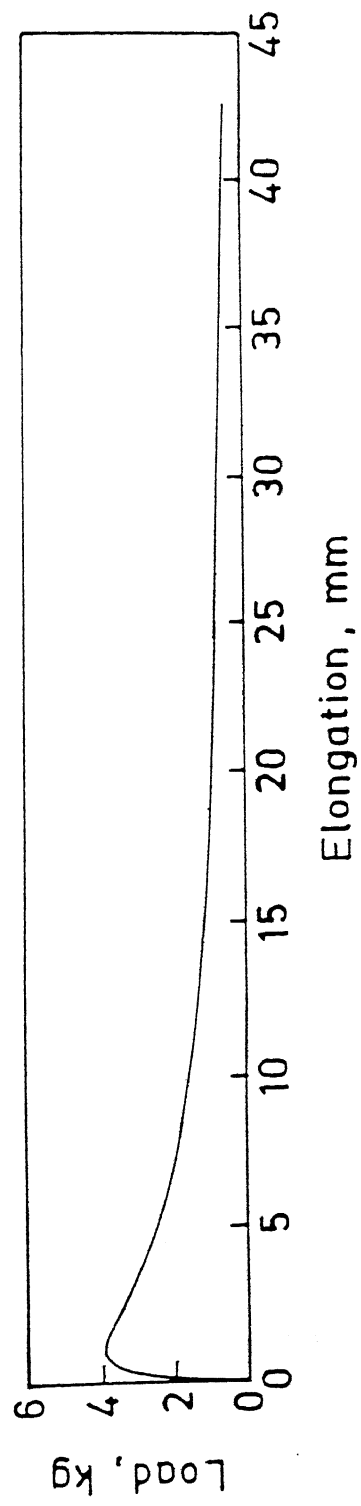


Fig. 4.39 (b) Load vs Elongation Curve For Route 3 Sample Tested At 925°C  
and Strain rate :  $5.5 \times 10^{-3}$ .

(3.92 MPa) for sample deformed at 925°C than that deformed at 900°C (5.8 MPa). On the other hand, the total tensile elongation was found to be higher in sample tested at 900°C. An elongation of 871% was recorded at 900°C while at 925°C, the elongation was 809%. This behaviour is in agreement with the fact that in the strain rate jump tests done at 900°C at the strain rate of  $5.5 \times 10^{-3}/s^{-1}$  the value of strain rate sensitivity was 0.65 while for 925°C and the same strain rate it was 0.55. This behaviour can be explained in terms of the  $\beta$  phase content during deformation because the  $\alpha/\beta$  phase ratio plays an important role in the deformation behaviour of ( $\alpha + \beta$ ) titanium alloys [52]. The importance of the strain rates is associated with the significant differences in properties between  $\alpha$  and  $\beta$  phase. For instance, in the temperature range used for superplastic forming of titanium alloys, the  $\beta$  phase is considered to be softer and its diffusivity is two orders of magnitude higher than that of the  $\alpha$  phase. Therefore, a finite fraction of the  $\alpha$  phase significantly restricts the grain growth because, in order to transfer highly partitioned alloying elements, long range diffusion is necessary. In the absence of second phase, the  $\beta$  phase will rapidly grow to diameters well in excess of 50  $\mu m$  at temperatures above  $\sim 760^\circ C$ .

As the temperature increases, volume fraction of the  $\beta$  phase increases at the expense of  $\alpha$  phase. Consequently, rapid grain growth is expected to occur in the  $\beta$  phase, thus reducing the  $m$  value and consequently the superplasticity. At about 850°C, the volume fraction of  $\beta$  phase is very small, which may be attributed to the lower  $m$  values than at 900°C and 925°C. On the other hand, at 925°C the  $\beta$  phase fraction is expected to be more than the optimum. The results of earlier investigation [60] have shown that the volume fraction of the  $\beta$  phase can also increase during superplastic deformation. At the lower temperatures, it is hypothesized that diffusivities of  $\alpha$  and  $\beta$  phases are too low and even with strain enhancement, no additional stabilization of  $\beta$  phase takes place [60]. From the above results, it is inferred that the optimum temperature for superplastic deformation of Ti-632Si alloy, thermo-mechanically processed through Route 3, is 900°C and optimum strain rate is  $10^{-3}/s$ . However, Kaibyshev has reported the optimum temperature for superplastic deformation of this alloy to be 950°C. The decrease in superplastic forming temperature in the present case is attributed to the microstructural state through processing by the newly designed Route 3.

The sample before testing were not subjected to recrystallization annealing and were in their as-rolled and water-quenched condition with hot rolling being done at 850°C. The X-ray diffraction pattern from the samples prior to their testing is shown in Figure 4.40. This figure indicates that the structure of the alloy prior to superplastic deformation consisted of a mixture of the hcp  $\alpha$ , the orthorhombic martensitic phase  $\alpha''$  and the metastable bcc beta.  $\beta_m$  instead of ( $\alpha+\beta$ ) structure. Huang and Lipheng [61] have shown that the orthorhombic martensite  $\alpha''$  can be stabilized in ( $\alpha+\beta$ ) Ti alloys through proper heat treatments and  $\alpha''$  reduces the optimum superplastic temperature of titanium alloys. It has been shown that for the alloy Ti-6Al-1.5 Cr-2.5Mo-0.5Fe-0.3S the optimum superplastic deformation temperature of approximately 900°C which is optimized by means of conventional heat treatments can be reduced to 800°C when the alloy contains  $\alpha''$  phase. It has been suggested [61] that during heating  $\alpha''$  and  $\beta_m$  get transformed to ( $\alpha+\beta$ ) with many vacancies formed in the transformed structure. Due to the presence of vacancies, the binding force of grain boundary is weakened, the resistance to grain boundary sliding is lessened, so that superplastic forming process can be proceeded easily with less flow stress at lower temperatures. Therefore, it may be inferred that since Ti-632Si alloy processed through Route 3 contains the orthorhombic phase  $\alpha''$ , its optimum superplastic deformation temperature gets reduced. This suggestion, however, requires more work to be done. Further, it requires to be seen whether  $\alpha''$  forms or not in the alloy processed through Route 1 and Route 2.

#### 4.5.3 Microstructural Changes in Ti-632Si Alloy during Superplastic Deformation:

Microscopic examination (SEM) was also done on the superplastically deformed sample which had shown maximum elongation at 900°C with strain rate  $5.5 \times 10^{-3}/s$ . Figure 4.41 show the microstructures of sample at its various locations. The tensile direction is also marked in the figure. Although it appears from these microstructures that the overall features remain primarily equiaxed, a closer look at them reveals that the structure is relatively coarser near the fracture tip and it becomes gradually finer as one moves away from the fracture tip towards the shoulder. This leads to the understanding that the grain growth during tensile testing is more pronounced in the central part, and is maximum near the fracture tip. This is quite likely because, as the plastic instability of the sample is more towards the central zone higher stresses develop in it

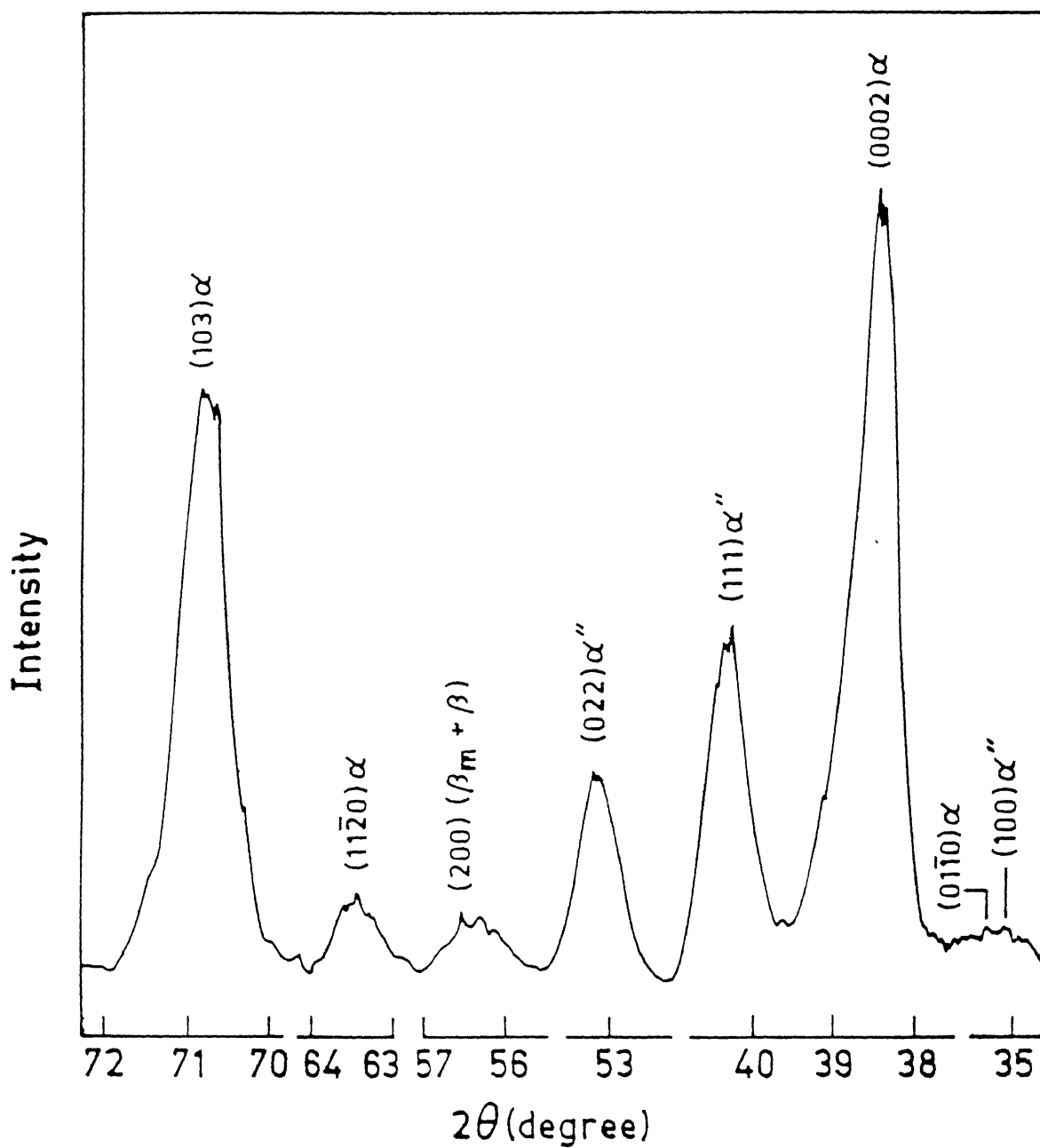


Fig. 4.40 X-Ray Diffraction Pattern For The Specimen (Route 3) Quenched In Water After Rolling At 850°C.

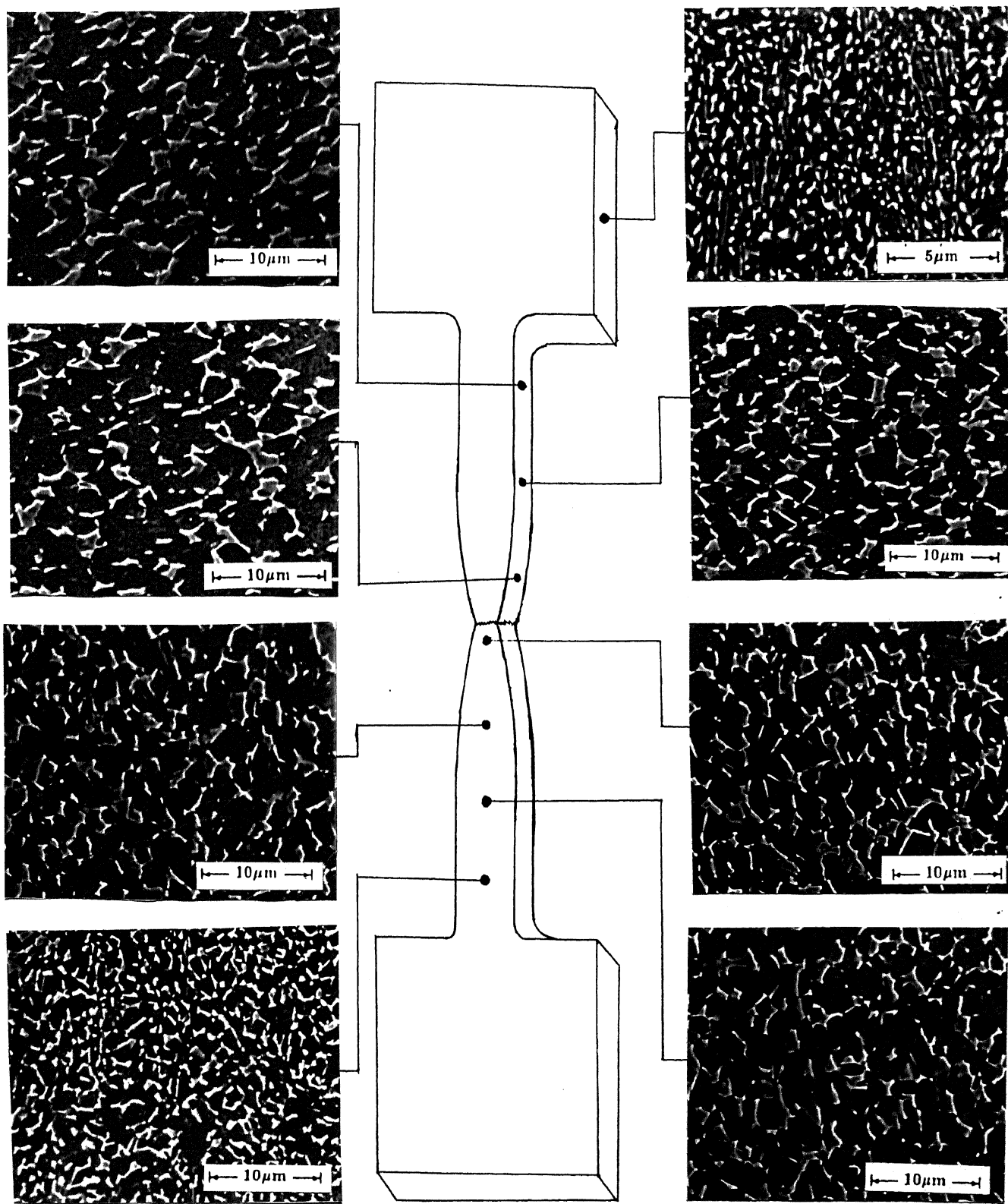


Fig. 4.41 Microstructures Of The Elongated Sample At Various Locations.  
Testing Conditions : 900°C,  $5.5 \times 10^{-3} \text{s}^{-1}$

central zone. Therefore due to the combination of higher stresses and temperature, the rate of grain coarsening increases in the central zone. As the grain size increases the superplastic ability of the material reduces and leads to fracture. This may be the reason for coarser grains near the fracture tip. In addition to the coarsening, it is also observed that the grains near the fracture tip get slightly elongated in the tensile direction.

Figure 4.42 shows the microstructure just-near the fractured part of the specimen tested at 900°C with strain rate  $5.5 \times 10^{-3}/s$  which contains cracks. It can be observed that these cracks or voids tend to extend towards the direction perpendicular to the tensile axis and occur near  $\alpha/\beta$  phase boundaries.

#### 4.5.4 Activation Energy for Superplastic Deformation:

The data obtained from the strain rate jump tests was used for determining the activation energy of superplasticity for Ti-632Si alloy in the temperature range 850 to 925°C. Figure 4.43 shows the plot of  $\ln \dot{\epsilon}$  vs  $\ln (-1/RT)$  at different true stresses. Activation energy was determined from the change in strain rate with the change in temperature as shown in the following equation

$$Q = [\partial \ln \dot{\epsilon}] / [\partial (1/(-RT))]$$

where  $\dot{\epsilon}$  = strain rate, R = gas constant and T = absolute temperature.

The activation energy obtained was 38-42 Kcal/mole. The obtained activation energy is higher than those of self diffusion ( $Q_{\text{self Diffusion of } \alpha} = 40.4$  and  $Q_{\text{self diffusion of } \beta} = 31.3$ ). The reason that the activation energy is higher is perhaps due to the fact that microstructure does not remain stable with the change in temperature as normally assumed. The increase in temperature is likely to exaggerate the strain rate enhancement thereby giving a high activation energy.

#### 4.5.5 Effect of Recrystallization on the Superplastic Behaviour

For studying the effect of recrystallization on superplastic behaviour, the as ( $\alpha + \beta$ ) roll sheets obtained from Route 3 were recrystallized at 850°C for 1 hr and 4 hrs respectively.

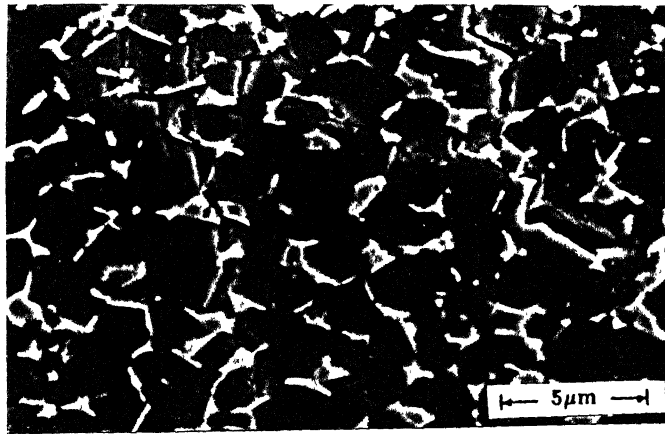


Fig.4.42      Microstructure of the specimen adjacent to the fracture tip showing the propagation of cracks  
(Testing Conditions: Temperature 900°C,  
Strain rate  $5.5 \times 10^{-3}$ )



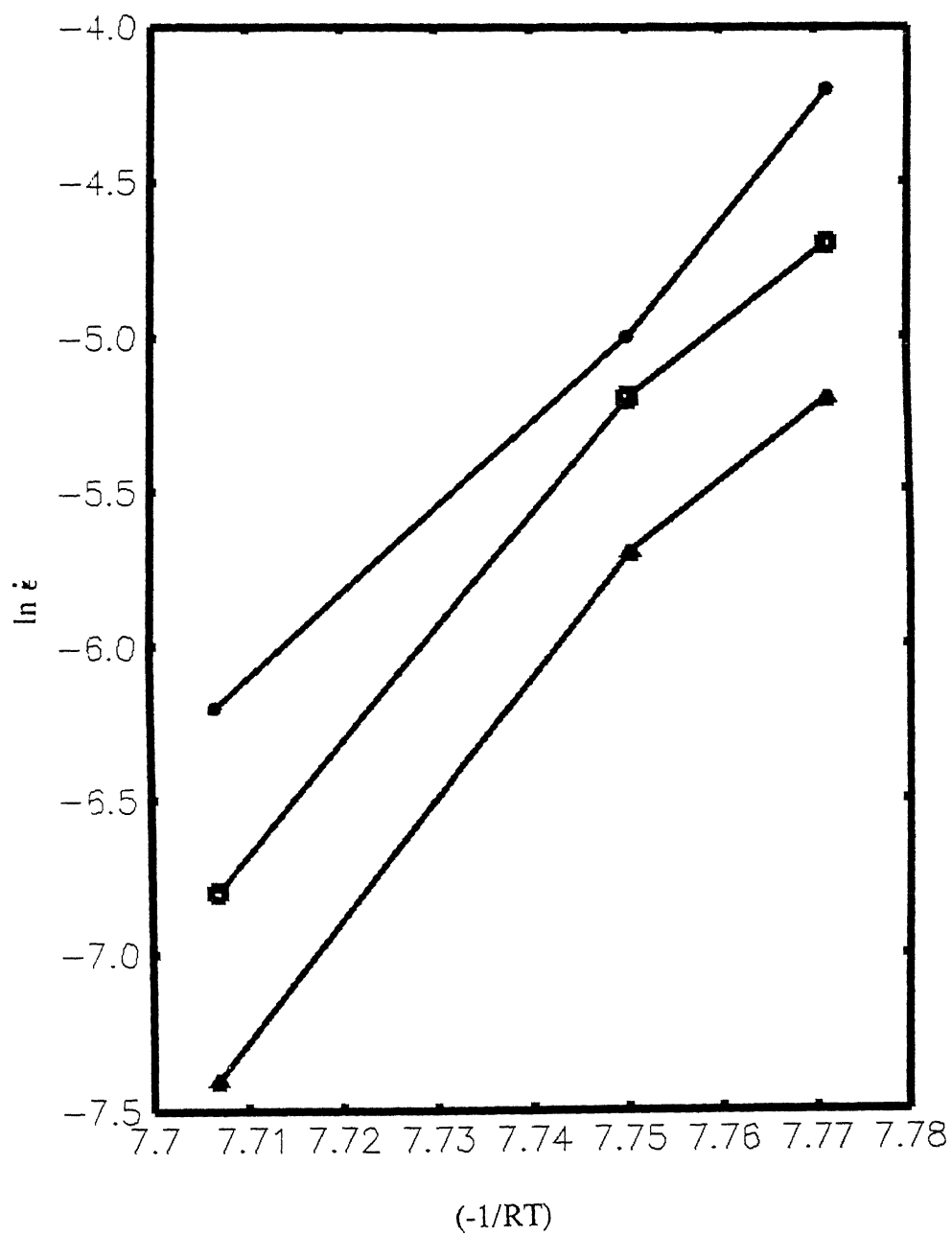


Fig. 4.43

Graph Of  $\ln(\text{Strain Rate})$  vs  $[1/(RT)]$  For Three Different Flow Stresses Obtained From

Fig. 4.37

While the grain size of the as-rolled material was  $1.2\ \mu\text{m}$  that of recrystallized material was  $2\ \mu\text{m}$  and  $2.3\ \mu\text{m}$  respectively for the recrystallization times of 1 hr and 4 hrs respectively. (Micrographs of recrystallized structure are already shown in Figure 4.41). The temperature of testing for these specimens was  $900^\circ\text{C}$  and the strain rates varied from  $10^{-4}/\text{s}$  to  $5.5 \times 10^{-1}/\text{s}$ . The load vs elongation curves obtained from the test are shown in the Figure 4.44 and 4.45 unrecrystallized, 1 hr annealed at 850 and 4 hrs annealed at 850 respectively from these curves the  $\log$  (flow stress) vs  $\log$  (strain rate) were plotted. From these load elongation curves,  $m$  values were calculated. The  $m$  values as a function of strain rate for the as rolled and annealed samples are shown in Figure 4.46. From the values of flow stress and  $m$ , it is observed that as the grain size increased due to recrystallization, the flow stress also increased and  $m$  values decreased. Maximum  $m$  value for the recrystallized alloy was observed at the strain rate of  $10^{-3}/\text{s}$  in the as rolled sample, i.e., with recrystallization, the superplastic deformability decreases. It is possible that recrystallization of  $\alpha$  prior to use in superplastic forming allows detrimental grain growth to occur during the heat up period of the material.

Figure 4.47 shows the structure of the as rolled ( $\alpha + \beta$ ) alloy reheated at  $900^\circ\text{C}$ , soaked for 15 minutes and water quenched. The structure consists of very fine  $\alpha$  grains which are nearly equiaxed in nature with average  $\alpha$  grain size of  $\approx 1.5\ \mu\text{m}$  i.e., just before superplastic deformation at  $900^\circ\text{C}$ , the structure is equiaxed and fine. While if we use recrystallized samples for superplastic deformation the specimens have a grain size of  $2.25\ \mu\text{m}$  even before reheating at the superplastic deformation temperature. This large difference in the grain size makes an effect on the superplastic deformability of this alloy. If the annealing treatment is eliminated, lower flow stresses and higher strain rate sensitivity result.

Thus the above results indicate that reheating after hot rolling is undesirable, and that the material should be in the as deformed state. This is supported by Gordon et. al [ ] on cold rolled Ti6Al4V. Plate specimens with initial grain size of  $5\ \mu\text{m}$  were cold rolled with 25, 50 and 75% reduction. Some of these specimens were further recrystallized by annealing at  $900^\circ\text{C}$  for 3 hr. Tensile tests made on these specimens at  $900^\circ\text{C}$  with a strain rate of  $3 \times 10^{-4}/\text{s}$  revealed that the as cold rolled specimens gave a much larger total elongation than the recrystallized specimens. While total elongation of 75% cold rolled specimens was 1115%, the

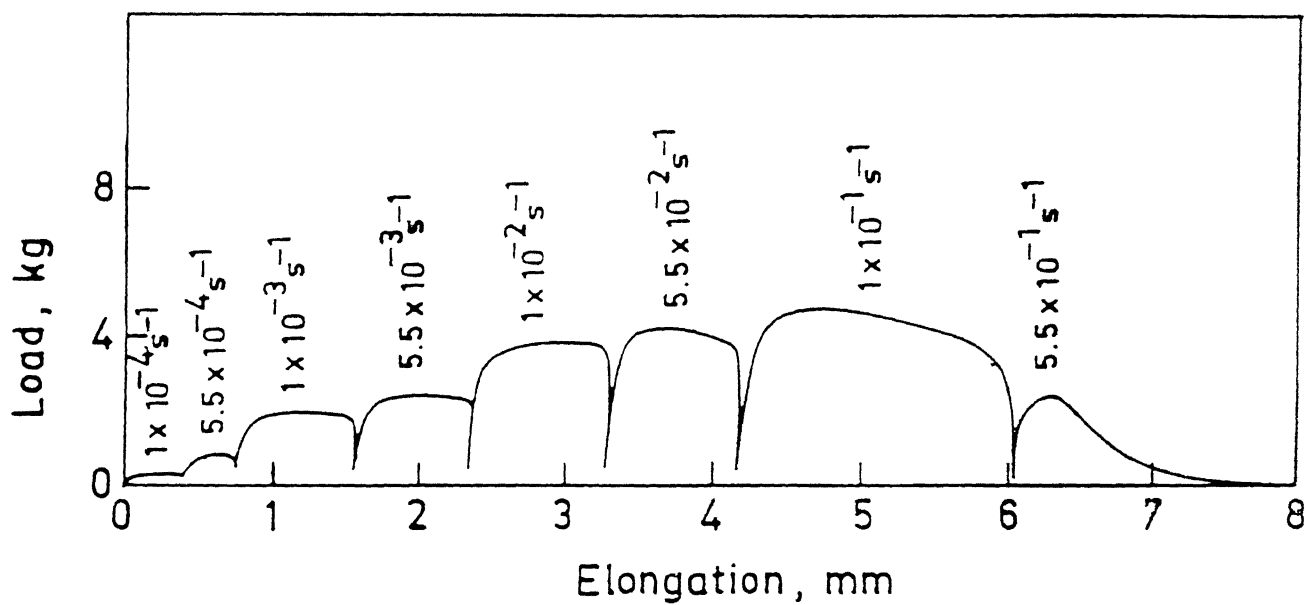


Fig. 4.44 Load vs Elongation Curve For Annealed ( 850°C , 1 hour )  
Route 3 Sample Tested At 900°C.

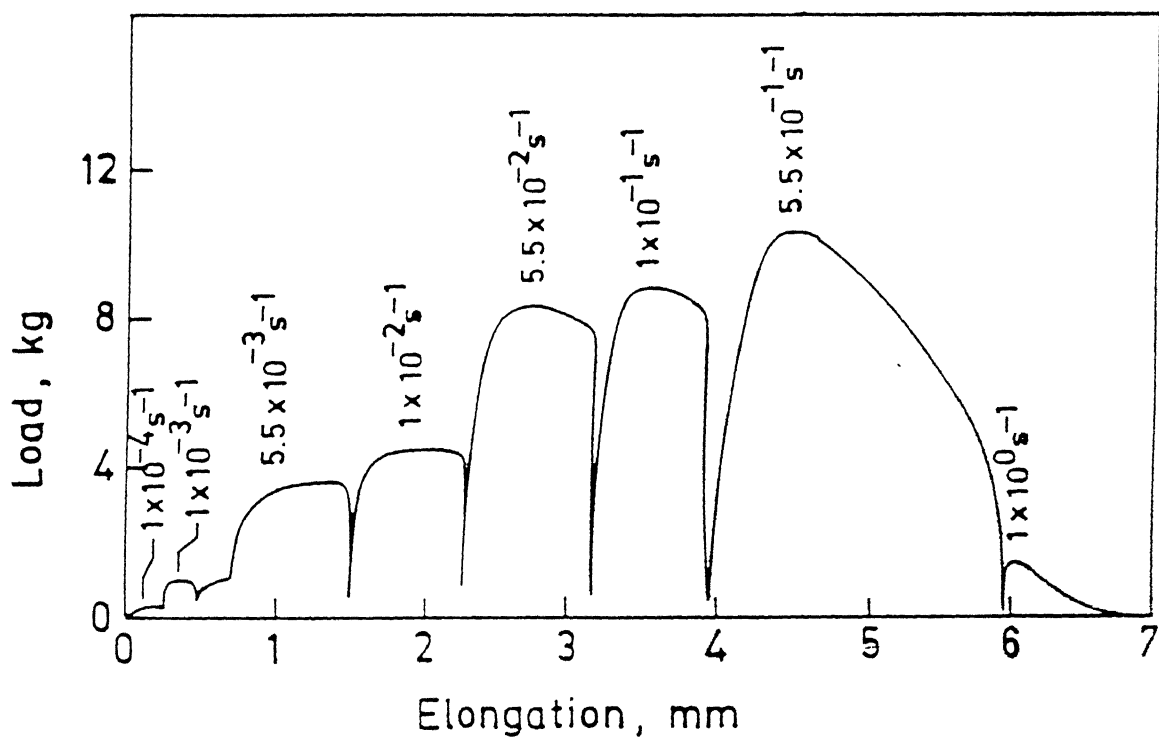


Fig. 4.45 Load vs Elongation Curve For Annealed ( 850°C , 4 hours )  
Route 3 Sample Tested At 900°C.

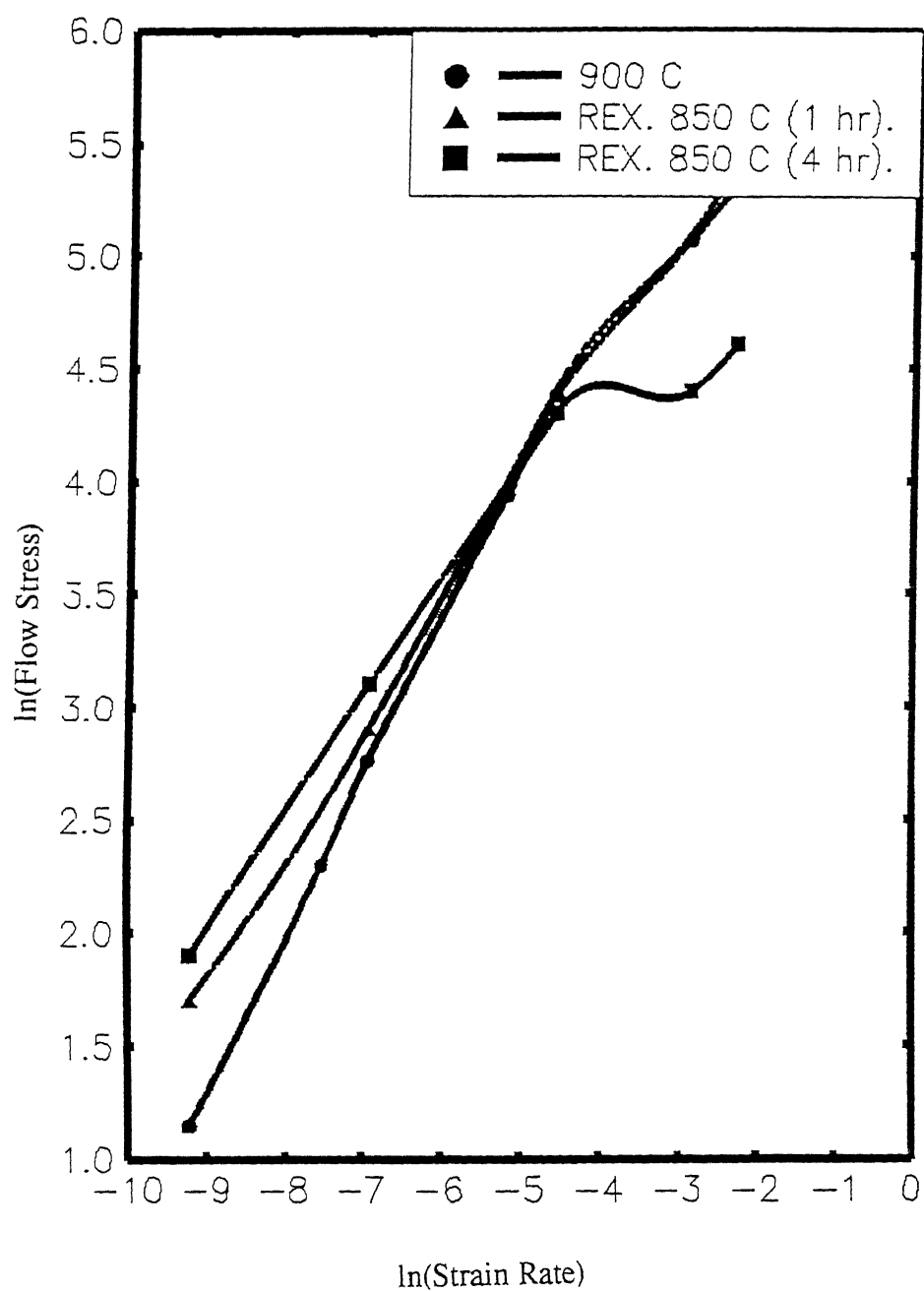


Fig. 4.46  $\ln(\text{Flow Stress})$  vs  $\ln(\text{Strain Rate})$  For Annealed Route 3 Samples.

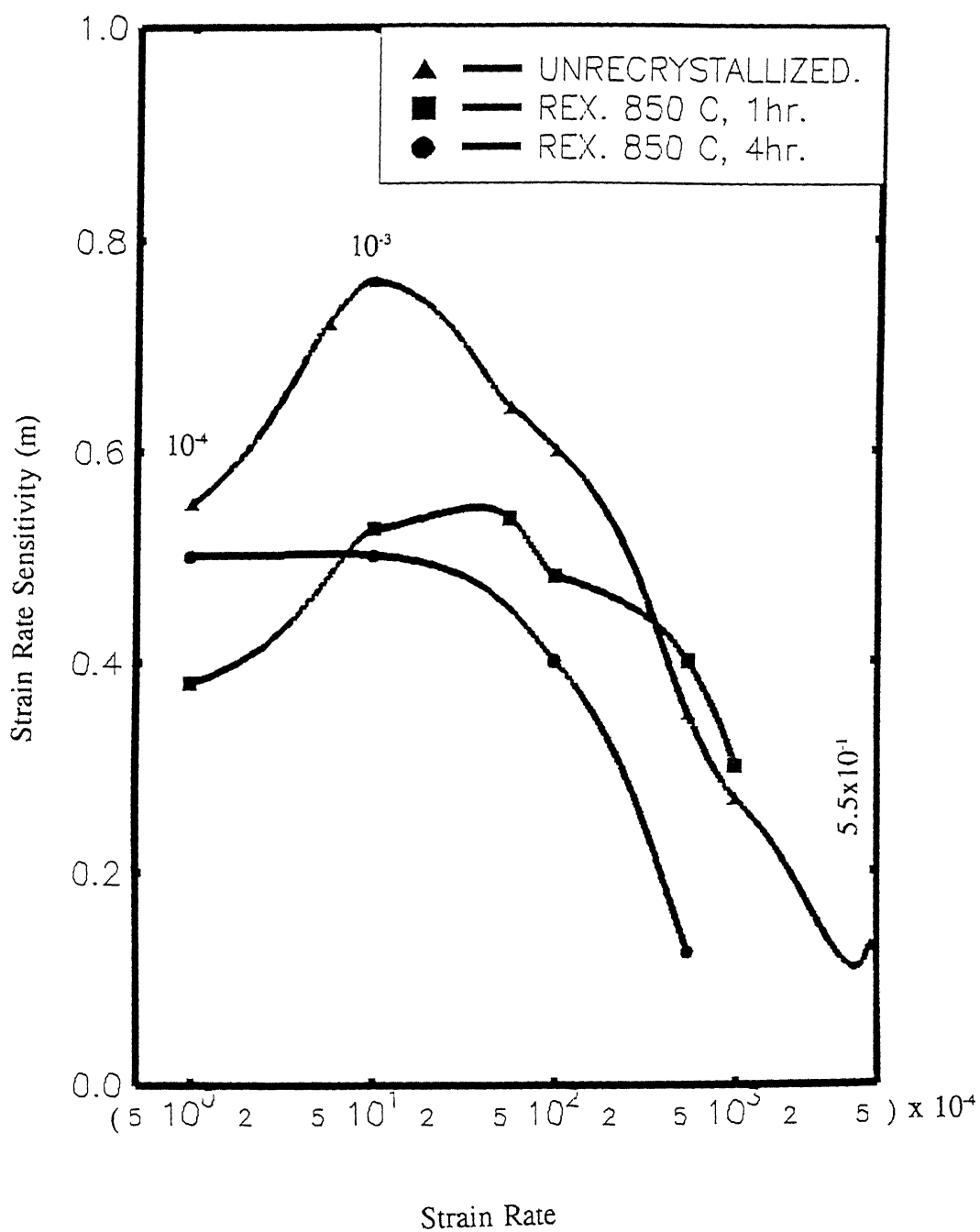


Fig. 4.46 A Effect Of Recrystallisation on Variation Of Strain Rate Sensitivity With Strain Rate .

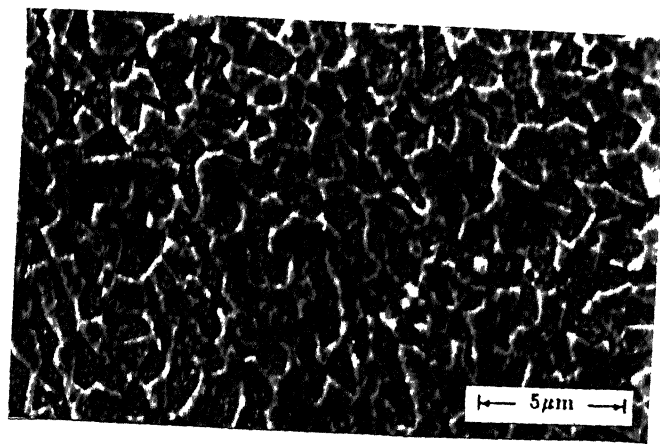


Fig. 4.47      Microstructure of the as rolled ( $\alpha+\beta$ ) alloy reheated at 900°C, soaked for 15 minutes and subsequently water quenched

specimens further recrystallized at 900°C yielded a total elongation of 925%. Similar results were also reported by Inagaki [63] who observed an elongation of 1400% in Ti6AlV unrecrystallized sheet which decreased to 400% when annealed at 950°C.

#### 4.5.6 Effect of Thermo-Mechanical Processing on Elongation till Failure:

Elongation to failure tests were carried out on specimens produced by different routes. The temperature of test was 900°C and strain rate was  $5.5 \times 10^{-3} \text{ s}^{-1}$ . Figure 4.48 (a,b,c) shows the load vs elongation curves for the samples tested. Figure 4.49 shows the flow stress obtained during the elongation to failure test with respect to the temperature routes. It was seen from the Figure 4.49 that flow stress was maximum for the specimen with the finest ( $\alpha + \beta$ ) morphology i.e. for the one obtained through Route 2. In contrast, the minimum flow stress was obtained for specimen with less fine ( $\alpha + \beta$ ) morphology which was obtained from Route 3. Figure 4.50 shows that maximum elongation values were obtained by specimens processed through Route 3, followed by those obtained through Route 1, and finally by those processed through Route 2. These observations appear to contradict since with finest structure route and sample showed less elongation which should have otherwise shown maximum elongation due to its finer structure.

This behaviour can be explained as the specimens showing the minimum tensile elongation had undergone different initial  $\beta$  processing steps. If we compare the samples of Route 3 and Route 2, then this means that  $\beta$  annealing structure in the  $\beta$  processing step of route 3 has improved the deformability than the route 2 sample which had  $\beta$  rolled structure in the processing step. This indicates that  $\beta$  annealing in  $\beta$  processing step improves the deformability of the ( $\alpha + \beta$ ) processed samples. This behaviour was also reported by Novikov et. al [64] in the same alloy in the temperature range 750 to 880°C where they have concluded that structure recrystallization in the  $\beta$  phase field improves the deformability of titanium alloys in the ( $\alpha + \beta$ ) range.

If we compare route 1 and route 3 then it was seen that route 3 had finer  $\beta$  structure ( $= 300 \mu\text{m}$ ) (after  $\beta$  annealing) than the as homogenized  $\beta$  structure [ $g_s = 600 \mu\text{m}$ ] of route 1. This means that with decreasing  $\beta$  grain size after  $\beta$ -processing prior to  $\alpha + \beta$  processing, superplastic deformation increases.



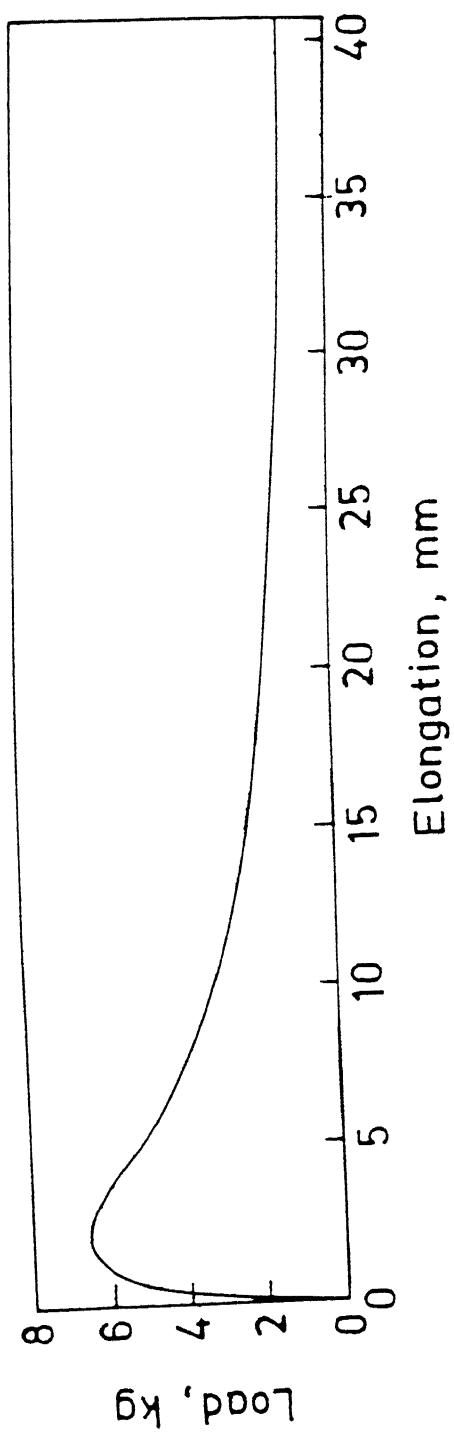


Fig. 4.48 (a) Load vs Elongation Curve For Route 1 Sample Tested At 900 °C.

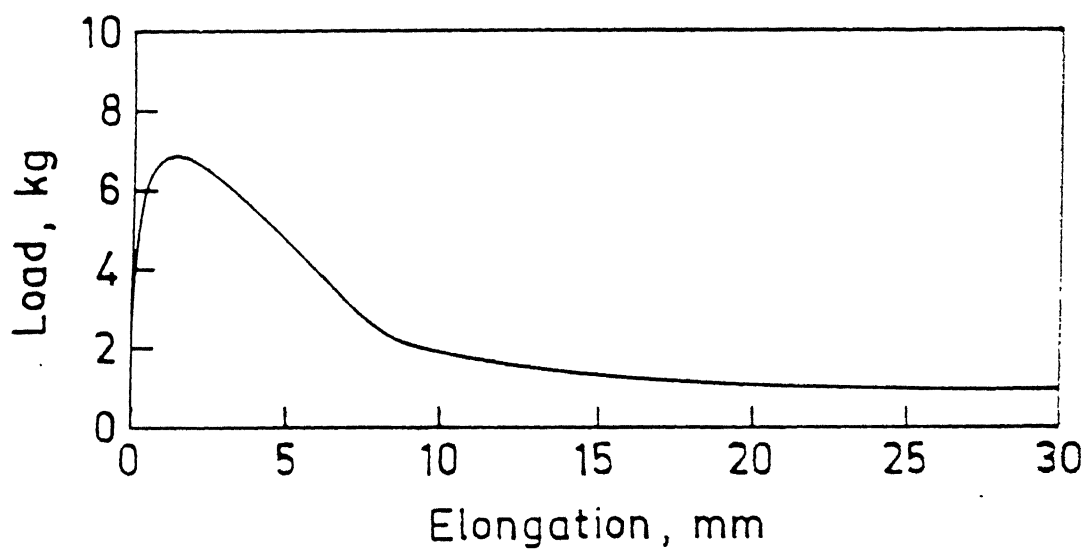


Fig. 4.48 (b) Load vs Elongation Curve For Route 2 Sample Tested At 900 °C.

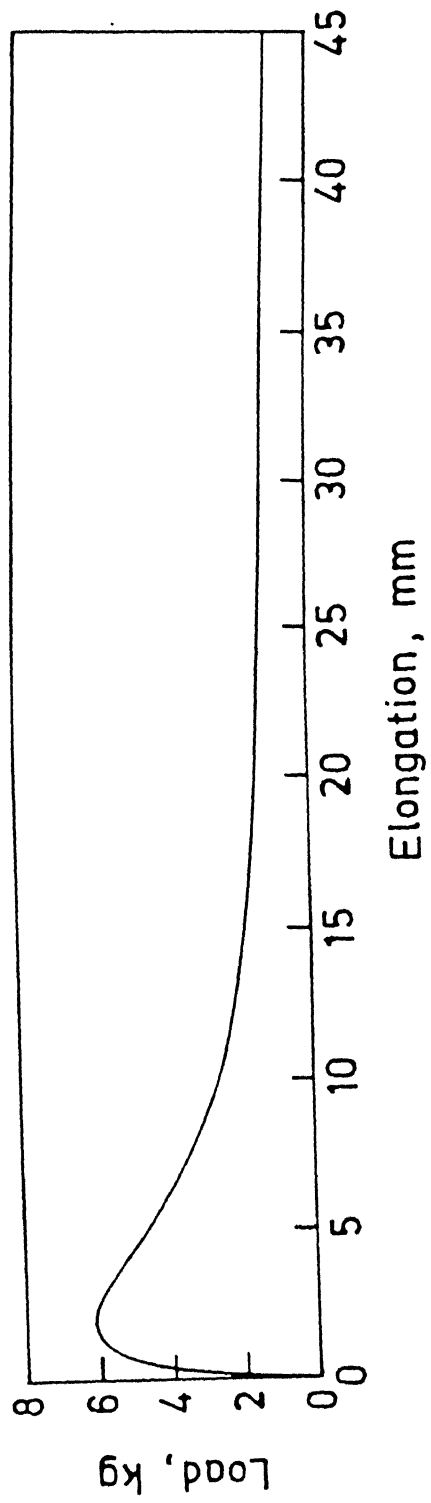


Fig. 4.48 (c) Load vs Elongation Curve For Route 3 Sample Tested At 900 °C.

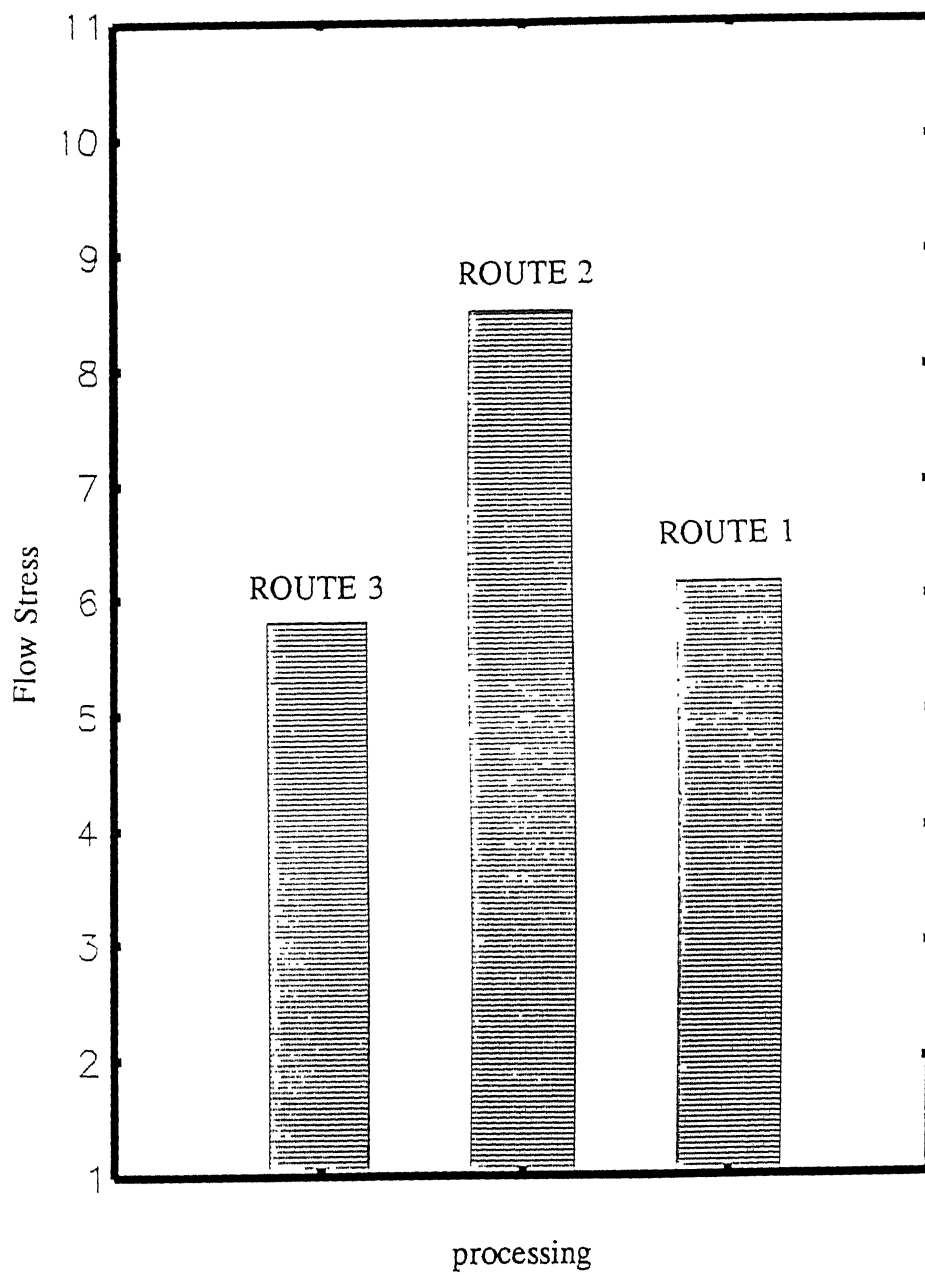


Fig. 4.49 Comparison of Flow Stress For Different Thermomechanically Processed Samples. Testing Conditions :  $900^{\circ}\text{C}$ ,  $5.5 \cdot 10^{-3} \text{s}^{-1}$

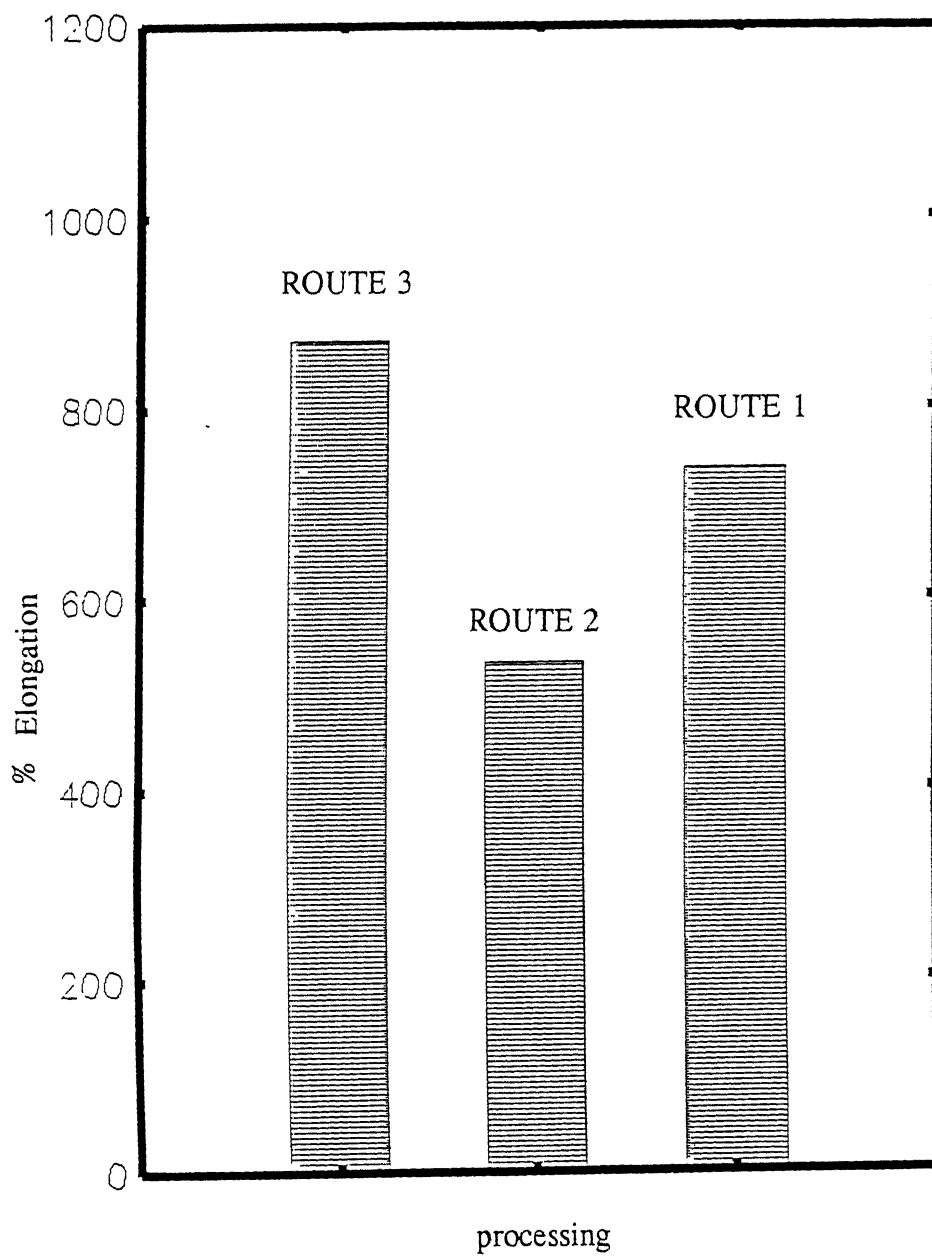


Fig. 4.50 Comparison of Maximum Elongation Obtained For Different Thermomechanically Processed Samples. Testing Conditions :  $900^{\circ}\text{C}$ ,  $5.5 \times 10^{-3}\text{s}^{-1}$

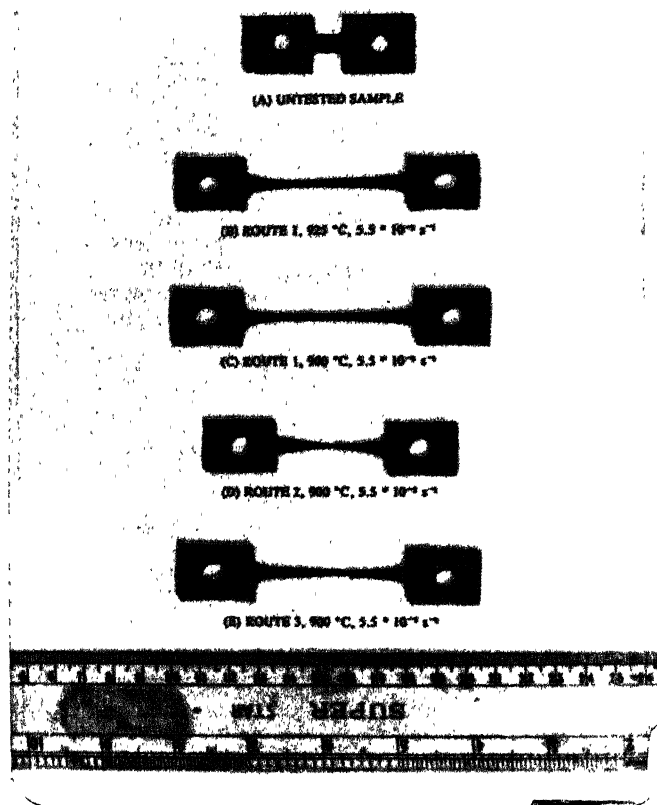


Fig. 4.51 Photograph Showing Elongated Samples After Superplastic Tensile Testing.

Thus at the end of this subsection we can say that initial  $\beta$  processing history has a marked effect on superplasticity of the TMP sheets. With  $\beta$  annealing and fine grain size in the initial  $\beta$  processing steps of the whole thermomechanical process, the superplastic formability can be improved.

## CONCLUSIONS

The following conclusions can be drawn from the results of the present study:

(1) The alloy Ti-632Si, during its processing in the  $\beta$  phase field does not undergo dynamic recrystallisation even at temperatures as high as 1250 °C, which is 250 °C above the  $\beta$ -transus temperature. However, the alloy rapidly undergoes static recrystallisation.

(2) The morphology of martensite  $\alpha'$  changes considerably with the conditioning of  $\beta$  phase i.e. (i) coarse or fine recrystallised  $\beta$  grains and (ii) pancaked unrecrystallised  $\beta$  grains. Aspect ratio of the martensitic plates could be varied between 15 to 30 by water quenching the samples obtained by following three alternative routes: (a) recrystallisation annealing carried out at about 50 °C above the  $\beta$  transus temperature, (b) rolling the alloy for different thickness reductions in the single phase  $\beta$  field at temperatures of 50 °C, 150 °C and 250 °C above the  $\beta$ -transus temperature, (c) subjecting pancaked grains by a recrystallisation annealing treatment at a temperature of 10-20 °C above the  $\beta$ -transus temperature.

(3) The acicular  $\alpha$  morphology obtained by the transformation of  $\alpha'$  to  $\alpha$  at different hot rolling temperatures has an influence on acicular  $\alpha$  thickness and aspect ratio. Thus, mixed type of structures containing acicular/equiaxed primary  $\alpha$  morphology of different aspect ratio is produced by 60% rolling deformation at the temperatures of 850 °C, 900 °C and 950 °C. The mean grain size of primary  $\alpha$ , however, is achieved by rolling at 850 °C. The breakdown of acicular  $\alpha$  morphology can be achieved through pinching by  $\beta$  phase.

(4) The condition of  $\beta$  grains prior to their quenching has also considerable effect on the refinement of the structure during rolling in the  $(\alpha+\beta)$  phase field by 60% reduction at 850 °C. The finest mean grain size of primary  $\alpha$  results when  $\beta$  phase is in unrecrystallised condition.

(5) Recrystallisation annealing helps in transforming the structure from mixed morphology consisting of acicular/equiaxed primary  $\alpha$  to nearly equiaxed. However, this also leads to grain coarsening of  $\alpha$ . The mean grain size of primary  $\alpha$  in the as rolled structure in the alloy processed through route 3 was found to be 1.2  $\mu\text{m}$  and that after recrystallisation annealing at



the temperature of 850 °C for a period of 4 hours becomes about 2.5  $\mu\text{m}$ .

(6) Characterisation of superplastic behaviour of differently thermomechanically processed samples show a maximum strain rate sensitivity of 0.75 in the samples processed through Route 3 involving conditioning of  $\beta$  phase to fine recrystallised at the testing temperature of 900 °C and strain rate of  $1 \times 10^{-3}$ . Under these conditions, total elongation of about 875 % was obtained which is considerably higher at lower deformation temperatures i.e. 100 °C below the  $\beta$ -transus temperature than that achievable in conventionally processed Ti-632Si. It is inferred that the  $\beta$  structure prior to  $(\alpha + \beta)$  has a marked effect on the superplastic elongation.

(7) The conventional processing generally requires recrystallisation annealing for obtaining higher strain rate sensitivity and total % elongation, while the superplastic behaviour of the thermomechanically treated Ti-632Si worsened after the recrystallisation annealing treatment. This means that one can directly use the as rolled sheets for superplastic forming without going for recrystallisation annealing treatments.

## SUGGESTIONS FOR FURTHER WORK

1. Detailed investigations should be done to study the deformation behaviour and recrystallization kinetics while processing in the  $\beta$ -phase field with special emphasis on evolution of final structure for the betterment of existing mechanical properties.
2. TEM investigations should be done to study the deformation behaviour in the  $(\alpha + \beta)$  phase fields vis-a-vis its effects on evolution of equiaxed morphology.
3. The formation of metastable phases and their implications in the evolution of microstructure during their decomposition while reheating are important.
4. Effect of equiaxed morphology, evolved by different routes on mechanical properties should be investigated.
5. Microstructural changes occurring during superplastic deformation of this alloy with different starting microstructural morphology should be studied assisted with TEM investigation.
6. Effect of metastable phases on the superplastic deformation / overall mechanical properties should be studied.
7. Post-Superplastic-Deformation properties should be investigated.
8. The effect of different starting textures on the superplastic deformation and the change / disappearance of texture during deformation should be studied.
9. Elucidation of the deformation mechanisms ; the extent to which the current theories of superplasticity are successful in modelling the behaviour of this alloy and predicting the effects of varying temperature, grain size and distribution , initial microstructure.

## REFERENCES

1. M. J. Donachie, Jr., in Titanium and Titanium Alloys : A Source Book, ASM, (1982)
2. S. R. Seagle and L.J. Barillo, in Titanium and Titanium Allouys : A Source Bok, ASM, (1982).
3. J.C.Williams and G.Luetjering, Titanium '80 Science and Technology, AIME, New York, Vol.1, pp671, (1980).
4. P.Dadras and J.F.Thomas.Jr, Met. Trans, A, Vol 12A, pp1867-76, (1981) .
5. N.E.Paton, C.H.Hamilton , Met Trans, A. Vol10A, pp231-250, (1979).
6. E.W.Collings, The Physical Metallurgy Of Titanium Alloys, ASM, pp181-207. (1984).
7. H.J.McQueen and D.L.Bourell, J.Metals, Vol 9, pp 28-35, (1987).
8. V.Shukla and S. Bhargava, NSTS-96, Conf.Proc.,Hyderabad, 28-29, (July 1996).
9. D.Bourell and H.J.McQueen, J.Appl.Metal Work, Vol 5, pp 53-73, (1987).
10. J. C. Chesnutt, C.G. Rhodes and J. C. Williams, Fractgraphy - Microscopic Cracking Processes, ASTM. 99-138, (1976).
11. C.H. Hommillon and G.E. Stacher, Metal Progress. March, 34. (1976).
12. F.H. Froes, J.C. Chesnutt, C.F. Yolton, C.H. Hamilton and M.F. Rosenblum, Titanium '80 Science and Technology, Kyoto, Japan, May 19-22, 1025-1031, Eds. H. Kimura. and O. Izumi,(1980).
13. I. Weirs, F.H. Froes, d. Dylon and G.E. Welsch, Met. Trans. A., 17A, Nov., 1935-1947,(1986).
14. W. Cho, J.W. Jones, J.E. Allison, W.T. Donlon: Proc. 6th World Conference on Titanium, Les. Ed. de Physique, Paris, Vol. 1, pp. 187-192,(1988).
15. H. M. Flower, P. R. Swann and D.R.F. West, Met. Trans., Vol. 2, pp. 3289-97, (1971).
16. C. Ramchandra and V. Singh ; Scripta met, Vol. 21, pp. 633-636, (1986).
17. W.J. Plumbridge and M. Stanley, Int. J. Fatigue, 1986, Vol. 8, pp. 209-16.
18. Titanium : A Technical Guide, Mathew J. Donachic Jr., ASM, 1988.
19. Molchanova, E.K., Phase Diagrams of Ti alloys, Israel Program for Scientific Translations, 1965.

20. Zwicker. U, Titan und Titanlegierungen, Springer Verlag, 1974.
21. Rosenberg H.W., Titanium Alloying in Theory and Practice in the Sci. Tech and Application of Titanium (Proc. first Int. Conference on Titanium, London, R.I. Jaffee and N.E. Promisel, Ed., Pergamon Press, 1970, pp. 851-859.
22. J.E. Gould, W.A. Balblact III, and J.C. Williams, in Ad. Proc. Methods for Titanium. Proc. Conf. The Met. Soc. of AMIE, TMS Fall, Kentucky, Oct. 13-15, 1981, Ed. D.F. Harson and C.H. Hamilton, pp. 203-225.
23. Wood, R.A., Titanium Alloys Handbook, Metals and Ceramics Information Centre, Battelle, Pub. No. MCIC-HB-02, Dec. 1972.
24. Salmon D. R., Low Temperature Data Handbook, Titanium and Titanium Alloys, National Physical Labs, NPL Report Q453 (N8023448), May 1979.
25. Froes, F.H., Eylon D. and Bomberger H. B. Ed., Titanium Technology : Present Status and Future Trends. Titanium Development Association. 1985.
26. Gorynin I.V., Chechulin, B.B., Ushkov, S.S. and Belova, O.S., A study of the nature of the Ductile - Brittle Transition in Beta Titanium Alloys, in Titanium Sci and Tech. (Proc. second Int. Conf. on Titanium Boston, Eds: Jaffee II and Brute, H.M. Plenum Prss, 1973.
27. K. H. Mishra, Materials Engg., 79-80, July 1974, 61-76, 1974, Reinhold Publishing Comp. Inc.
28. S.M.L. Sastry, P. S. Rao and K. K. Sankaran, Titanium '80 Science and Technology, Conf. Proc., Eds: Kimura and Izumi, Kyoto, Japan, May 19-22. 1980, 873-886.
29. Wayne, A. Reinsch, Metal Progress, Feb. 1982, 51-53.
30. T.L. Trenogina and R. M. Lerinman, proc. of 3rd International Conference on Titanium, Moscow, 1976, pp. 1623-1632.
31. J.C. Williams, Titanium Science and Technology, Plenum Press, New York, Vol. 3, 1973, pp 1433.
32. R.I. Jaffee, Titanium Science and Technology, Plenum Press, New York, Vol. 3, 1973, pp. 1665.
33. M. Peters and G. Luetjering, Titanium '80 Science and Technology, 1980, Kyoto, Japan, pp. 925.
34. J.C. Williams and G. Luetjerings, Titanium '80 Science and Technology, AIME, New

York, Vol. 180, pp. 671.

35. K. Gazioiler, J.J. Grundhoff and P. Fuoke and W. Bunk, Z. Metallkd, 67(1976)209.
36. G.A. Stubbinton and A.W. Bonlen, J. Mat. Sci., 9, 1974, 941.
37. J. C. Williams and E.A. Starke Jr., Deformation, processing and Structure, G. Krauss, ed. ASM, Metals Park, Ohio, 1984, pp. 279-354.
38. Sakhanova, Titanium '80, Science and Technology, Kyoto, Japan, pp. 849.
39. K. Moru, H. Mecking and G. Luetjering, Proc. of Int. Conf. on Strength of Metals and Alloys, Pergamon Press, New York (1985), 251.
40. H. Inagaki, Z. Metallkd, Aug. 1990, pp. 540.
41. H. Margolin and P. Cohen, Titanium'80 Science and Tech, Kyoto, Japan. pp 1565.
42. T. Sheppard and J. Norley, Mat. Sci. and Tech. Oct. 1988.
43. Hammond C. and Nutting J. The Physical Metall of Superalloys and Titanium alloys in forging and properties of aerospace materials, TMS, 1978, pp. 75-102.
44. S. F. Frederick, and G. A. Ilenning, Met. Trans. 6B (1975) 601.
45. M. F. Amateau, D. L. Dull and L. Raymonds, Met. Trans. 5A(1974) 561.
46. H.J. McQueen and J. J. Jonas, Treatise on Materials Science and Tech.. Plastic Deformation of Materials, R.J. Arsenault ed., Academic Press, New York, 1975. vol. 6, pp. 393.
47. R. A. Adamesku et al, Fiz, Metal. Metalloned, 63, No. 5, 987-991, 1987.
48. A.S.M. Committee on Ti and Ti Alloys, Metals handbook Ninth Ed., Vol. 3, 361-371, 1980 ASM.
49. A. K. Ghosh and C.H. Hamilton, Met. Trans. 10A, 699, (1979).
50. Murcoy, W. Mahoney, Technical Notes, in Handbook Of Titanium, 1101-1109.
51. O.A. Kaibyshev, I.V. Kazachkov and R. M. Galeev, JI. of Mat. Sci. 16, 250 (1981).
52. C.H. Hamilton, in Superplastic Forming Conf. Proc. Ed. S. Agarwal, ASM, Los Angeles, Mar 22, 1984, pp13-22.
53. F. Dymant, Titanium '80, Eds. H. Kimura and O. Izumi, AIME, 19(1980)
54. N.E.W. Dereca and C.M. Libanati, Acta Met. 16, 1297 (1968).
55. A.E. Pontau and O. Hazrus, Phys. Rev. B., 19, 4027, (1979).
56. M.Peters, G.Luetjering, and G.Ziegler, Materials Sci. Tech., Oct. 1988, Vol 4, 274-282.

57. I.Weiss, F.H.Froes,D.Eylon, G.E.Welcsh, Met Trans A, Vol 17A, 1986, 1935-1946.
58. O.A.Kaybyshev, R.A.Lutfullin and G.A.Salishchev, Fiz. Metal Metalloved,66,no 6, 1163-1171, 1988.
59. M.E.Rosenblum, P.R.Smith and F.H.Froes, Titanium '80 Science and Technology, Conf. Proc, Ed:H.Kimura, O.Izumi, Tokyo, Japan, pp 1015-1025.
60. C.H.Hamilton and A.K.Ghosh, ibid,pp 1001-1014.
61. Huang Liping, In Superplasticity and Superplastic Forming, Conf. Proc. (TMS),Blaine, Washington, 1988, pp 435-440, Eds:C.H.Hamilton and N.E.Paton.
62. G.Gordon, L.Snarsky, A.Cohen, A.Rosen ,Materials Sci. Tech.,1, (1985), 466-469.
63. H.Inagaki, Z.Metallkd, 86, (1995) 9.
64. I.I.Novikov, V.K.Portnoy, N.L.Anikanov, I.A.Akmulin and G.I.Lekh, Fiz. Metal Metalloved, 68, No 1, 156-160, 1989.